Stellingen

behorende bij het proefschrift

Partial Discharge and Breakdown Testing at High DC Voltage

Udo Fromm
Delft, 19 september 1995

1. The three dimensional q-Δt_{suc} histogram (number of discharges as a function of the discharge magnitude and the time to the successive discharge) is a good base for discharge classification at DC voltage. When using it, all the methods currently used for discharge classification at AC can be adopted for use at DC as well.

2. The study of physical discharge properties can be based on standard discharge measurements by plotting the mean time to the successive discharge and the mean time to the previous discharge against the discharge magnitude.

3. Although the occurrence of errors is a necessary condition for the generation of knowledge, errors are evaluated as being negative.

4. The ultimate goal of technical science is to write recipe books for the engineer.

5. Never buy the first version of a product, if possible!

6. Despite the increasing availability of computers, there is as yet no acceptable replacement for pencil and paper.

7. Despite the enormous developments in information technology, citizens of neighbouring countries still lack sufficient knowledge of each other.

8. A (political, economic, financial) system can be more resourceful if the decisions are made by those who have to carry the consequences.

9. Not taking everything seriously while being serious does not have to be a contradiction.

Partial discharge and Breakdown Testing at High DC Voltage

Partial discharge and Breakdown Testing at High DC Voltage

Partial discharge and Breakdown Testing at High DC Voltage

PROEFSCHRIFT

ter verkrijging van de graad van doctor
aan de Technische Universiteit Delft,
op gezag van de Rector Magnificus, Prof. ir. K.F. Wakker,
in het openbaar te verdedigen ten overstaan van een commissie,
door het College van Dekanen aangewezen,
op dinsdag 19 september 1995, te 10.30 uur

door

Udo FROMM

Diplom Ingenieur für Elektrotechnik, TU Dresden
geboren te Koßdorf, Duitsland

Delft University of Technology, 1995

Dit proefschrift is goedgekeurd door de promotor

Prof. dr. ir. F.H. Kreuger

Samenstelling promotiecommissie:
Rector Magnificus, voorzitter
Prof. dr. ir. F.H. Kreuger, TU Delft, promotor
Prof. dr. ir. H. Blok, TU Delft
Prof. ir. L. van der Sluis, TU Delft
Prof. dr. ir. G.C. Damstra, TU Eindhoven
Prof. ir. W.L. Kling, S.E.P. Arnhem
Dr. ir. P.H.F. Morshuis, TU Delft
Dr. ir. J.J. Smit, KEMA Arnhem

Published and distributed by:
Delft University Press
Stevinweg 1, 2628 CN Delft
Telephone +31 15 783254
Fax +31 15 781661

CIP-DATA KONINKLIJKE BIBLIOTHEEK, DEN HAAG

Fromm, U.
Partial Discharge and Breakdown Testing at High DC Voltage/
U. Fromm - Delft: Delft University Press, - Ill.
Thesis Delft University of Technology. - With ref. - With summary in Dutch. - With summary in German.
ISBN 90-407-1155-0
NUGI 832
Subject headings: high dc voltage, partial discharges, breakdown, discharge recognition

Printed in the Netherlands

Contents

Summary

The production of reliable high voltage components requires the availability of suitable test methods. For the design of test methods, knowledge of the mechanisms which cause ageing and finally lead to breakdown is necessary. In this thesis partial discharges and breakdown are studied at high DC voltages. The goal is the development of test procedures and diagnostic tools for equipment which is stressed under application of DC voltage.

In chapter 1 an introduction is given to the problems of dealing with high DC voltage.

In chapter 2 the experimental methods used in this study are described, which are
- a classical detection system in combination with a computer aided discharge analyzer.
- a time-resolved detection system for internal partial discharges.
- a set-up for an ageing test.

In chapter 3 internal partial discharges are studied. The physical mechanism is investigated and the statistical behaviour is analysed. A model of the statistical discharge behaviour is presented and experimentally validated. The model is based on the mutual relation of time lag, discharge magnitude and recovery time for a single discharge.

In chapter 4, the statistical behaviour of partial discharges in air is examined. A similar statistical model to that developed for internal discharges can be used for the description of corona discharges. Surface discharges appear to be more complex. As a characteristic description for surface discharges, the three dimensional q-Δt_{suc} histogram (number of discharges depending on discharge magnitude and time to the successive discharge) can be used.

Chapter 5 concerns the partial discharges in dielectric liquids. An overview of mechanisms leading to breakdown is given. Some measurement results for partial discharges in transformer oil are presented.

In chapter 6, ageing and breakdown at DC voltage is investigated. The results of ageing tests are presented for samples of epoxy resin which contain an air-

filled void. For the evaluation, the inverse power law relation is assumed. A life exponent $9 < n < 12$ has been obtained for the epoxy samples.

In chapter 7, methods of testing and methods of discharge diagnostics are discussed for DC voltage. The methods for voltage testing are concluded to be similar to that which is known for AC voltage. Further, a partial discharge test is suggested. Concerning discharge diagnostics at DC voltage, the three dimensional q-Δt_{suc} -histogram (number of discharges depending on discharge magnitude and time to the successive discharge) is suggested to be used as a base for discharge classification. Then, all the methods used currently for the discharge classification at AC voltage can be adopted to be used for DC voltage as well.

Chapter 1

Introduction

In the beginning there was DC voltage.
The electrical science based on the discoveries by the pioneers Galvani, Volta, Oersted, Ohm and Ampère and in later years the practical application of electricity began with DC voltage.

1.1 Historical sketch

1.1.1 HVDC energy application [5,37]

The first electric power station in the world, on Pearl Street, in New York, was built by Thomas E. Edison and began operation in 1882. It supplied 110 V DC voltage. The electricity was produced by dynamo machines driven by steam engines. Within a few years, similar stations had been built in most large cities of the world. In Germany for instance, in 1887 there were 375 electric power stations operating; 170 of them in Berlin. Such a station consisted, for instance, of 4 dynamos driven by 4 steam engines of 100 horsepower power each. The generation and consumption of electric power were closely located to each other. The invention of the AC transformation had a great impact on the transmission technique. At that time there was much discussion about the advantages and disadvantages of AC and DC. The introduction of the 3-phase AC voltage decided the discussion in favour of AC. After that the DC voltage was restricted to a few fields such as electric railways and the chemical industry (electrolysis).

With the development of large transmission lines, the engineers remembered the advantages of DC voltage. There are no reactive current components, no dielectric losses and when compared with AC, less insulation effort is required. The absence of reactive current components made long cable connections, such as submarine cables, possible. The first commercially used HVDC transmission line was built in 1954. It connects the island Gotland with the Swedish mainland.

At the same time test procedures were developed to ensure reliable operation under all possible conditions [88]. Heat caused by power losses has to be taken

in account, so that the tests consist of combined heat cycles and overvoltage stress [49,67,81]. Most of the cables still have paper-oil insulation, which is known to be very reliable. In addition to the paper-oil cables, polyethylene cables are under development [15].

1.1.2 HVDC non-energy application

The first widespread practical application of electricity was the DC telegraphy driven by electrochemical batteries. Later on, other applications like electric dust filtering or electrostatic painting were developed, where the working principle is based on electrostatic forces.

The invention of the electron tube led to the development of a whole group of non-energy applications like X-ray, electron microscopy and spectroscopy, etc. In these fields high DC voltage is used to generate an electron beam. In the past these high voltage components did not receive much attention. Recently, the miniaturisation of these products has caused problems which started new technological development. The aim of this development is to create reliable and inexpensive insulation constructions with small dimensions. This will lead to the development of better test and design rules.

Another field dealing with high voltage DC problems is spacecraft engineering. Charge accumulation at the surfaces of spacecraft due to space radiation and the effect of ensuing partial discharges on the electronic components have been considered as a problem [65]. In order to ensure reliable operation, the measurement of partial discharges has been used [3,4,16].

1.2 The electric field and space charge accumulation at DC voltage

1.2.1 The electric field at DC voltage

In general, the electrical field at DC voltage E_{DC} consists of two components

$$E_{DC} = E_{\epsilon} + E_{\rho} \tag{1.1}$$

The ϵ-field E_{ϵ} is determined by the ϵ distribution, identical to an AC field. The field E_{ρ} is caused by accumulated space charge. The field at DC voltage E_{DC} undergoes various situations because each field component shows a different behaviour in the course of time.

switching on the voltage
An external voltage V_0 is applied to an insulator at time t_0 (see Figure 1.1). The time during which the voltage is increased up to V_0 is usually much smaller than the time required to accumulate a considerable amount of space charge. At t_0 the component E_ρ is negligible, so that

$$E_{DC}\ (t_0) = E_\epsilon \tag{1.2}$$

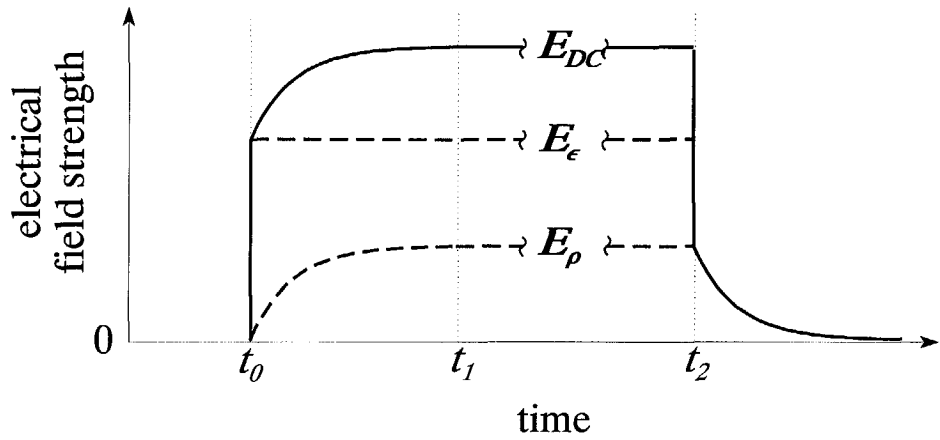

Figure 1.1 *Different field situations at DC voltage. At $t=t_0$ a voltage V_0 is applied to the insulator. At $t=t_1$ the steady DC field is reached. At $t=t_2$ the voltage is switched off.*

The space charge will accumulate between t_0 and t_1 (see Figure 1.1), so that the field E_{DC} changes continuously during that period (depending on the materials used this may take minutes or days).

steady DC field
A steady DC field E_{DC} is reached when the charge accumulation is finished (for $t>t_1$ in Figure 1.1). The field E_{DC} is determined by the distribution of the specific conductivity σ.

$$E_{DC}\ (t>t_1) = E_\sigma \tag{1.3}$$

With eq. (1.1) and eq. (1.3), the accumulated space charge can be calculated (see Appendix A):

$$\rho = \sigma \boldsymbol{E}_{\sigma} \cdot \nabla \frac{\epsilon}{\sigma} \tag{1.4}$$

charge-induced field
After switching off the voltage (for $t > t_2$ in Figure 1.1) the charge-induced field $\boldsymbol{E}_{\rho}$ remains. Caused by conduction the accumulated charge dissipates. The dissipation of the charge can last from minutes to weeks.

polarity reversal
Polarity reversal causes the superposition of the charge-induced field at one polarity and the ϵ-field of the opposite polarity. After redistribution of the space charge, a new steady DC state is reached.

superimposed voltage impulses
The appearance of voltage impulses on the operating voltage is treated as a superimposed ϵ-field on the current field E_{DC}.

In order to determine locations with a critical field strength, field calculation programs are generally used. These programs (e.g.[89]) usually solve the ϵ-field $\boldsymbol{E}_{\epsilon}$ given by $\nabla \cdot \epsilon \nabla V = 0$ and the σ-field $\boldsymbol{E}_{\sigma}$ given by $\nabla \cdot \sigma \nabla V = 0$. Thus the field distribution at the steady DC state and the field distribution directly after a change of the voltage (switching on or off, polarity reversal, superimposed voltage impulses) can be calculated.

The transition period to the stationary DC field cannot be described in this way. The charge-induced field during that period needs to be treated as a time function. During the transition to the stationary DC field, the local field stress might exceed both the stationary AC and DC stress [30], which prompted the development of a program to plot the field during the field transition [82]. To the best knowledge of the author, such software is not yet commercially available. Therefore the field transition is illustrated here by the following example:

> At time t=0 a DC voltage is applied to a sample consisting of 3 different materials. The field transition is simulated on an *RC* network (Figure 1.2). At first the field distribution is capacitive ($E_{\rho}=0$). Thereafter charges are accumulated at the interfaces.

When considering the fields E_ϵ and E_σ only, layers 1 and 3 in Figure 1.2 would be concluded to be the most stressed. Considering the time-dependent voltage distribution over the different layers (see Figure 1.2) it turns out, that the highest stress occurs in the second layer.

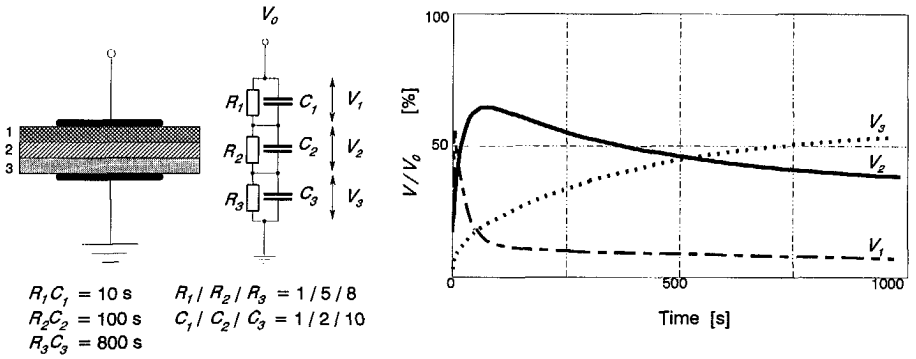

***Figure 1.2** Transient voltages across the layers of an insulator.*

This simple example implies two conclusions:

- The transition period to a steady DC field must be considered to be critical. Therefore, for the evaluation of DC constructions, calculations or approximation methods that simulate the transition from the ϵ-field to the σ-field may be necessary.
- When testing DC constructions, the test time has to be at least as long as the transition time for the change from the ϵ-field to the σ-field.

1.2.2 Mechanism of charge accumulation

According to equation (1.4), external influences must be taken into account if they cause a gradient of ϵ/σ [17]; e.g., power losses in cables cause a temperature gradient which leads to a gradient of ϵ/σ; external radiation (X-ray or nuclear radiation) may locally enhance the conductivity and therefore cause a gradient of ϵ/σ.

Even in the case of a DC field in a *single* material, space charge might be accumulated. Whether space charge will accumulate and the polarity of that charge depend on the conduction mechanisms through the electrode/insulator interface and in the bulk of the dielectric. Concerning the polarity of space charge, it can be distinguished in (see Figure 1.3):

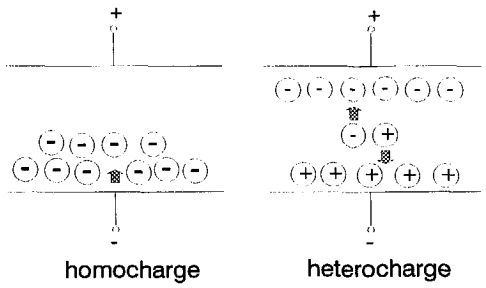

***Figure 1.3** The accumulation of homocharge and heterocharge.*

a) Homocharge

The polarity of the space charge is the same as that of the nearest electrode. Homocharge accumulates if the charge transport through the electrode/insulator contact exceeds the charge transport through the bulk of the dielectric, so that the current of the whole system is bulk limited. Homocharge reduces the dielectric thickness, which can lead to breakdown [57].

b) Heterocharge

The polarity of the space charge is opposite to that of the nearest electrode. Heterocharge accumulates if the electrode/insulator contact blocks the extraction of mobile charges. Thus the transport through the bulk is larger than the limited current through the electrode/insulator contact. The accumulation of heterocharge in the vicinity of the electrodes causes field enhancement and might lead to local damage.

For many years, a direct analysis of the process of charge accumulation was impossible since the experimentally observable variables gave only an average of what was taking place in the sample under study. Over the years, methods were developed which enabled the direct observation of space charge accumulation. A review is given by Lewiner [46].

For a better understanding of the mechanism of charge accumulation, the macroscopical description of the insulation in terms of permittivities ϵ and conductivities σ is not sufficient. A microscopical understanding of the influence of the structure of the dielectric (homogeneity, isotropy) upon the generation and transport of the charge carrier is required. The nature and location of trapping centres needs to be studied. The resulting models may be similar to those used nowadays in semiconductor engineering.

1.3 Partial discharges at DC voltage

The destructive character of partial discharges is well known. There is a lot of knowledge and experience of the detection and evaluation of characteristic discharge parameters at AC voltage. For DC voltage, there is a lack of knowledge. For the development of test procedures and design rules of DC equipment, research on partial discharges and their effect on the reliability and the lifetime of the insulation is required. The discharge reveals itself in a number of ways [40]. Electrical discharge detection makes use of the charge displacement which causes a current in the leads to the object. In general there are two methods of electrical discharge detection:

- classic discharge detection
- time-resolved discharge detection

(a) Classic discharge detection

The classic detection equipment integrates the displacement current over its time of occurrence. This integrated value is called the discharge magnitude q. The basic measurement circuit is shown in Figure 1.4.

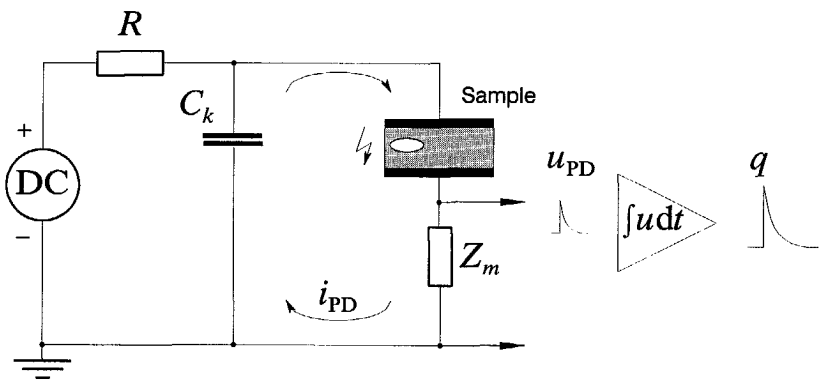

***Figure 1.4** Straight detection circuit.*

At DC voltage all discharges within the sample cause a current of the same polarity. Discharges outside the sample cause a current of the opposite polarity, which fact can be used to suppress external noise. Another method to suppress external disturbances is the balanced detection circuit as shown in Figure 1.5.

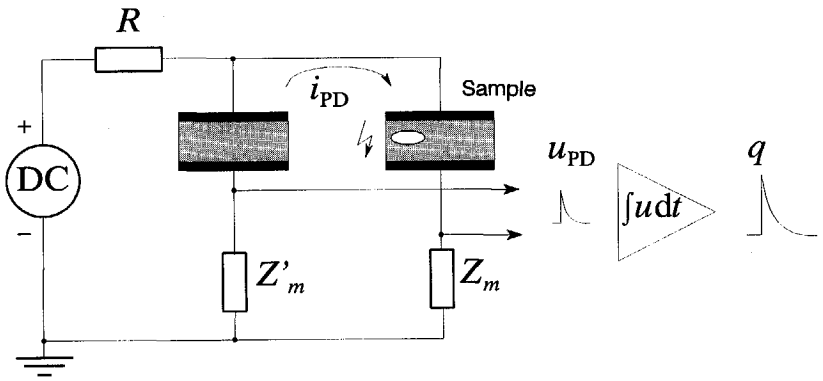

***Figure 1.5** Balanced detection circuit.*

There is very little published work on partial discharge measurement at DC voltage. Most of the measurements were carried out on simple sample configurations [12,23,24,43,59,68,72,80]. A few researchers report measurements on real industrial objects [3,69,76,87]. However, there is a lack of knowledge in interpreting the measured data.

(b) Time-resolved discharge detection
The study of the physical discharge mechanism requires the direct measurement of the displacement current in the leads of the test object. For this purpose time-resolved measurement is used. With time-resolved measurements as a base, the conditions for the development of Townsend-like and the streamer-like discharges are discussed by Devins [12]. The relation between the discharge mechanism and insulation degradation for AC voltage has been studied by Morshuis [56]. Such a comprehensive study has not yet been made at DC voltage, but some measurements have been reported [83].

Compared to the classic discharge detection, the time-resolved discharge measurement requires a more advanced measurement technique and a discharge circuit with a very high bandwidth. For industrial discharge measurement, it is restricted to some test objects only (cables, GIS). However, the knowledge of the discharge mechanism facilitates the interpretation of the discharge data measured by the classical method.

1.4 Ageing and breakdown

1.4.1 Mechanisms leading to breakdown

In order to ensure the reliable functioning of high voltage components, the investigation of ageing under operating conditions is necessary. Detailed knowledge of the breakdown mechanism enables the design of improved materials and constructions. In classic high voltage engineering, different types of breakdown mechanisms are distinguished [14]:

1. *Intrinsic breakdown*
   Intrinsic breakdown may occur because of the enhanced generation of charge carriers due to avalanche multiplication above a certain field strength (electronic breakdown [62]), or if the forces produced by the electrostatic attraction of the electrodes exceed the mechanical strength of the dielectric (electromechanical breakdown).

2. *Thermal breakdown*
   Almost all insulators might undergo thermal breakdown at a sufficiently high temperature, since the electrical conductivity is usually an exponentially increasing function of the temperature, and the thermal conduction is a slowly decreasing function of the temperature [61].

   The breakdown is usually not initiated on a broad front across the insulation area but at weak spots. This led other workers to consider the filamentary thermal breakdown [14].

3. *Treeing*
   Treeing occurs in inhomogeneous fields if the local field strength exceeds the intrinsic strength, which leads to a channel growth. Caused by charge transport through the channel, the field at the tip of the channel again may exceed the intrinsic strength, which leads to further channel growth and branching. The structure thus created looks like a tree and gives the mechanism its name. Breakdown occurs if the insulating distance is bridged by a tree. The tree development is not necessarily accompanied by the occurrence of partial discharges [48,85].

4. *Discharge erosion*
   At AC voltage the activity of partial discharges leads to material erosion, which causes a decrease of the insulation thickness, thus bringing about field enhancement. Pit formation can cause further field concentration, which leads to treeing and finally to breakdown [56,77].

At DC voltage no evidence is found for such a causal relation. No discharge erosion has been observed in experiments with artificial voids in polyethylene [57,72]. Therefore, partial discharges are not assumed to cause ageing in fields up to 25 kV/mm [72]. However, the occurrence of partial discharges indicates weak spots within the insulation construction, where breakdown might be initiated by other mechanisms.

5. *Chemical deterioration*
Chemical ageing is one aspect of the problem of stability of polymers [29]. It proceeds via the formation of polymer free radicals. Free radicals are very reactive and lead to propagating chain scission or cross-linking [14]. The initiation step may be thermal, oxidative, caused by UV absorbtion, ionising radiation or mechanical. Local electric currents may affect the chemical deterioration by Joule heating. The chemical reactions are sensitive to electric fields if charged species such as radical ions are formed as intermediates, or if they bring about changes in the dielectric constant by altering the concentration of polar species. Electric DC fields can also be responsible for dissociation and transport of ionised and ionisable by-products resulting in electrochemical decomposition (ionization) of the dielectric or the electrodes [84].

All of these processes may be participating factors in a real breakdown; e.g., the contribution of the thermal and mechanical process to the DC electrical breakdown on polyethylene has been shown in [58].

1.4.2 Breakdown statistics

Breakdown data are stochastically distributed. Therefore, they are evaluated by statistical methods. The two-parameter WEIBULL distribution is commonly used for characterizing the time to failure for solid insulation [14,18,34,66].

$$P_F(t) = 1-\exp[-(\frac{t}{t_S})^{\beta}] \tag{1.5}$$

The parameter t_S is known as the characteristic time to breakdown. Assuming the inverse power law relation

$$\begin{aligned} t_S &\sim V^{-n} \\ t_S &= C^{-1/\beta}V^{-\gamma/\beta}\ , \end{aligned} \tag{1.6}$$

where n and C are constants, results in a breakdown probability as a function of time and voltage stress:

$$P_F(V,t) = 1-\exp(-Ct^{\beta}V^{\gamma}) , \qquad (1.7)$$

During long-term DC tests on polyethylene cables [18,66] and on different epoxy samples [34], values of $n = 8..20$ were obtained. The breakdown data showed a large scatter. In contradiction to this, Shihab [72] measured a voltage level above which all samples broke down within one hour; below that level no breakdown was registered until 500 h.

Today the WEIBULL distribution is generally accepted as the most appropriate for solid insulation constructions. However, its first use was based on experience; it simply fitted the data. Later, a physical justification for the use of the WEIBULL statistics in the assessment of dielectric breakdown was given [13,14].

1.5 Object of the present study

The aim of present research developments in the HVDC non-energy field is to find reliable and inexpensive insulation constructions with small dimensions. This in turn implies a need for the development of test and design rules. The object of the present study is the development of a set of test rules for HVDC equipment.

Similar to AC tests, the DC tests should consist of partial discharge measurement and breakdown testing. The partial discharge measurement at DC voltage requires:

- development of measurement equipment
- definition of the quantities to be measured.

In order to interpret the measured discharge data

- the better understanding of the discharge mechanism is required.

The aim is

- the development of diagnostic tools for discharge tests at DC voltage.

In order to define conditions for overvoltage tests, the knowledge of the breakdown mechanism is required. Therefore

- the influence of partial discharge on breakdown at DC voltage

and

- the long-term behaviour of epoxy resin with applied DC stress is part of the present study.

Chapter 2

Experimental methods

2.1 Classical discharge detection

Classical discharge detection was the main tool for the discharge measurements reported in this work. It was used to study the statistical behaviour of various discharge sources.

2.1.1 General aspects

Concerning partial discharge measurement, the displacement current in the leads of the test object caused by a discharge is usually integrated. The amplitude of the resulting signal is proportional to the discharge magnitude q (see Figures 1.4, 1.5).

The problem is to "translate" the measured discharge magnitudes into an understandable "picture" of the discharge behaviour. At AC voltage, the discharge behaviour is generally made visible by superimposing the discharge pulses on the power frequency ellipse. At DC voltage, there is no generally accepted standard yet. In order to solve this problem different data representations have been used:

- the magnitude distribution [43,50,52,68,72]
- the distribution of the time intervals between the discharges [43,50]
- the discharge frequency as a function of time [43,72]
- the discharge frequency as a function of the discharge magnitude [68,69]
- the apparent discharge current [57]
- conditioned distributions [7].

Different data representations have the disadvantage that they are not comparable. Further, there is no indication that a single data representation provides all the necessary information on the discharge process.

The solution to this problem is to record the basic quantities of a DC discharge process, which are the magnitude and the time of occurrence of each discharge.

Then deduced quantities like the ones mentioned above can be calculated. The advantage of this method is that the data sets are comparable, even after the introduction of new deduced quantities. The first practical PD detector that works along these lines is reported in [53]. There, the discharge data were recorded on magnetic tape. The disadvantage was the off-line evaluation of the data and the requirement of new hardware for the generation of a new data representation.

New computer techniques enable the storage of a huge amount of data in computer memory. It also makes the data evaluation much quicker and more flexible, so that on-line evaluation can be performed. The software can easily be changed, so that the introduction of a different data representation is easily possible.

With the considerations above, we can define the requirements that a measurement system must fulfill:

- The recording in computer memory of the magnitude and the time of occurrence of the discharge. This is required over long periods of time, which is necessary for the dielectric properties (space charge, conduction mechanisms) to reach a stable state.
- On-line evaluation and graphic display of the discharge data (requirement for all modern measurement systems).
- Good noise rejection: all experience gained with AC discharge detection can be used; on top of that polarity-dependent noise rejection is possible (see Chapter 1.3) [43].

2.1.2 Hardware

The principle of the system is shown in Figure 2.1. Four main parts can be distinguished:

- **Conventional discharge detector:** band width 200 kHz; the crest value of the output signal is proportional to the discharge magnitude, the polarity of the output signal is equal to the polarity of the discharge current at the input.

- **Signal conditioner:** the discharge to be recorded is distinguished from background noise by a trigger level. A discharge signal exceeding this trigger level leads to the detection of its top value and to the generation of a trigger pulse, which starts the A/D conversion. The signal conditioner is polarity selective, so that only discharges of the selected polarity lead to the generation of a trigger pulse.
- The **data acquisition card** includes an A/D converter (to obtain the discharge magnitude), a timer (to obtain the time of discharge occurrence), a D/A converter (to provide an analogue trigger level for the signal conditioner). The A/D converter has a an 8-bit resolution, the timer is a 32-bit counter triggered with 1 MHz, which limits the minimum detectable discharge frequency to 0.00023 Hz (1 discharge per 71 min).
- **Computer**: a 386 PC/AT compatible with 3 Mbyte extended memory is used.

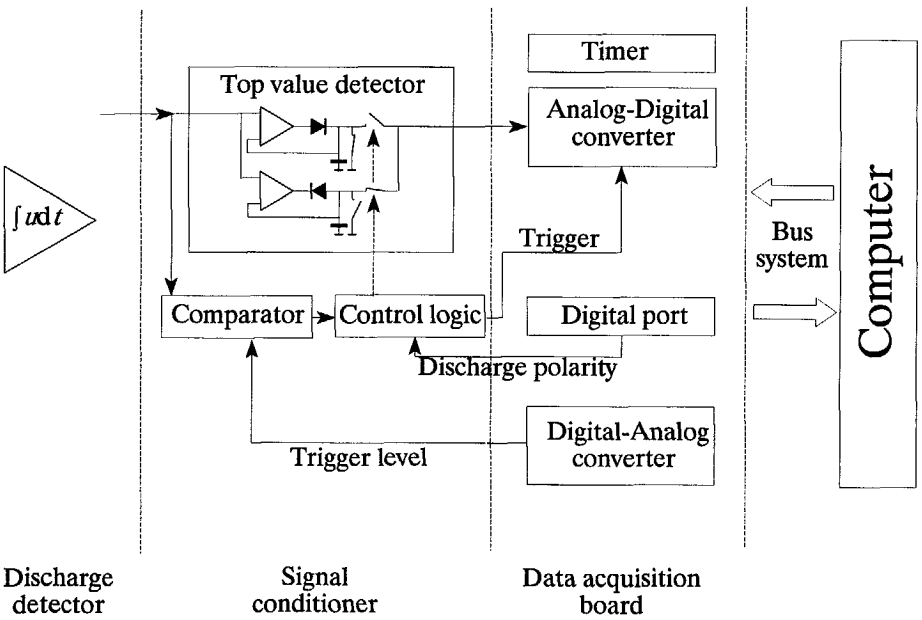

***Figure 2.1** The measurement system for the classical discharge detection.*

2.1.3 Software

The software consists of three main parts:

1. Basic system functions and procedures

The basic system includes all functions and procedures organizing memory access, managing file operation and basic graphic control functions.

2. Data acquisition

Before starting the measurement procedure, the polarity of the discharges to be recorded, the trigger level (see Figure 2.1) and the blind time t_{blind} are set. The blind t_{blind} time is necessary for the detector output to reach a steady state after discharge occurrence; during that time no discharge can be recorded. If a discharge above the trigger level is detected, the control logic of the signal conditioner generates a trigger signal, which starts the A/D conversion. When finishing the A/D conversion a hardware interrupt is generated. The interrupt routine stores the A/D converted value of the discharge magnitude (1 byte) and the time of occurrence (by reading a timer: 4 byte, 1 MHz clock) in the extended memory of the PC.

3. User interface

The user interface enables the user to evaluate on-line the data accumulated by the acquisition part during the measurement. The following output functions were used within the scope of this study:

a) Time functions of:
- discharge frequency f_{PD}.
- the time Δt between two discharges.
- discharge magnitude q.
- average discharge magnitude (median).

b) Distribution and density functions of:
- the discharge magnitude q.
- the time Δt between two discharges.
- three dimensional distributions of discharge magnitude and the time to the previous or to the successive discharge, $H(q, \Delta t_{pre})$ and $H(q, \Delta t_{suc})$.

c) Other functions
- the mean discharge magnitude $\overline{q}_{suc}$ of the successor as a function of the magnitude q.
- the time to the previous discharge $\overline{\Delta t}_{pre}$ as a function of the discharge magnitude q.
- the time to the successive discharge $\overline{\Delta t}_{suc}$ as a function of the discharge

magnitude q.

2.1.4 Noise rejection and data loss

At DC voltage all discharges within the sample cause a current of the same polarity (see Figure 1.4). Discharges outside the sample cause a current of the opposite polarity, which can be used to suppress interference by external discharges. This suppression is accompanied by a data loss, because during the time an interfering signal is rejected no discharge can be recorded.

In order to distinguish between two successive discharges, the detector output must reach a steady zero state before a new discharge is registered. Therefore a blind time t_{blind} is needed during which no discharge is recorded. The blind time is software selective (80 μs .. 10 ms) and determines the maximum resolution. The blind time results in a data loss L_{data} (see Appendix B):

$$L_{data} = t_{blind} f_{outside} \quad , \tag{2.1}$$

where f_{outside} is the average frequency of disturbances caused by discharges outside the sample. A frequency f_{outside} of 120 Hz would cause a data loss of 1 % at a blind time of $t_{\text{blind}} = 80$ μs.

2.1.5 Summarized system specifications

discharge detector:	200 kHz bandwidth
A/D conversion:	8 bit (128 positive, 128 negative)
time recording:	4 byte, 1 MHz clock frequency
time resolution between two successive discharges:	minimal 80 μs ...10 ms (software selective) maximal 71 min
maximum number of recorded PD:	600.000 (at 3 Mbyte extended memory)
polarity of the recorded discharge:	software selective
trigger level:	software selective

2.2 Time-resolved measurements

Time-resolved measurements have been carried out for internal discharges (chapter 3) in order to study the physical discharge mechanism.

2.2.1 Test samples

The test samples were constructed employing the "sandwich method". A test sample consists of three layers of material, each 0.1 mm thick. A hole punched in the middle layer serves as a cylindrical void. In all experiments the void diameter d_V was 6 mm. The void height h_V was 0.1 mm and the height of the sample h_S was 0.3 mm (see Figure 2.2).

2.2.2 Set-up for the time-resolved discharge measurements

The measurement set-up is shown in Figure 2.2. The electrode configuration is similar to that used by Morshuis [56]. In order to prevent an extremely high field strength at the edge of the high-voltage electrode, a field-grading electrode at earth potential has been used. The sample is placed on the top of the positive high-voltage electrode and supported by oil-impregnated paper. A small amount of oil is added on the top layer of the sample before placing the upper electrode. This guaranties an air-free contact between the electrode and the sample. A weight of 6 kg on top of the upper electrode generates a pressure of about 9 kN/m^2 on the sandwich construction, so that discharges between the sheets are prevented.

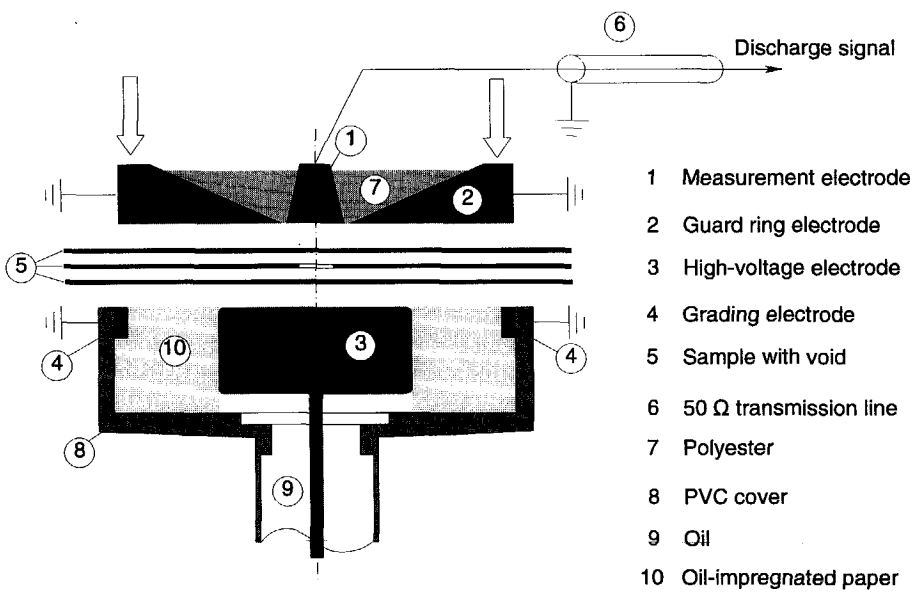

Figure 2.2 Measurement set-up.

The earthed guard ring is coaxial with the measurement electrode and acts as a coupling capacitor. The measurement impedance is formed by the wave impedance of a 50 Ω transmission line. The transmission line is connected to a digitizing oscilloscope and terminated with 50 Ω. The oscilloscope has a sampling rate of 500 Msamples/second and an analogue bandwidth of 300 MHz.

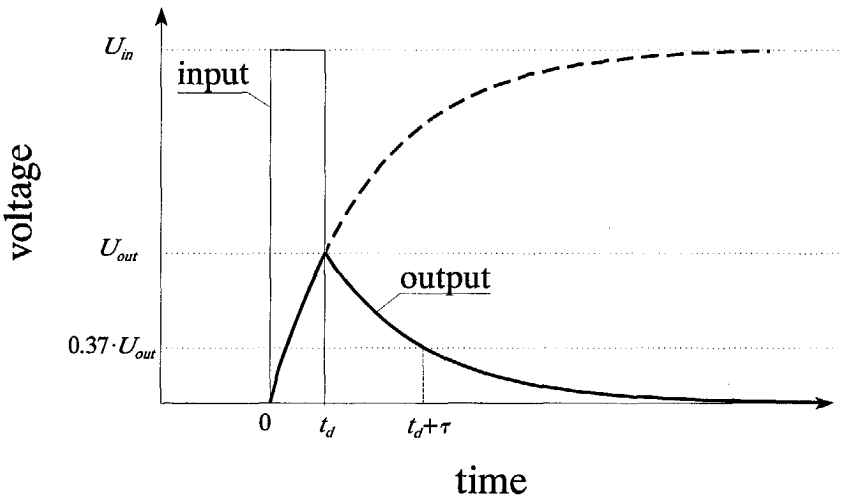

***Figure 2.3** Signal deformation due to a low-pass filter.*

The time constant of the entire system can be estimated as follows. A block impulse of the duration t_d and the amplitude U_{in} is deformed by a low-pass filter with time constant τ (see Figure 2.3). The output pulse has a smaller amplitude $U_{out} < U_{in}$ and the tail of the output pulse is determined by τ. The time constant of the entire system can be estimated to be about 20 ns, if the tail of the shortest measured pulse (e.g. Figure 3.8) is determined by the time constant of the system. The value of 20 ns is not sufficient to maintain the original shape of the discharge signal, which is specially true for streamer-like discharges. It is, however, short enough to distinguish clearly between the Townsend-like and the streamer-like discharge mechanism as described by Morshuis [56] for AC.

2.2.3 Automated registration of time-resolved discharge parameters

In order to evaluate the stochastic discharge process, an automized registration is used. Due to the limited dynamic range of the oscilloscope, the measurement is carried out for different ranges of magnitude. First, a set of data is collected at a range 0.05..0.8 mA. The number of pulses exceeding 0.8 mA is recorded in the range 0.8..3.2 mA.

In order to distinguish between discharges within the sample and discharges from outside the sample, the mean value of the recorded signal is used as a discriminator. A negative mean indicates the discharge occurrence outside the void for a positive test voltage (compare chapter 2.1.4).

For the statistical evaluation, the pulse height and the 50% pulse width of each detected discharge are registered. These data are displayed in two-dimensional and three-dimensional histograms.

2.3 Ageing tests

2.3.1 Test samples

A further aim of the study was to determine the effect of internal voids on the long term stability of epoxy resin. One problem of lifetime tests is to ensure that the breakdown takes place in the sample and not along the surface.

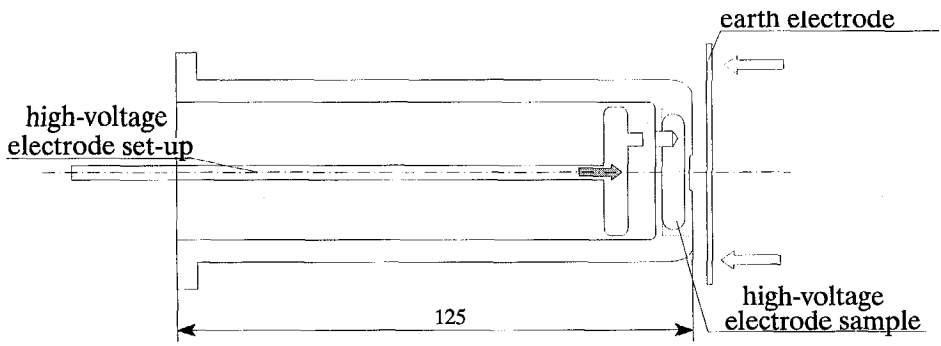

***Figure 2.4** Sample for the ageing tests.*

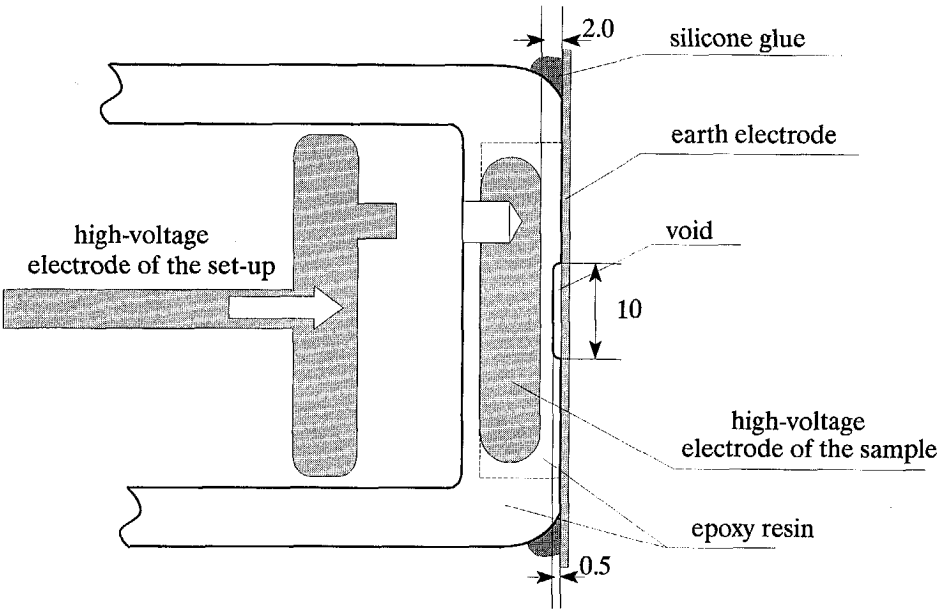

Figure 2.5 *Enlarged part of the sample in Figure 2.4.*

The design of the test sample (see Figure 2.4) is based on that of a high-voltage connector (socket) DIN 6838. The high voltage-electrode (aluminium) has been cast in epoxy (resin/harder/filler(Microdol) = 100/90/195 (massa-%)). The earth electrode (print-board) was placed on the top of the sample and glued to it with silicone paste. Thus, an electrode bounded void (void diameter d_V=10 mm, void height h_V=0.5 mm) was formed in series with 1.5 mm of epoxy resin, see Figure 2.5.

2.3.2 Set-up for the ageing tests

The test circuit, which is used is shown in Figure 2.6. The samples are placed under oil and are connected to the high voltage with a serial resistance of 1 GΩ. The resistance of the sample was measured to be larger than $5 \cdot 10^{11}\Omega$ (measured at 50 kV) so that the fault due to the series resistance of 1 GΩ is less than 1 %.

After a breakdown, the current through the sample is limited by the 1 GΩ resistance. The voltage across the 10 kΩ resistance increases then by $V_0 \times (10\text{k}\Omega/1\text{G}\Omega) \approx 0.7..1.2$ V, which is used to register the breakdown time with an *x-t* recorder. The *x-t* recorder is protected by a low-pass filter (see Figure 2.6).

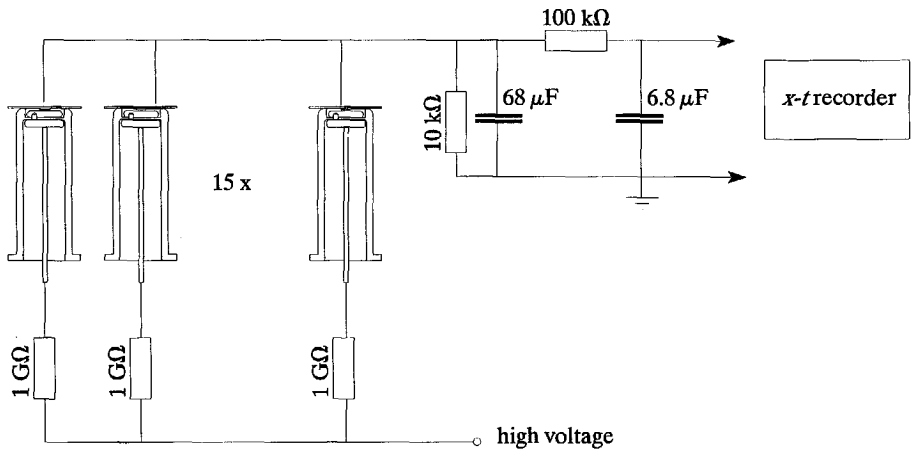

Figure 2.6 *Test circuit for the lifetime tests.*

Chapter 3

Internal discharges

Internal partial discharges occur in cavities in a solid dielectric. In general, the occurrence of partial discharges is understood as follows. The voltage across a gap increases until the breakdown voltage of the void is reached and a discharge occurs. The discharge leads to a charge build-up at the void surfaces, causing the extinction of the discharge. The residual voltage V_r remains.

In order to start a discharge two conditions must be fulfilled:

- The voltage across the void must exceed the minimal breakdown voltage V_{min}.
- A starting electron must be present. It may be supplied by external sources (e.g. radiation) or by previous discharges. Waiting for this electron causes a time lag t_L of the discharge ignition. During this time the voltage across the void further increases, so that the ignition voltage V_i exceeds the minimal breakdown voltage $V_{\min}$ by an overvoltage ΔV (see Figure 3.1, 3.2).

A discharge causes a voltage drop. In order to generate the consecutive discharge, the voltage must again exceed the minimal breakdown voltage. The time requested therefore is the recovery time t_R.

The relations between time lag t_L, discharge magnitude q and recovery time t_R are discussed in this chapter.

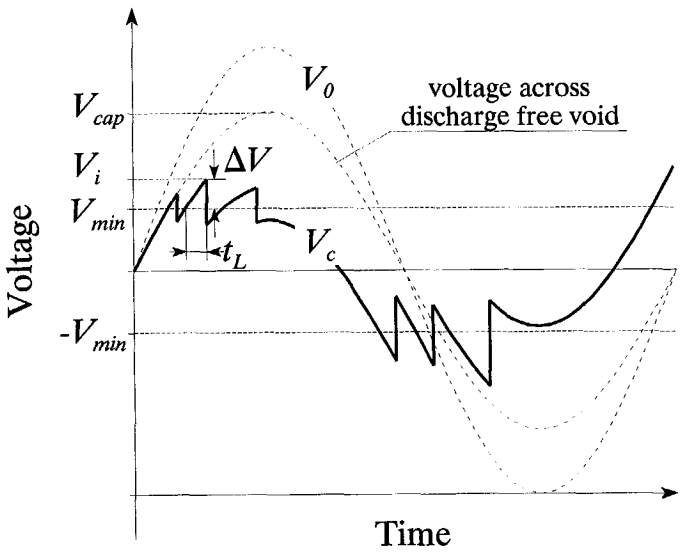

Figure 3.1 *Voltage across the void at AC.*

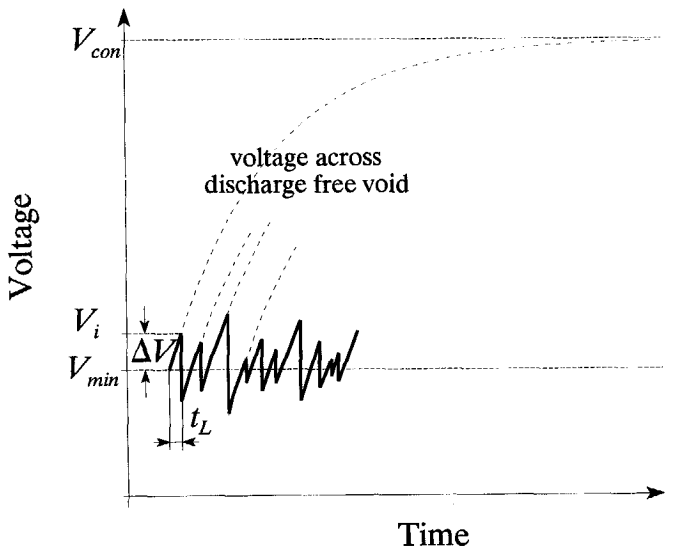

Figure 3.2 *Voltage across the void at DC.*

3.1 General aspects

For a simple but convenient description of internal partial discharges, an equivalent circuit consisting of capacitive and resistive elements is used (see Figure 3.3), where C_a and R_a represent the sample properties, C_b and R_b represent the properties of the part of the dielectric in series with the defect, C_c is the capacitance of the void and R_c is its surface resistance.

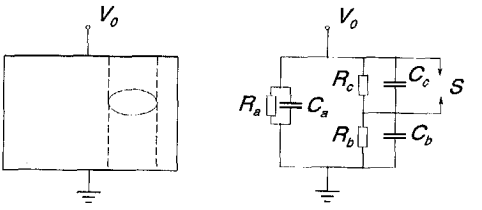

***Figure 3.3** The equivalent circuit.*

The discharge process is taken into account by a spark gap S. The equivalent circuit has as characteristic time constant τ:

$$\tau = \frac{R_b R_c (C_b + C_c)}{R_b + R_c} \tag{3.1}$$

At AC, the voltage across the void $V_c(t)$ (see Figure 3.1) can be assumed to be a capacitively divided part of the test voltage, because the time constant τ (usually 10..1000 s) exceeds the duration of a sine wave (20 ms for 50 Hz AC) by several orders.

At DC voltage (see Figure 3.2) this time constant has to be taken into account, when calculating the voltage across the void.

As mentioned above, discharges ignite with an overvoltage ΔV. The effect of the overvoltage on the discharge mechanism has been studied by Devins [12]. Two discharge mechanisms were introduced and named 'Townsend-like' and 'streamer-like'. A small overvoltage results in a Townsend-like discharge, whereas a large overvoltage leads to a streamer-like discharge. Properties of both types are given in Table 3.1. Townsend-like and streamer-like discharge mechanisms have been studied by Morshuis [56] at AC voltage. These mechanisms are studied at DC in §3.2 of this thesis.

Table 3.1 Properties of the different discharge types [12,56]

Townsend-like discharge	streamer-like discharge
• small overvoltage (a few volts) • small current amplitude • duration proportional to gap height • covers a large part of the void surface • residual voltage close to minimal breakdown voltage	• large overvoltage • large current amplitude • short duration • covers a fraction of the void surface • residual voltage close to zero

Compared to AC voltage, the discharges at DC voltage show some important differences:

I Discharges are unipolar
In contradiction to AC, the direction of the electric field does not alternate, so that all discharges have the same direction during voltage application and during the steady DC state. Only after switching off does the direction of the discharges alter.

II Supply of starting electrons
For the initial electron supply, the electron emission from the cathodic surfaces has been concluded to be dominant [60]. The occurrence of a discharge leads to a charge build-up on the void surface. This decreases the field across the void and causes the discharge to extinguish. The surface charge at the anodic surface consists of trapped electrons originated by the previous discharge. For AC voltage after field reversal, a part of the trapped electrons becomes available for electron emission. At DC voltage, the initial electrons at the cathode must be supplied by a conduction current through the bulk of the dielectric, because the discharge direction does not reverse. Therefore, the time lags for AC and DC cases are expected to be different.

III Rate of voltage rise across the void
As mentioned above, the discharge mechanism is determined by the overvoltage ΔV [12]. The overvoltage ΔV depends on the time lag t_L and on the voltage steepness dV/dt at $V(t) = V_{min}$ (see Figures 3.1, 3.2).

$$\Delta V \approx t_L \left.\frac{dV}{dt}\right|_{|V(t)=V_{min}} \tag{3.2}$$

The waveform of the voltage across the void is substantially different for AC and DC. Therefore the voltage steepness dV_{AC}/dt at AC and the voltage steepness dV_{DC}/dt at DC are discussed separately in the following sections with respect to the discharge mechanism. Further the significance of the inception voltage is discussed.

3.1.1 Voltage behaviour at AC

The test voltage V_0 exceeds the inception voltage V_{inc}, when the voltage across the void V_c exceeds the minimal breakdown voltage V_{min}, so that

$$V_{inc} = V_{min}\left(1+\frac{C_b}{C_c}\right) \quad . \tag{3.3}$$

The inception voltage is a parameter of the discharge process. The discharge frequency f_{PD} is

$$\begin{aligned} f_{PD} &= 0 && \text{for } V_0 < V_{inc} \\ f_{PD} &\geq 50 \text{ Hz} && \text{for } V_0 \geq V_{inc} \quad . \end{aligned} \tag{3.4}$$

At least one discharge occurs during each cycle at 50 Hz power frequency. Thus, the inception voltage is *clearly detectable*.

At discharge ignition, the voltage steepness is

$$\left.\frac{dV_{AC}}{dt}\right|_{|V(t_{min})=V_{min}} = \frac{d}{dt}[V_{cap}\sin(\omega t_{min})] = \omega V_{cap}\cos(\omega t_{min}) \quad . \tag{3.5}$$

The time between crossing the zero line and reaching the minimal breakdown voltage is t_{min}, so that $\omega t_{min} = \arcsin(V_{min}/V_{cap})$. Assuming $V_{cap} = k_{AC} V_{min}$, eq. (3.5) can be rewritten.

$$\left.\frac{dV_{AC}}{dt}\right|_{|V(t_{min})=V_{min}} = \omega k_{AC} V_{min}\cos\left[\arcsin\left(\frac{1}{k_{AC}}\right)\right] \tag{3.6}$$

A value $dV_{AC}/dt \approx 140$ V/ms is calculated when assuming a frequency of 50 Hz and $V_{min} = 1.44$ kV for a void of 0.2 mm height for a test voltage 5% above inception voltage ($k_{AC} = 1.05$). In order to generate Townsend-like discharges,

the overvoltage must not exceed a few tens of volts. This requires time lags of the order of 0.1 ms or less.

3.1.2 Voltage behaviour at DC

At DC, the voltage across the void is determined by the test voltage V_0 and by the characteristic time constant τ (eq. (3.1)) of the test sample.

$$V(t) = V_{con} - (V_{con} - V_r)\exp\left(-\frac{t}{\tau}\right) \tag{3.7}$$

with $V_{con} = \lim_{t\to\infty} V(t)$, if no discharge would occur (see Figure 3.2). V_{con} is determined by the resistances R_b and R_c.

$$V_{con} = V_0 \frac{R_c}{R_b + R_c} \tag{3.8}$$

The time behaviour of the voltage across the void can be described as follows. Due to a discharge, the voltage across the void drops down to the residual voltage V_r. Caused by recharging of C_c the voltage across the void will increase again. The recovery time t_R is the time between the occurrence of a discharge and reaching the minimal breakdown voltage V_{min} (Figure 3.4).

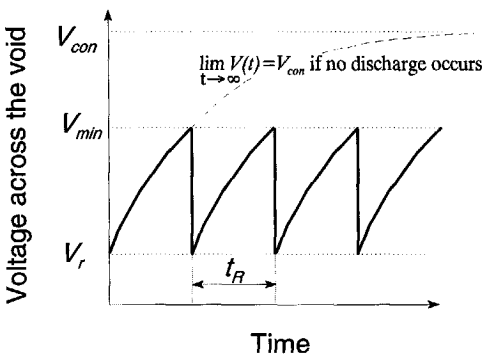

***Figure 3.4** The voltage across the void for $V_i = V_{min}$.*

$$t_R = -\tau \ln\frac{V_{con} - V_{min}}{V_{con} - V_r} \tag{3.9}$$

Assuming $V_i = V_{min}$ and defining a voltage excess $k_{DC} = V_{con}/V_{min}$ the discharge frequency f_{PD} is given by

$$f_{PD} = 0 \qquad \text{for} \quad k_{DC} \leq 1$$

$$f_{PD} = \frac{-1}{\tau \ln\left(\frac{V_{\min}(k_{DC}-1)}{k_{DC}V_{\min}-V_r}\right)} \qquad \text{for} \quad k_{DC} > 1 \tag{3.10}$$

The relation between f_{PD} and k_{DC} is shown in Figure 3.5. At discharge inception ($k_{DC}=1$) the discharge frequency is zero. According to the model, the discharge frequency increases almost linear with the voltage excess, so that the detected discharge inception voltage depends on the minimal measurable discharge frequency. This is in agreement with the experimental results of Shihab [72]. Therefore, the measured inception voltage is not a characteristic parameter of the discharge process only, but of the discharge process in combination with the smallest discharge frequency that is observed by the measuring system. As an alternative, the inception voltage is defined as that test voltage where the discharge frequency exceeds a certain value (e.g. 1 discharge/min).

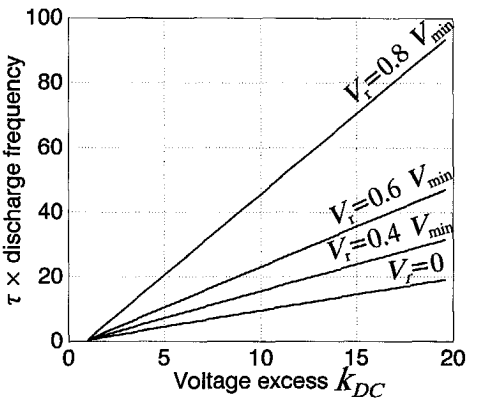

***Figure 3.5** Discharge frequency as a function of the voltage excess k_{DC} at DC voltage.*

When crossing the minimal breakdown voltage V_{min}, the voltage steepness can be estimated with eqs. (3.7) and (3.9).

$$\left.\frac{dV_{DC}}{dt}\right|_{|V(t_R)=V_{\min}} \leq (k_{DC}-1)\,\frac{V_{\min}}{\tau} \tag{3.11}$$

With $\cos[\arcsin(a)] \geq (1-a)$ for $0 \leq a \leq 1$ and with eqs. (3.11) and (3.6) for $k_{AC}=k_{DC}$ it can be stated:

$$\frac{\frac{dV_{AC}}{dt}}{\frac{dV_{DC}}{dt}} \geq \omega \times \tau \qquad (3.12)$$

$$= 3\times10^3 \ldots 3\times10^5 \text{ times} \qquad \text{for } \tau = 10 \ldots 1000\,\text{s}$$

For $k_{DC} \approx k_{AC}$ the steepness in the AC case is *several orders* larger than at DC voltage. Even if k_{DC} exceeds k_{AC} by several decades, the voltage steepness at DC is still much smaller than at AC. Therefore, for time lags comparable to those at AC, an enlarged probability of Townsend-like discharges is expected at DC voltage.

3.2 The discharge mechanism at DC voltage

Time-resolved measurements have been made on polyethylene samples (3 foils of 0.1 mm thickness each, hole of 6 mm diameter in the middle foil) with the measurement system as described in chapter 2.2. For a void height of h_V=0.1 mm the minimal breakdown voltage is V_{min}=980 V (determined with the PASCHEN curve [10]).

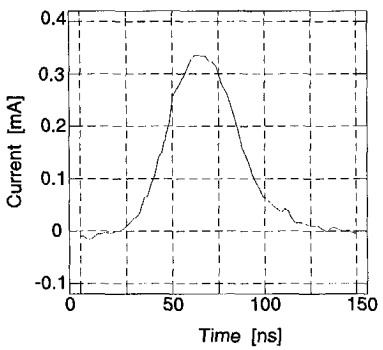

Figure 3.6
Townsend-like discharge. 50%-pulse-width ≈ 45ns pulse-height ≈ 0.35mA.

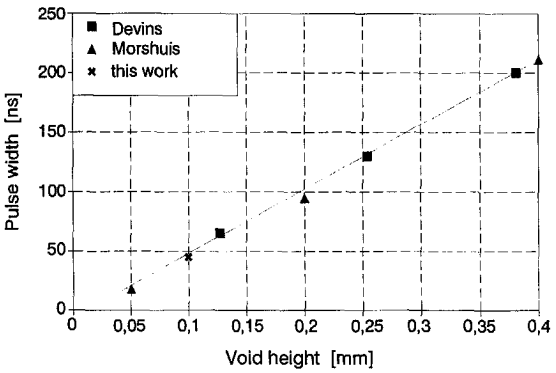

Figure 3.7 *The relation between the pulse-width and the void height for "Townsend-like" discharges measured by Devins* [12], *Morshuis* [56] *and by the author.*

Two types of pulses have been measured at DC voltage:

- The first type is characterized by a small pulse-height and a large pulse-width (Figure 3.6). Comparing the void height/pulse-width characteristic of the measured pulses with the Townsend-like pulses measured by other workers [12,56] (Figure 3.7) gives evidence of the Townsend-like character of the measured pulses. Elsewhere, this discharge type is referred to as pseudo-glow type [2] or pulseless type [38].
- The second type is shown in Figure 3.8. The characteristic short duration and large pulse-height indicates the streamer-like type. The discharges sometimes ignite in groups with a very short time period between consecutive discharges. An example is shown in Figure 3.9.

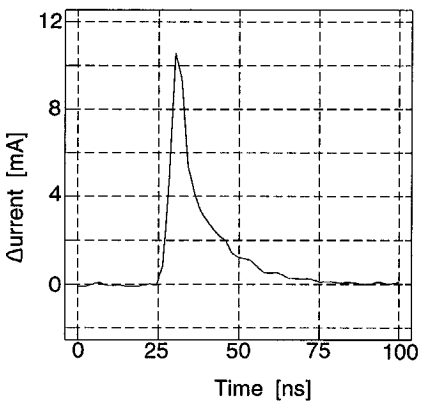

Figure 3.8 streamer-like discharge. 50% pulse-width ≈ 10 ns pulse-height ≈ 10 mA.

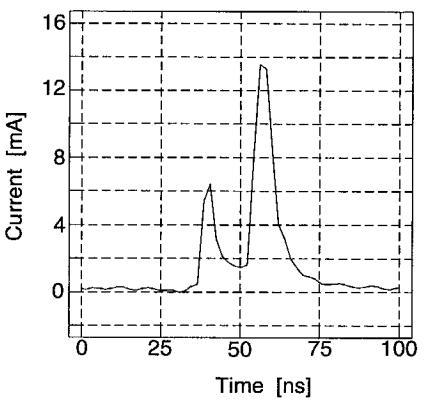

Figure 3.9 Two consecutive streamer-like discharges.

To recognize the the discharge mechanism, the measured data are displayed in two-dimensional and three-dimensional density histograms (see Figure 3.10-3.16). In all these figures the density is the number of discharges per window divided by the sum of all discharges.

3.2.1 Effect of the test voltage

(a) 10 kV test voltage

The measured density as a function of the pulse-height and the pulse-width are shown in Figure 3.10. The average pulse-width is about 40 ns. This is characteristic for Townsend-like discharges in a void of this height (compare

with Figure 3.7). The results are in agreement with the considerations above, that a (compared to AC) small voltage steepness at discharge ignition causes a small overvoltage ΔV, which results in the occurrence of Townsend-like discharges.

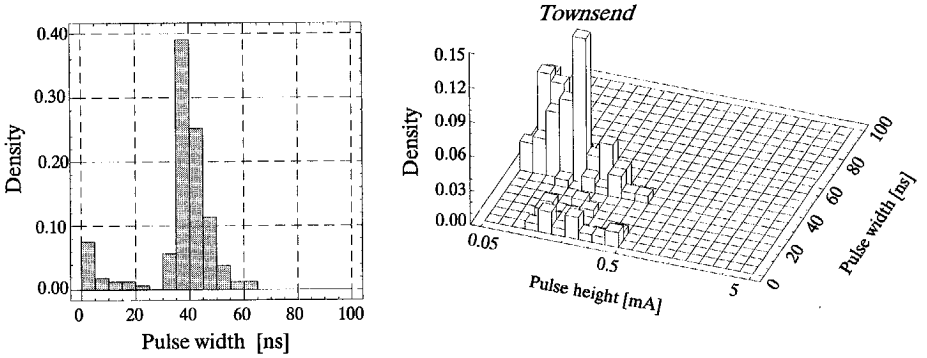

Figure 3.10 *Pulse-width and pulse-height distribution for discharges measured for PE at V_0=10 kV (d_V=6mm, h_S=0.3mm, h_V=0.1mm).*

(b) 15 kV test voltage

The measured density as a function of the pulse-height and the pulse-width are shown in Figure 3.11. A second peak becomes noticeable in the pulse-width histogram, caused by streamer-like discharges. These streamer-like discharges have a small pulse-width and a larger pulse-height than the Townsend-like discharges, as shown in the three dimensional histogram in Figure 3.11.

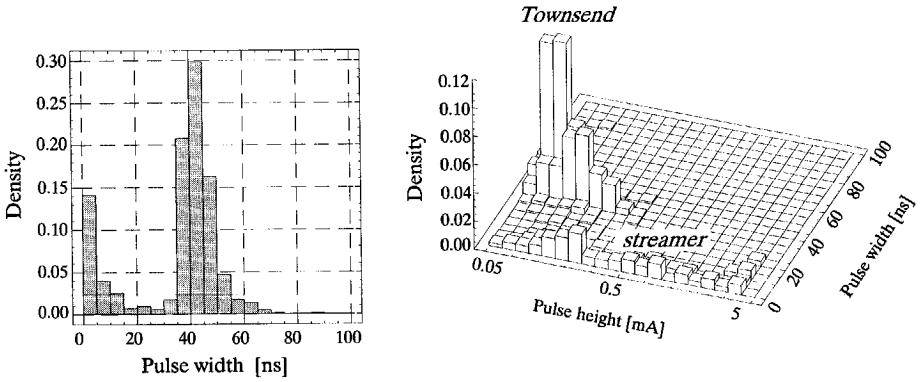

Figure 3.11 *Pulse-width and pulse-height distribution for discharges measured for PE at V_0=15 kV (d_V=6mm, h_S=0.3mm, h_V=0.1mm).*

This behaviour can be explained as follows: A larger test voltage leads to a faster voltage increase so that the overvoltage ΔV caused by a time lag is larger. A larger overvoltage results in an enhanced probability of streamer-like discharges.

(c) 20 kV test voltage

The measured density as a function of the pulse-height and the pulse-width are shown in Figure 3.12. The peak in the pulse-width histogram caused by the streamer-like discharges has increased. This behaviour is explained by a larger voltage increase across the void, so that the time lag causes larger overvoltages that enhance the probability of streamer-like discharges. The location of different areas for Townsend-like discharges and streamer-like discharges in the pulse-width-pulse-height surface can be clearly recognised in the three dimensional histogram of Figure 3.12.

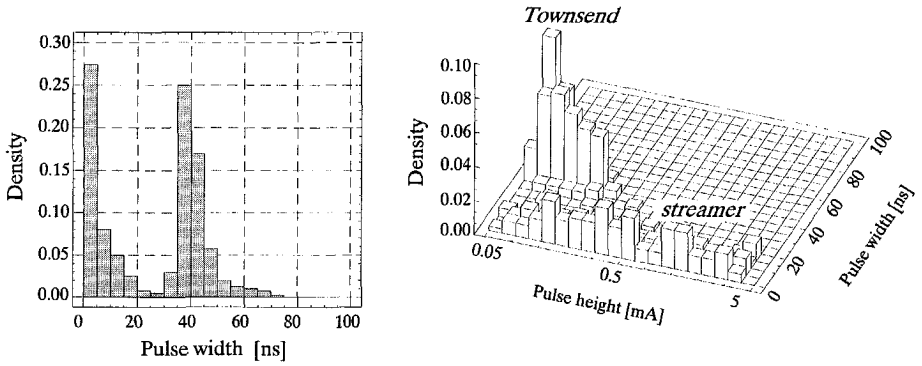

Figure 3.12 *Pulse-width and pulse-height distribution for discharges measured for PE at V_0=20 kV (d_V=6mm, h_S=0.3mm, h_V=0.1mm).*

3.2.2 Effect of the stress duration

At AC voltage, a transition from streamer-like discharges to Townsend-like discharges at prolonged stress duration was observed by Morshuis [54]. In order to check whether there is such a transition at DC as well, measurements were made. Therefore the test at 20 kV was prolonged for 25 h. The measured density as a function of the pulse-height and the pulse-width after 25 h are

shown in Figure 3.13. Clearly visible is the decrease of the density of the streamer-like discharges. A transition from the streamer-like discharge mechanism to the Townsend-like discharges has actually occurred.

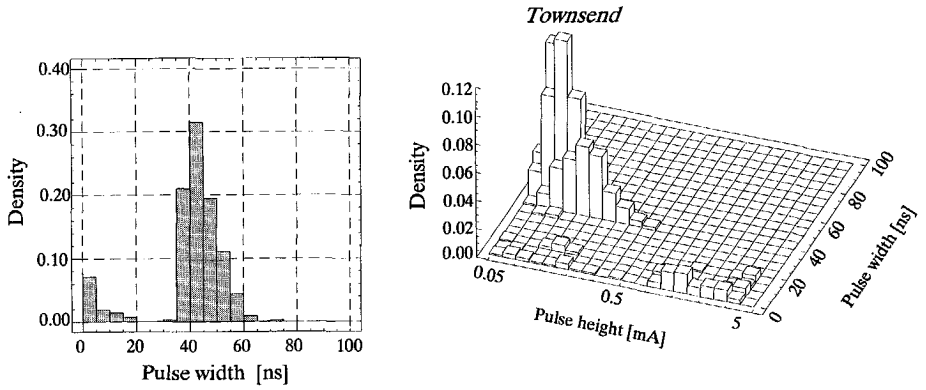

Figure 3.13 *Pulse-width and pulse-height distribution for discharges measured for PE at V_0=20 kV after 24 hours voltage stress (d_V=6mm, h_S=0.3mm, h_V=0.1mm).*

3.2.3 Effect of the insulating material

Time resolved measurements were made for different materials (two types of polycarbonate and cellulose-3-atcetat) at a test voltage of 20 kV. The measured pulse-width histograms are shown in Figure 3.14, 3.15, 3.16. In spite of the large differences in the discharge frequency (due to different values of τ), the pulse-width histograms are similar. The occurrence of both Townsend-like discharges (peak at about 40 ns) and streamer-like discharges (peak for pulse-width <5 ns) is observed. The largest repetition rate is observed for Townsend-like discharges.

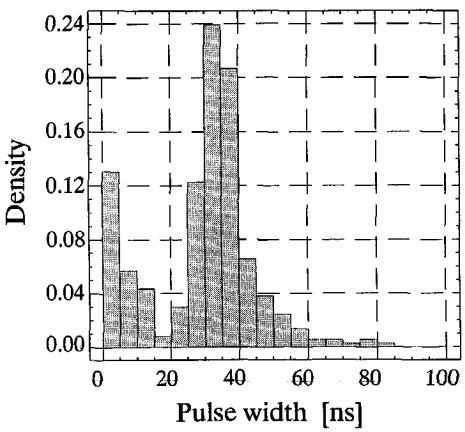

Figure 3.14 *Pulse-width distribution for discharges measured at polycarbonate (type 1) at V_0=20 kV (d_V=6mm, h_S=0.3mm, h_V=0.1mm, f_{PD}=1.8min^{-1}).*

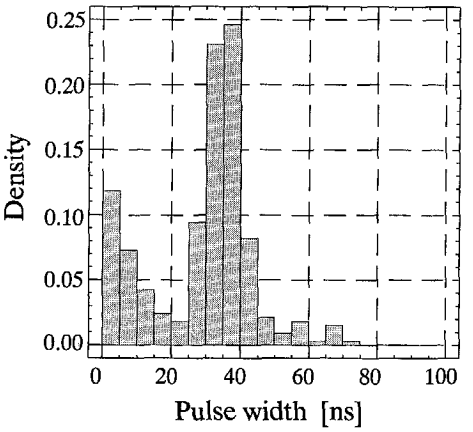

Figure 3.15 *Pulse-width distribution for discharges measured at polycarbonate (type 2) at* $V_0=20\ kV$ ($d_V=6mm$, $h_S=0.3mm$, $h_V=0.1mm$, $f_{PD}=1min^{-1}$).

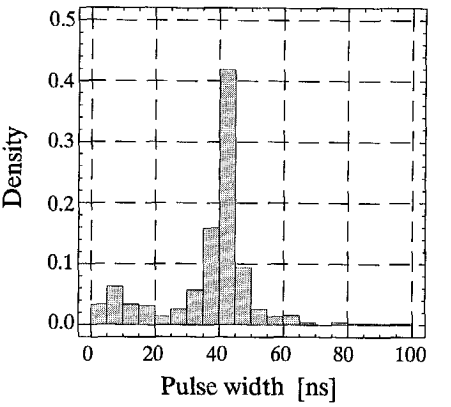

Figure 3.16 *Pulse-width distribution for discharges measured at cellulose-3-atcetat at* $V_0=20\ kV$ ($d_V=6mm$, $h_S=0.3mm$, $h_V=0.1mm$, $f_{PD}>45min^{-1}$).

3.2.4 Conclusions

At DC voltage, both the Townsend-like and the streamer-like discharge mechanism can be observed. For discharges in small voids (void height of the order of 0.1 mm) and moderate stresses, the Townsend-like discharge mechanism has appeared to be dominant. An increased field strength leads to an increased probability of streamer-like discharges. Only at a very high mean field strength in the test object (>50 kV/mm) might streamer-like discharges become dominant. For these cases, a transition from streamer-like to Townsend-like discharges after prolonged stress duration takes place, similar to the behaviour at AC voltage. At AC voltage, the transition from the streamer-like to the Townsend-like mechanism is caused by the creation of a layer of oxidation products [56]. Such a layer has been reported by Shihab [72] for DC voltage as well, after a sufficient test duration.

There may be two possible explanations for observed transition from streamer-like to Townsend-like discharges:

1. Assuming that the starting electron supply is mainly determined by surface emission [60], the surface condition is very important. The creation of a layer of oxidation products leads to an increased supply of start electrons. This leads to a decrease of the statistical time lag and a decrease of the

overvoltage, which results in a transition from streamer-like to Townsend-like discharges.

2. An increased conductivity of the void surface leads to a decreased R_c in the *abc* model (Figure 3.3). This causes a decrease of V_{con} (eq. (3.8)) leading to a decrease of $k_{DC}=V_{con}/V_{min}$. This leads to a decreased voltage steepness (eq. (3.11)) so that at a constant time lag t_L, the overvoltage ΔV would decrease (eq. (3.2)), which would explain the transition from the streamer-like to the Townsend-like discharge mechanism.

3.3 The statistical discharge behaviour

3.3.1 Model

After a discharge occurring at t_0, the recovery time t_R is required to reach the minimal breakdown voltage V_{min} (see Figure 3.17), so that

$$V_{\min}=V(t_0+t_R)=V_{con}-(V_{con}-V_r)\exp\left(-\frac{t_R}{\tau}\right) \quad . \tag{3.13}$$

As has been noted, the ignition voltage V_i exceeds the minimal breakdown voltage V_{min} by ΔV, due to the time lag t_L necessary for the supply of a starting electron, so that

$$V_i = V_{\min}+\Delta V = V_{con}-(V_{con}-V_r)\exp\left(-\frac{t_R+t_L}{\tau}\right) \quad , \tag{3.14}$$

where t_R is the recovery time after extinction of the previous discharge.

The supply of starting electrons is a stochastic process. Therefore, each discharge gets a different time lag. The time lag determines the overvoltage of a particular discharge. The overvoltage at which a discharge ignites determines the discharge magnitude as has been studied by Devins [12]. The discharge leads to a voltage drop across the void which causes the recovery time. In other words, time lag t_L, recovery time t_R, overvoltage ΔV and residual voltage V_r are

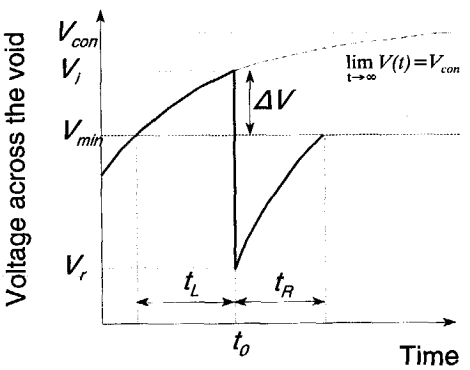

***Figure 3.17** The voltage across the void.*

mutually related. This relation is further examined below.

Assumptions

(a) *The dominant discharge mechanism is Townsend-like*
This is realistic as has been shown in section 3.2.

(b) *The entire void is discharging*
As shown in [56], such an assumption is realistic for Townsend-like discharges.

(c) *The discharge magnitude is a function of the time lag*
As has been shown by Devins [12] for Townsend-like discharges, the discharge magnitude is a function of the overvoltage. The *abc* model provides a functional relation between time lag t_L and the overvoltage ΔV, so that the discharge magnitude is concluded to be a function of the time lag.

$$q=F_1(t_L) \quad \text{or} \quad t_L=F_1^*(q) \quad . \tag{3.15}$$

(d) *The recovery time is a function of the discharge magnitude*
The *abc*-model (Figure 3.3) provides the recovery time t_R as a function of the residual voltage V_r (see eq. (3.9)). For Townsend-like discharges Morshuis [56] has shown that the residual voltage V_r is a function of the overvoltage ΔV. As has been noted, the overvoltage determines the discharge magnitude. Therefore the recovery time is concluded to be a function of the discharge magnitude

$$t_R=F_2(q) \quad . \tag{3.16}$$

(e) *The magnitude of a discharge is independent of its predecessor*
This is experimentally be verified in section 3.3.2. The independence means that a discharge does not 'remember' the magnitude of the previous discharge and does not influence the successive discharge. The discharge magnitude is related to the time lag (see eq. (3.15)). Therefore, the mean time lag of the successors of n arbitrarily chosen elements of a set of discharges is equal to the mean time lag of all discharges if n is large.

$$\frac{1}{n}\sum_{i=1}^{n} t_{L,suc(i)} = \overline{t_L} \tag{3.17}$$

Similarly, the mean recovery time of the predecessor of n arbitrarily chosen

elements of a set of discharges is equal to the mean recovery time of all discharges.

$$\frac{1}{n}\sum_{i=1}^{n} t_{R,pre(i)} = \overline{t_R} \tag{3.18}$$

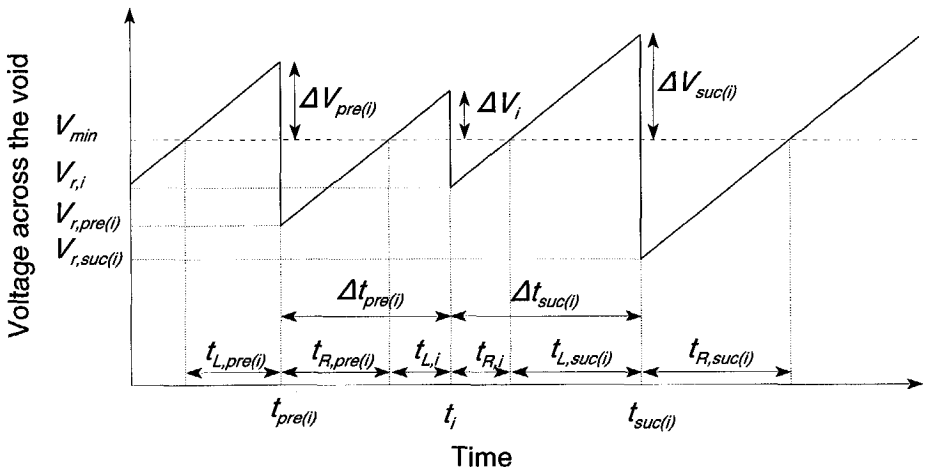

Figure 3.18 *The voltage across the void for successive discharges.*

Evaluation of time lag t_L and recovery time t_R

The time to the *previous* discharge is the sum of the time lag (which determines the discharge magnitude) and the recovery time of the previous discharge (Figure 3.18).

$$\Delta t_{pre(i)} = t_{R,pre(i)} + t_{L,i} \tag{3.19}$$

Similarly, the time to the *successive* discharge is the sum of the recovery time (determined by the discharge magnitude) and the time lag of the successive discharge.

$$\Delta t_{suc(i)} = t_{R,i} + t_{L,suc(i)} \tag{3.20}$$

Equations (3.19) and (3.20) can be used for the evaluation of time lag and recovery time. Let us consider n discharges. From eq. (3.19) the mean time to

the previous discharge is

$$\overline{\Delta t_{pre}} = \frac{1}{n}\sum_{i=1}^{n}(t_{R,pre(i)}+t_{L,i}) \quad . \tag{3.21}$$

Let us further assume that all n discharges are of the same discharge magnitude q. Then eq. (3.15) leads to $t_{L,i}=t_L(q)$, so that eq. (3.21) can be rewritten as

$$\overline{\Delta t_{pre}}(q) = t_L(q)+\frac{1}{n}\sum_{i=1}^{n} t_{R,pre(i)} \quad . \tag{3.22}$$

Eqs.(3.22) and (3.18) lead to

$$\overline{\Delta t_{pre}}(q) = t_L(q) + \overline{t_R} \quad . \tag{3.23}$$

The time to the successor is, analogously,

$$\overline{\Delta t_{suc}}(q) = t_R(q) + \overline{t_L} \quad . \tag{3.24}$$

Consequently, the model predicts a *mean time interval* between discharges that is different for *previous* and *successive* discharges.

In order to verify the model, the measured discharge data set is divided into sub-sets with a constant discharge magnitude. The mean time to the successor and to the predecessor can be evaluated for each discharge magnitude. The calculated values are plotted in a q-$\overline{\Delta t}_{suc}$-diagram and a q-$\overline{\Delta t}_{pre}$-diagram. If the two diagrams show a continuous relation between the discharge magnitude and the mean time to the successor, and a continuous relation between discharge magnitude and the mean time to the predecessor, the model as developed above is valid.

Further, the times $\overline{\Delta t}_{pre}(q=0)$ and $\overline{\Delta t}_{suc}(q=0)$ can be extrapolated to the zero line (Figure 3.22 and 3.23). According to eqs. (3.23) and (3.24)

$$\overline{\Delta t_{pre}}(q=0) = \overline{t_R} \tag{3.25}$$

$$\overline{\Delta t_{suc}}(q=0) = \overline{t_L} \quad , \tag{3.26}$$

because according to the model, $t_L \to 0$ and $t_R \to 0$ for $q \to 0$.

The mean time lag $\overline{t}_L$ and the mean recovery time $\overline{t}_R$ can be determined in this way.

3.3.2 Experimental

Test conditions

Measurements have been made on sandwich- type samples (3 PE foils, each 0.1 mm thick; the middle foil has a 6 mm diameter hole). The electrode system is shown in Figure 2.2. For the measurement of the statistical behaviour, the classic measurement system as shown in Figure 2.1 has been used. The sensitivity limit was 1.5 pC.

Time behaviour

After voltage application, the discharge frequency decreases until a stable state is reached (Figure 3.19). This is caused by the leakage current through the sample. A large current (short after voltage appli-cation) leads to a quick recharging of C_c in the equivalent circuit (Fig-ure 3.3), causing a larger discharge frequency than the lower current after reaching the stable state. The close relation between discharge frequency and current through the sample has been experimentally verified by Shihab [72].

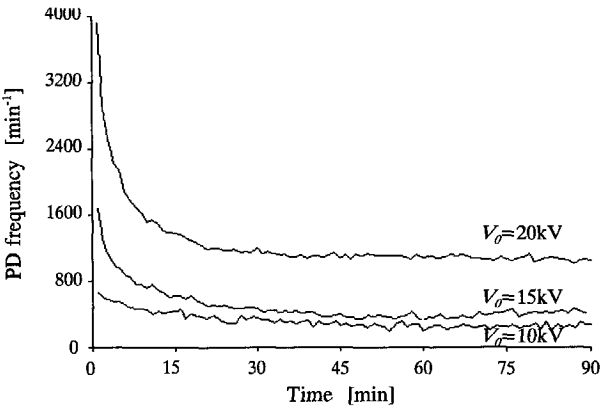

Figure 3.19 *The discharge frequency as a function of time at V_0=10kV, 15kV, 20kV (d_V=6mm, h_S=0.6mm, h_V=0.2mm).*

Distribution of the discharge magnitude

The measured density func tion of the discharge magnitude at 20 kV is shown in Fig-ure 3.20. In agreement with the results of other workers, [12,72] the density is maximal for the smallest measured dis-

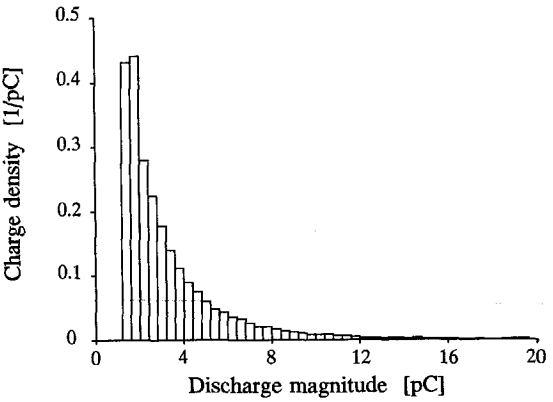

Figure 3.20 *The density function of the discharge magnitude (d_V=6mm, h_S=0.3mm, h_V=0.1mm, V_0=20kV). mean discharge magnitude: 4.1 pC.*

charges.

Independence of the successive discharges

In order to check the independence of successive discharges, the mean magnitude value of the discharges, which succeed the discharges of a constant magnitude has been derived from the measured data. The results are shown in Figure 3.21. The mean discharge magnitude of the successive discharge does not depend on the discharge magnitude of the predecessor and it is equal to the mean value of all discharges (compare to Figure 3.20). This supports the assumption **(e)**.

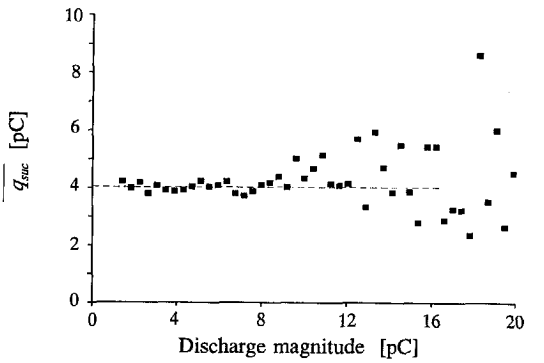

Figure 3.21 *The mean magnitude of the successor as a function of the discharge magnitude (d_V=6mm, h_S=0.3mm, h_V=0.1mm, V_0=20kV).*

Time lag, recovery time

The mean times to the predecessor and to the successor at different discharge magnitudes are shown in Figures 3.22 and 3.23, respectively. For small discharge magnitudes, there is an almost linear relationship between q and $\overline{\Delta t}_{suc}$ and $\overline{\Delta t}_{pre}$. This result confirms the proposed model. Consequently, for small discharges, the assumptions made in the beginning are realistic. Using linear extrapolation, the values $\overline{\Delta t}_{suc}(q=0)$ and $\overline{\Delta t}_{pre}(q=0)$ can be determined (Figures 3.22 and 3.23).

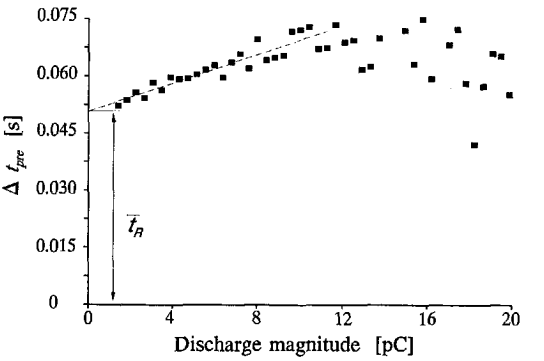

Figure 3.22 *The time to the previous discharge as a function of the discharge magnitude (d_V=6mm, h_S=0.3mm, h_V=0.1mm, V_0=20kV).*

According to eqs. (3.25) and (3.26) the mean time lag and the mean recovery time appear to be $\overline{t}_R \approx 50$ ms $\overline{t}_L \approx 45$ ms for this particular sample. Because of the limited measurement sensitivity, the measured average time distances between the discharges exceed the real values. Therefore, the evaluated values for $\overline{t}_R$ and $\overline{t}_L$ are upper limits. For large discharge magnitudes in Figures 3.22 and 3.23, a rather large scatter is observed. The reasons therefore might be as follows.

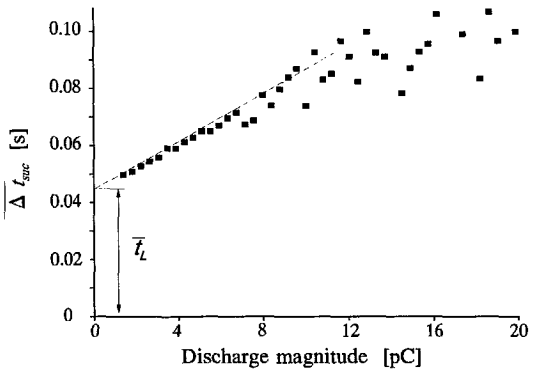

Figure 3.23 *The time to the successive discharge as a function of the discharge magnitude (d_V=6mm, h_S=0.3mm, h_V=0.1mm, V_0=20kV).*

1. The small density for large discharge magnitude leads to a small number of events per charge interval (Figure 3.20). The calculation of a mean value of a few events only leads to a larger scatter.
2. The time-resolved discharge measurements have shown that streamer-like discharges have a larger magnitude than Townsend-like discharges. The model is based on discharging of the complete void surface, which is approximately true for Townsend-like discharges, but not for streamer-like discharges [56].

Effect of the test voltage

(a) Observations

Measurements as described above have been carried out at different test voltages. All tests have been performed using the same sample. The tests at lower voltages were made first. The measurement durations were 2 h at 10 kV and 15 kV, 1 h at 20 kV and 25 kV, and 0.5 h at 30 kV.

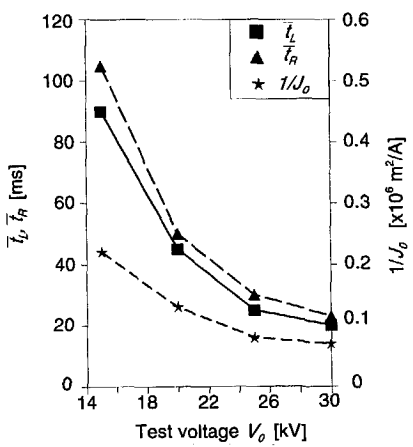

Figure 3.24 *The mean time lag, the mean recovery time and the reciprocal of the current density as functions of the test voltage (d_V=6 mm, h_S=0.3 mm, h_V=0.1 mm).*

The time lag and the recovery time are

determined by the method described above. The median of the magnitude distribution has been used as a measure of the discharge magnitude. Additionally, the current density in 0.2 mm thick foils (as thick as that the void containing material) has been measured. The results are shown in Figures 3.24 and 3.25. Based on these results the following is concluded.

1. The values of the time lag and the recovery time decrease with increasing test voltage (Figure 3.24) as may be expected.
2. The median of the discharge magnitude is not much affected by an increasing test voltage (Figure 3.25), which is in agreement with the results reported elsewhere [72]. Because the discharge magnitude is determined by the overvoltage, it must be concluded that the overvoltage ΔV is not greatly affected by a change of the test voltage.

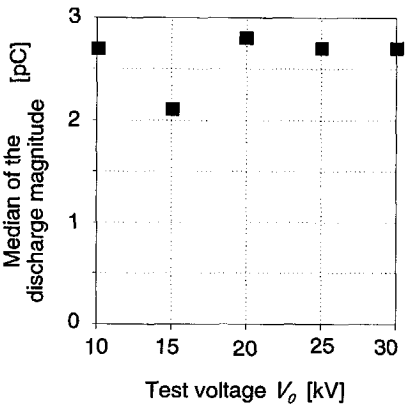

Figure 3.25 *The median of the discharge magnitude as function of the test voltage. (d_V=6 mm, h_S=0.3 mm, h_V=0.1 mm).*

Based on these observations the overvoltage ΔV and the voltage drop caused by the discharge are calculated in the following. Further the relation between the discharge frequency and the conduction current and the influence of a ripple on the test voltage are discussed.

(b) Calculation of the overvoltage ΔV

Assuming discharges of a constant discharge magnitude, eq. (3.13) and eq. (3.14) lead to

$$\Delta V = V_i - V_{\min} = -(V_{con} - V_r)\left[\exp\left(-\frac{t_L + t_R}{\tau}\right) - \exp\left(-\frac{t_R}{\tau}\right)\right] \quad . \tag{3.27}$$

The time constant τ is in the order of 30 ... 50 s, so that $(t_L + t_R) << \tau$

$$\begin{aligned}\Delta V &= -(V_{con}-V_r)\left[\left(1-\frac{t_L+t_R}{\tau}\right)-\left(1-\frac{t_R}{\tau}\right)\right] \\ &= (V_{con}-V_r)\frac{t_L}{\tau} \\ &\leq V_{con}\frac{t_L}{\tau} \quad .\end{aligned} \tag{3.28}$$

Substituting eq. (3.1) and eq. (3.8) into eq. (3.28) we obtain

$$t_L \geq \Delta V \frac{R_b(C_b+C_c)}{V_0} \tag{3.29}$$

The resistances R_b and R_a are made out of the same material, so that

$$\rho = R_b\frac{A_V}{h_S-h_V} = R_a\frac{A_S-A_V}{h_S} \quad , \tag{3.30}$$

where ρ is the resistivity of the dielectric material, A_V is the cross-section of the void, A_S is the cross-section of the sample, h_V is the height of the void, and h_S is the height of the sample. For a large field strength, the resistivity of the sample may not be constant. Then eq. (3.30) must be restricted to the cases where the field in R_b is approximately as large as the field in R_c. That requires

$$h_V \ll h_S \quad . \tag{3.31}$$

With eqs. (3.30) and (3.31), eq. (3.29) leads to

$$\frac{J_0\, A_V\, t_L}{C_b+C_c} \geq \Delta V \quad , \tag{3.32}$$

where $J_0 = V_0/[R_a(A_S-A_V)]$.

In order to calculate the overvoltage, current measurements have been made. Because the void dimensions could not be neglected for the measured samples, the current density J_0 has been determined by measuring the current through a PE layer as thick as the dielectric surrounding the void (0.2 mm). The overvoltage ΔV for an average discharge has been calculated with eq. (3.32).

With a measured $J_0=7.8\times10^{-6}$ A/m^2, $A=\pi 9$mm^2 and $t_L=45$ ms at $V_0=20$ kV and the calculated capacitances $(C_b+C_c)\approx 6$ pF, the overvoltage is calculated to be $\Delta V\leq 1.6$ V.

For large test voltages ($V_{con}\gg V_r$) eq. (3.32) can be rewritten (compare eq. (3.28)) as

$$t_L\approx\frac{1}{J_0}\frac{\Delta V(C_b+C_c)}{A_V} \quad , \tag{3.32}$$

whereas for lower voltages,

$$t_L\geq\frac{1}{J_0}\frac{\Delta V(C_b+C_c)}{A_V} \quad . \tag{3.33}$$

Considering ΔV to be almost independent of the test voltage, t_L must decrease more with increasing test voltage than $1/J_0$. The measured results (Figure 3.24) are in agreement with such a prediction.

(c) Calculation of voltage drop V_{min}-V_r

The voltage drop due to an average discharge can be calculated using eq. (3.14):

$$\begin{aligned} V_i-V_r &= V_{con}-V_r-(V_{con}-V_r)\exp\left(-\frac{t_R+t_L}{\tau}\right) \\ &= (V_{con}-V_r)\left[1-\exp\left(-\frac{t_R+t_L}{\tau}\right)\right] \quad , \end{aligned} \tag{3.34}$$

where t_R is the recovery time of the previous discharge and t_L is the time lag of the current discharge. The time constant τ is of the order of 30 ...50 s, so that $(t_L+t_R)<<\tau$. Eq. (3.34) can be rewritten.

$$\begin{aligned} V_i-V_r &= (V_{con}-V_r)\left[1-\left(1-\frac{t_R+t_L}{\tau}\right)\right] \\ &= (V_{con}-V_r)\ \frac{t_R+t_L}{\tau} \\ &\leq V_{con}\ \frac{t_R+t_L}{\tau} \end{aligned} \tag{3.35}$$

Inserting eqs. (3.1) and (3.8) into eq. (3.35) we obtain

$$V_i - V_r \leq V_0 \frac{t_R + t_L}{R_b(C_b + C_c)} \tag{3.36}$$

With eqs. (3.30) and (3.31), eq. (3.36) leads to

$$V_i - V_r \leq J_0 \frac{(t_R + t_L)A_V}{C_b + C_c} \tag{3.37}$$

With $J_0 = 7.8 \times 10^{-6}$ A/m^2, $t_L + t_R = 95$ ms at $V_0 = 20$ kV and the calculated capacitances $(C_b + C_c) \approx 6$ pF, the voltage drop is calculated to be $V_i - V_r \leq 3.5$ V. This value is small compared to the minimal breakdown voltage $V_{min} = 980$ V (determined with the Paschen curve [10]), so that the residual voltage is almost equal to the ignition voltage and the voltage across the void describes an extremely small zig-zag. This is noteworthy since in the literature the residual voltage is often taken to be zero. Furthermore, the small voltage drop is an indication that the discharges are Townsend-like discharges [56].

With eq. (3.40) and with $f_{PD} = 1/(t_L + t_R)$, eq. (3.37) leads to

$$f_{PD}\, q\, \frac{(C_b + C_c)^2}{A_V\, C_b\, C_c} \leq J_0 \quad , \tag{3.38}$$

whereas for large test voltages (compare eq. (3.34)), it can be written as

$$f_{PD}\, q\, \frac{(C_b + C_c)^2}{A_V\, C_b\, C_c} \approx J_0 \quad . \tag{3.39}$$

Considering q to be almost independent of the test voltage, f_{PD} must increase more with increasing test voltage than J_0. This is in agreement with the measurements presented here (Figure 3.26) and with previous measurements by Watanabe [80].

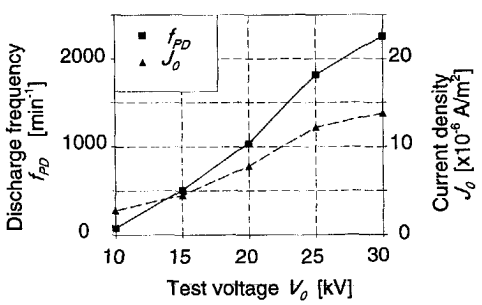

Figure 3.26 *The current density and the discharge frequency as functions of the test voltage ($d_V = 6$ mm, $h_S = 0.3$ mm, $h_V = 0.1$ mm).*

(d) Calculation of the discharge magnitude
The measurable discharge magnitude is

$$q_m = (V_i - V_r)\frac{C_b C_c}{C_b + C_c} \quad . \tag{3.40}$$

With V_i-V_r=3.5 V and C_b=C_c=3 pF, the discharge magnitude is q=5.2 pC. This value is within the measured range of the discharge magnitude (Figure 3.20) and confirms the proposed approach.

(e) Influence of voltage ripple
The measured Δt-density functions show a superposed oscillation, as shown in Figure 3.27 for a test voltage of 20 kV. This oscillation is a result of the 50 Hz voltage ripple and can be explained as follows.

The voltage across the cavity changes between the ignition voltage and the residual voltage. As has been shown, the difference between V_i and V_r is only a few volts. The voltage ripple is capacitively divided, i.e. in the case of the test samples, about half the ripple appears across the cavity.

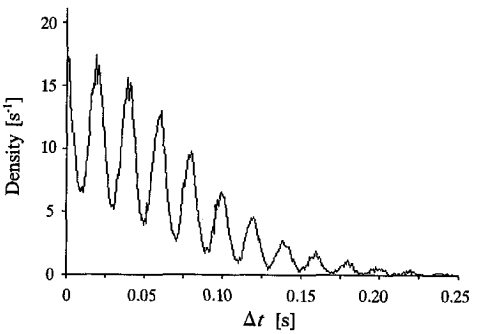

***Figure 3.27** Density function of the time separations between successive discharges (d_V=6 mm, h_S=0.3 mm, h_V=0.1 mm, V_0=20 kV).*

The occurrence of a discharge requires an ignition voltage V_i above the minimal breakdown voltage V_{min}. The ripple on the test voltage leads to a decreased discharge probability at the bottom of the ripple because the voltage across the void may not reach the minimal breakdown voltage V_{min}.

Further the discharge magnitude depends strongly on the overvoltage at which the discharge ignites [12]. Therefore discharges occurring at the top of the ripple are larger than discharges occurring between the tops, which may lead to enhanced detected density of discharges at the top of the ripple.

In the tested case, the 50 Hz voltage ripple (1.5 V at V_0=10 kV) is on the same order as the voltage difference between V_i and V_r, which explains the large influence on the occurrence of discharges. In actual industrial equipment this

capacitive voltage division is far smaller and the effect of the ripple will be far less.

3.4 Conclusions

Concerning the behaviour of internal discharges at DC voltage, the following conclusions are drawn:

1. There is no clearly detectable discharge inception voltage. As an alternative, an inception voltage can be defined as the voltage at which the discharge frequency exceeds a certain value (e.g. 1/min).

2. Compared to AC voltage, the probability of Townsend-like discharges at DC is enlarged. This is caused by the different voltage behaviour across the void.

3. The statistical discharge behaviour has been investigated. The following is concluded:
   - A discharge does not affect the magnitude of its successor.
   - An increased time to the predecessor Δt_{pre} causes an increased discharge magnitude.
   - An increased discharge magnitude causes an increased time to the successor Δt_{suc}.
   - The mean time lag and the mean recovery time can be derived from the graphs $\overline{\Delta t}_{suc}=f_1(q)$ and $\overline{\Delta t}_{pre}=f_2(q)$.

Chapter 4

Partial discharges in air

Corona and surface discharges are typical discharges in air. The purpose of this chapter is to characterise corona and surface discharges by using statistical means. This can help later on to recognize these defects in industrial components.

4.1 General time lag - recovery time model

For the general description of the statistical behaviour of partial discharges, a similar model is used as that introduced for internal discharges in §3.3.1. In order to cause a discharge two conditions must be fulfilled:
1. Field strength: In order to cause breakdown the electric field must exceed the minimal breakdown field strength E_{min}.
2. A starting electron must be present. Waiting for this electron causes a time lag t_L of the discharge ignition.

The occurrence of a partial discharge causes the generation of a space charge or a surface charge near the discharge location. This leads to a drop in the field strength, so that the discharge extinguishes. In order to cause the next discharge, the field must again exceed the minimal breakdown field strength E_{min} The field increases which is caused by the decay of the charge accumulated near the discharge location. A recovery time t_R is required in order to reach E_{min} again.

In general, the minimal breakdown field strength E_{min} cannot assumed to be a constant. The ionization coefficient can be influenced by metastable species generated by previous discharges [6], so that temporary variations of E_{min} are possible as will be shown for corona later on.

For the statistical studies, the following symbols are used. The discharge occurring at t_i has a time lag $t_{L,i}$ and affects the recovery time $t_{R,i}$ (see Figure 4.1). The predecessor of the discharge at t_i occurred at $t_{pre(i)}$, the successor occurs at $t_{suc(i)}$. The time between the discharge at t_i and its predecessor is $\Delta t_{pre(i)}$. The time between the discharge at t_i and its successor is $\Delta t_{suc(i)}$.

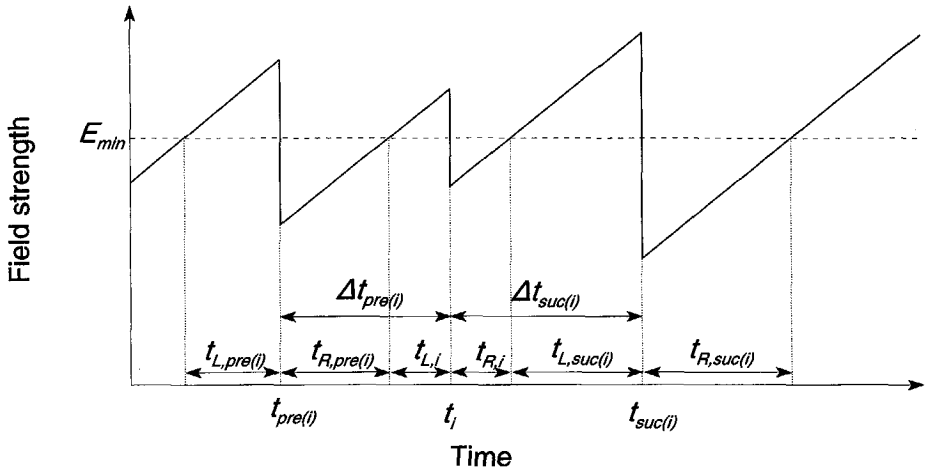

Figure 4.1 *The relationship between the time lag t_L, the recovery time t_R and the time to the previous and successive discharge.*

4.2 Corona discharges

4.2.1 General behaviour

Corona discharges occur at sharp metallic points. This type of partial discharge has been observed by many investigators e.g. [6,52,86]. A detailed review is given in [6].

The discharge measurements reported here were made using the classical measurement system (§2.1). The measurement circuit is shown in Figure 4.2. The distance between the needle and the earth electrode is very large (>0.5 m) compared to the tip radius of the needle (40 μm). Corona has a clearly detectable inception voltage. The inception voltage for positive corona (about 7 kV) is larger than that for negative corona (about 5.5 kV). Just after corona inception the discharges were less reproducible, so

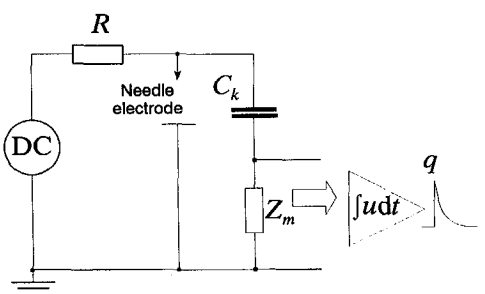

Figure 4.2 *Measurement circuit for corona discharges.*

that registration was started after a stressing time of several minutes.

The discharge magnitude depends on the sample geometry and on the voltage polarity. The measured discharge magnitude is smaller for the negative needle (~27 pC) than for the positive needle (~45 pC). The discharge magnitude is not greatly affected by the test voltage (Figures 4.3 and 4.4).

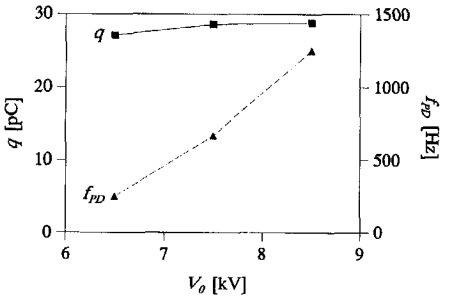

Figure 4.3 *The discharge magnitude and the discharge frequency as function of the test voltage for negative corona.*

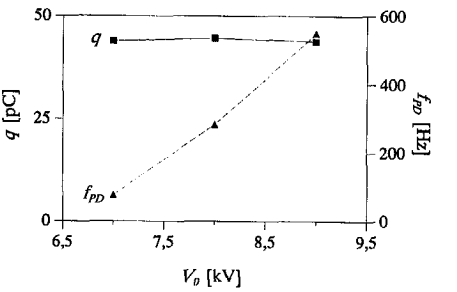

Figure 4.4 *The discharge magnitude and the discharge frequency as function of the test voltage for positive corona.*

The test voltage does have effect on the discharge frequency. An increased test voltage causes an increased repetition rate, where this relation is stronger for negative corona (Figure 4.3) than for positive corona (Figure 4.4).

4.2.2 Statistical behaviour

The statistical behaviour will be discussed for negative corona measured at 6.5 kV and for positive corona measured at 8 kV, which is 15-20% above inception voltage.

(a) Discharge magnitude

The distributions of the discharge magnitude for negative and positive corona are shown in Figures 4.5(a) and 4.5(d) respectively.

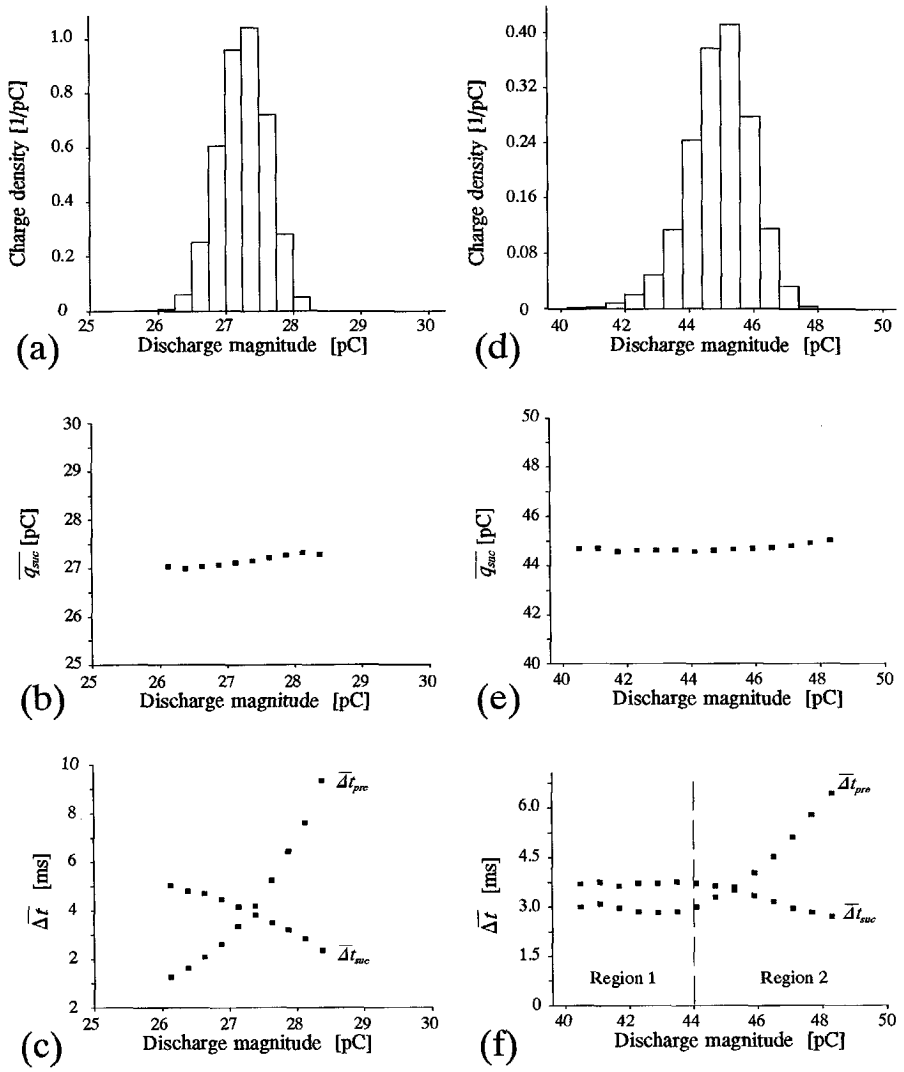

Figure 4.5 *Results for the discharge measurements. (a), (b), (c) negative needle at V_0=6.5 kV; (d), (e), (f) positive needle at V_0=8 kV.*
Discharge magnitude histogram: (a), (d)
Mean discharge magnitude as function of the discharge magnitude: (b), (e)
Mean time to the previous discharge $\overline{\Delta t}_{pre}$ and mean time to the successive discharge $\overline{\Delta t}_{suc}$ as function of the discharge magnitude: (c), (f)

(b) Relation between the magnitudes of successive discharges
The average magnitude of the successive discharge as a function of the discharge magnitude for negative and positive corona is shown in Figures 4.5(b) and 4.5(e) respectively. The average magnitude of the successive discharge does not depend on the discharge magnitude. Therefore eqs. (3.17) and (3.18) are valid here as well.

$$\frac{1}{n}\sum_{i=1}^{n} t_{L,suc(i)} = \overline{t_L} \tag{4.1}$$

$$\frac{1}{n}\sum_{i=1}^{n} t_{R,pre(i)} = \overline{t_R} \tag{4.2}$$

These equations lead to eqs. (4.3) and (4.4) (see §3.3.1), which are used for the interpretation of the measured $\overline{\Delta t}_{pre}$-$q$ and $\overline{\Delta t}_{suc}$-$q$ relations.

$$\overline{\Delta t_{pre}}(q) = t_L(q) + \overline{t_R} \tag{4.3}$$

$$\overline{\Delta t_{suc}}(q) = t_R(q) + \overline{t_L} \tag{4.4}$$

(c) The time to the predecessor $\overline{\Delta t}_{pre}$ and to the successor $\overline{\Delta t}_{suc}$ as function of the discharge magnitude
The average time to the predecessor $\overline{\Delta t}_{pre}$ and to the successor $\overline{\Delta t}_{suc}$ as a function of the discharge magnitude are shown for negative corona in Figure 4.5(c) and for positive corona in Figure 4.5(f).

(I) Negative corona
Eq. (4.3) and Figure 4.5(c) lead to the conclusion, that an enlarged discharge magnitude is caused by a prolonged time lag. Such behaviour is expected, because a prolonged time lag leads to a discharge ignition at higher field strength and discharge ignition at a higher field strength in its turn causes a larger discharge magnitude, because more space charge is required to extinguish the discharge process.

Eq. (4.4) and Figure 4.5(c) lead to the conclusion, that an enlarged discharge magnitude causes a shorter recovery time. Such behaviour can be explained as follows. The dependence of the recovery time t_R on q is determined by two competing effects:

1. Field reduction as a result of ion space charge generated by the previous discharge: In course of time the space charge disappears, causing again an increase of the field strength. A larger discharge magnitude is accompanied by a larger space charge, so that the recovery time t_R (necessary to reach again the minimal breakdown field strength E_{min}) will increase.

2. Enhancement of the ionisation coefficient in the gas volume where the next discharge develops, caused by the metastable species generated by the previous discharge [6]. The enhanced ionisation coefficient causes a decrease of the minimal breakdown field strength, so that a shorter recovery time is required in order to reach again the minimal breakdown field strength.

The second effect obviously dominates the measured data and leads to a decreased recovery time t_R for an increased discharge magnitude.

(II) Positive corona

For positive corona the picture is not as clear as for negative corona. Two regions can be distinguished: Region 1 for discharges smaller than about 44 pC and region 2 for discharges larger than 44 pC (see Figure 4.5(f)).

Region 2

In region 2 the mean time to the previous discharge $\overline{\Delta t}_{pre}$ increases before discharges of an increased magnitude, whereas the mean time to the successive discharge $\overline{\Delta t}_{suc}$ decreases. The explanation might be similar to that for negative corona. The dependence of the recovery time t_R on q is determined by the two competing effects (1. Field reduction, 2. Enhancement of the ionisation coefficient). The second effect obviously dominates within region 2 and leads to the decreased $\overline{\Delta t}_{suc}$ for an increased discharge magnitude.

Region 1

In region 1 the time to the previous discharge $\overline{\Delta t}_{pre}$ and the mean time to the successive discharge $\overline{\Delta t}_{suc}$ are no function of the discharge magnitude (Figure 4.5(f)). Together with the eqs. (4.3) and (4.4) two conclusions are drawn:

1. The recovery time t_R is no function of the discharge magnitude q. Such behaviour can be explained by the compensation of the two competing effects (compare *Negative corona*):
   - Field reduction by ion space charge leads to an increased t_R for increased q

- Enhancement of the ionisation coefficient leads to an decreased t_R for increased q

2. The time lag t_L does not determine the discharge magnitude q. More investigations are required before an explanation can be given.

4.3 Surface Discharges

Surface discharges occur along interfaces, if the tangential field strength exceeds the breakdown strength of one of the materials. Compared to internal discharges, there is no spacial limitation of the discharge.

A discharge along a surface generates a surface charge. The surface charge causes a decreased field at the discharge location, so that the discharge stops. Conduction causes a charge decay, which results in field enhancement thus causing the next discharge. The physics of charge carrier multiplication along a surface is reviewed by Craig Miller [9]. In this section discharge measurements along a air-solid interface are reported.

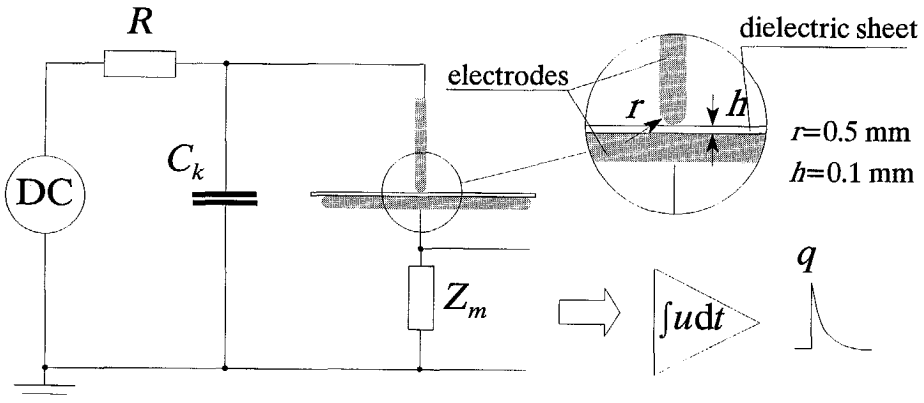

***Figure 4.6** Measurement circuit for surface discharges.*

The discharge measurements were made with the classical discharge measurement system at the configuration shown in Figure 4.6. The measurements were carried out with different dielectric materials:

- polycarbonate (PC)
- polyethylene (PE)
- cellulose-3-acetate (CTA)

The test voltage varied between 6 kV and 15 kV. The measurements were started a few seconds after voltage application, so that the discharges, which occurred during voltage application, have not been registered.

4.3.1 General behaviour

(a) Discharge magnitude

The discharge measurements showed for all materials a discharge magnitude of the order of nC. For PC no discharges were measured at V_0=10 kV. Therefore the effect of the test voltage (V_0=6 kV...10 kV) on the discharge magnitude has been studied for PE and CTA. A voltage step up test was performed, measuring at 6 kV, 7 kV, 8 kV, 9 kV and 10 kV. The measuring time was 0.5 h at each voltage level. The mean discharge magnitude as function of the test voltage is shown in Figure 4.7 for a positive test voltage and in Figure 4.8 for a negative test voltage. The following facts can be stated:

1. The discharge magnitude is larger for a positive test voltage than for a negative test voltage.

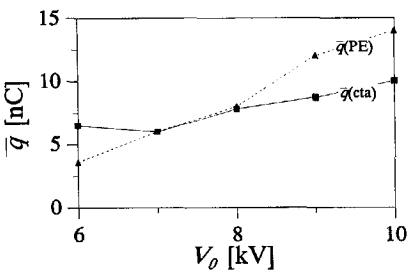

Figure 4.7 *The mean discharge magnitude $\overline{q}$ as function of the positive test voltage for PE and CTA.*

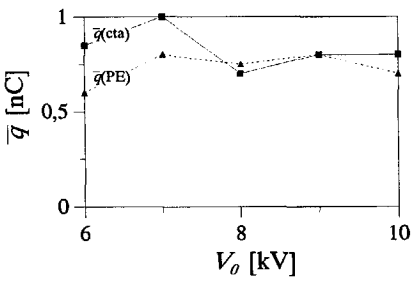

Figure 4.8 *The mean discharge magnitude $\overline{q}$ as function of the negative test voltage for PE and CTA.*

2. For a positive test voltage the discharge magnitude increases with increasing test voltage.

In some cases both large discharges (order of nC) and small discharges (order of pC) were observed. This leads to the assumption that discharges of different

mechanisms can occur at the same time. In order to study such phenomena, a detector with a large dynamic range is required. Therefore the amplifier, which integrates the discharge current (see Figure 4.6) should preferably be logarithmic over a range of four or more decades.

(b) Discharge repetition

Surface discharges appear to have no regular time behaviour. The discharge activity might stop for a while (see Figure 4.9) and then continue again. The time between successive discharges may increase until there is no longer any discharge registered, as shown in Figure 4.9 for PE. In other cases the discharge frequency might suddenly increase as shown in Figure 4.10.

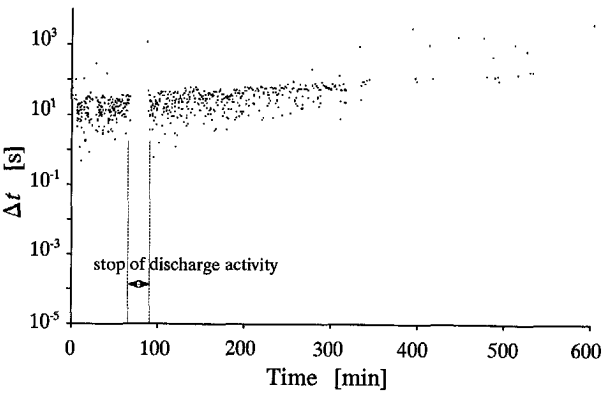

Figure 4.9 *The time between successive discharges $\overline{\Delta t}$ for surface discharges on PE at $V_0 = -10$ kV; each discharge is plotted as one pixel.*

Though the discharge repetition is badly reproducible, the tendency of an increased discharge frequency at increased test voltages has been observed for both polarities.

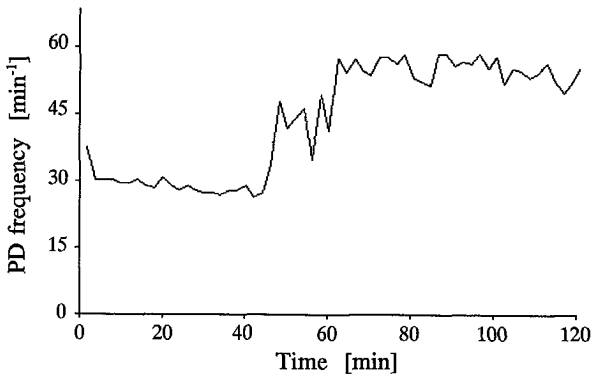

Figure 4.10 *The discharge frequency as time function for surface discharges on CTA at $V_0 = 10$ kV.*

There is no discharge inception with high repetition as in the case of corona, so that the measured inception voltage depends on the lowest measurable discharge frequency. This behaviour is similar to that of internal discharges.

4.3.2 Statistical behaviour

In order to use the model given in §4.1 for the explanation of the statistical discharge behaviour, a large number of discharges occurring under similar circumstances must be registered. There are two reasons causing difficulties in such a statistical evaluation.

1. Because of the low repetition rate, long measuring times are required. However, the discharge frequency is generally not constant for long periods (compare §4.3.1).
2. Because of the small dynamic range of the used discharge detector, it is probable that not all discharges are registered.

Therefore the calculation of the mean magnitude of the previous or successive discharge, or the calculation of the mean time to the previous or successive discharge as functions of the discharge magnitude are meaningless.

For this reason the histogram of measured basic quantities (discharge magnitude, time of occurrence) is proposed here for the description of the statistical discharge behaviour. The time of occurrence is replaced by the time between the discharges. Two distributions are possible:

- q-Δt_{pre} histogram
- q-Δt_{suc} histogram

It has been chosen for the q-Δt_{suc} histogram, because only little difference has been found between them. These plots can be used in order to distinguish different discharge sources:

(a) Corona

The almost constant discharge magnitude and the almost constant time between successive discharges at a constant test voltage is characteristic for corona. This behaviour results in a very narrow q-Δt_{suc} histogram, as shown in Figure 4.11 for positive corona at $V_0 = 8$ kV.

(b) Internal discharges

Internal discharges have the highest density for the smallest measured magnitude as shown in Figure 4.12.

(c) Surface discharges

Surface discharges (Figures 4.13-4.15) have their density maximum usually for magnitudes larger than the smallest measured values (compare *(b) Internal discharges*). The magnitudes of surface discharges are distributed over a wide range, unlike in the case of corona.

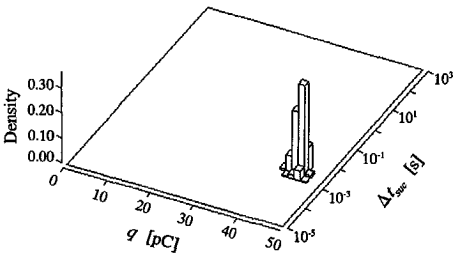

Figure 4.11 *q-Δt_{suc} histogram for positive corona at V_0=8 kV.*

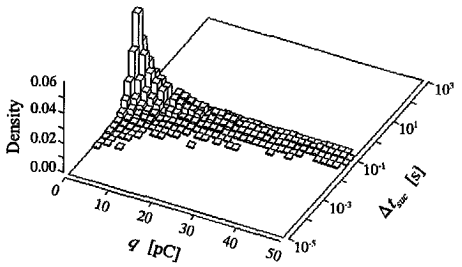

Figure 4.12 *q-Δt_{suc} histogram for internal discharges in PE at V_0=15 kV; (h_V=0.2 mm, d_V=10 mm, h_S=0.6 mm).*

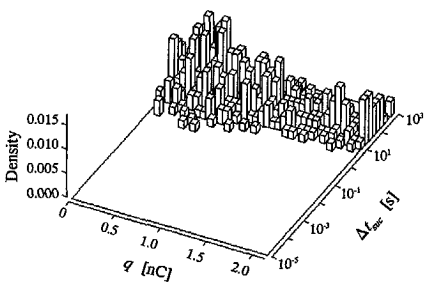

Figure 4.13 *q-Δt_{suc} histogram for surface discharges on a PE surface at V_0=−10 kV.*

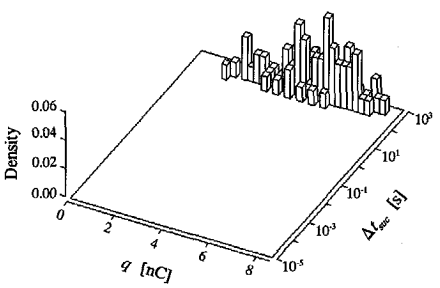

Figure 4.14 *q-Δt_{suc} histogram for surface discharges on a PC surface at V_0=15 kV.*

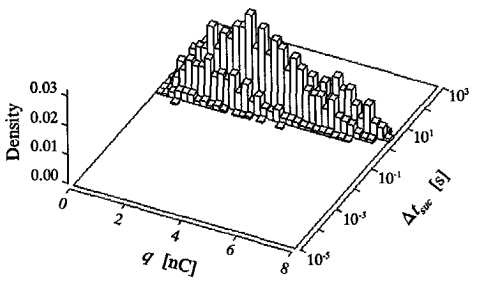

Figure 4.15 *q-Δt_{suc} histogram for surface discharges on a CTA surface at V_0=10 kV.*

4.4 Conclusions

For the description of the statistical discharge behaviour, a general *time lag - recovery time model* has been introduced. Discharge measurements have been made for corona and surface discharges.

Corona discharges have a regular time behaviour. Therefore the statistical behaviour can be described using the *time lag - recovery time model.*

Surface discharges do usually not have a regular time behaviour. The discharge magnitude can range from the order of pC to the order of nC. Both these facts make it difficult to register enough data to enable use of the *time lag - recovery time model.*

In order to distinguish different discharge sources, the q-Δt_{suc} histogram can be used. Different discharge sources result in characteristic patterns, which can be used for recognition purposes.

Chapter 5

Partial discharges in dielectric liquids

This chapter is aimed at completing the picture about discharges at DC voltage. A systematic study of the discharge behaviour in liquids has not been carried out, so that the measurements are limited to corona in oil. First an overview of the mechanisms leading to breakdown is given and secondly measurements carried out with a classical discharge detector are presented.

5.1 Discharge initiation and propagation

As dielectric liquids one understands generally both polar (e.g. phthalate esters, castor oil) or non-polar (e.g. mineral oil, silicon oil) liquids with a relative permittivity ϵ_R usually smaller than 10 and with DC resistivities higher than 10^{10} Ω [19].

At low voltages the conduction is dominated by ion transport. Negative ions are formed by attaching injected electrons. The electron injection is controlled by the characteristics of the metal/dielectric interface. Only a small fraction of the electrode surface participates in the injection process. At DC voltage, the observed current is mainly caused by events taking place in the immediate vicinity of the two electrodes and has little to do with the charge transport across the dielectric [19]. At low fields, only a few electrons can pass the potential barrier of the injection site. At higher fields, the number of injected electrons and their average kinetic energy increase, which is caused by the SCHOTTKY effect. Even higher fields will favour the tunnelling of electrons across the potential barrier.

The electrons leaving the metal have, on average, a kinetic energy greater than the molecules of the dielectric. These electrons can cause three types of interaction [19]: thermal expansion, breaking of bonds (>3eV), impact ionization (>6eV). At sufficiently high field strengths the probability of the latter two increases significantly. Also the heating process becomes more effective and leads to localized vaporization of the liquid. As the vapour phase expands, its internal pressure drops and according to PASCHEN's law breakdown of this region occurs when a critical low pressure is reached. The breakdown

of the vaporized region can be measured as partial discharge. In other word, partial discharges in liquids are gas discharges. All models and measurement methods for gas discharges can be used for discharges in liquids as well. The partial discharge inception in liquids indicates the generation of a vaporized region [20].

The discharges are reported to occur as bursts or pulse trains with different behaviour for the positive and negative point electrode, whereas the growth of the vaporised region is reported to be uniform. The growth of the vaporised region still continues after the current pulses have ended [36]. Therefore, the growth of the vaporised region is assumed to proceed independently on the occurrence of partial discharges [19] and it is suggested that it is driven by electrostatic forces [74]. Breakdown occurs if the vaporised region bridges the distance between the electrodes.

In other words, when comparing the partial discharge behaviour of different systems, no conclusions concerning the breakdown voltage can be drawn. The growth of the vaporised region has been the subject of many investigations (e.g. [1,11,36,74])

5.2 Measurement of corona discharges in transformer oil

Classical discharge measurements can be used for the statistical characterization of the discharge processes. The measured discharge magnitude is generally the integrated charge of a pulse train, because the discharges within a pulse train have time distances less than a micro second [36,74], whereas the upper frequency limit of the discharge detector is usually about 200 kHz.

Experiments were made with a point(positive)-plane configuration, using a needle with a point radius of 35 μm having a distance to the plane of 50 mm. The arrangement was placed under transformer oil. Measurements were made with an increasing test voltage (steps of 10 kV for 10 minutes). At 50 kV the occurrence of the first few discharges was detected. Measurements have been carried out at 50 kV, 60 kV, 70 kV and 80 kV. The measurement

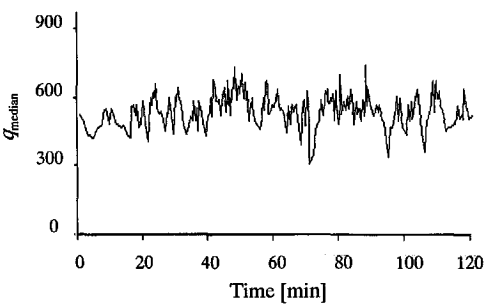

***Figure 5.1** The average discharge magnitude (median) as time function (one median value is calculated for 50 discharges); $V_0 = 70$ kV.*

duration was two hours.

At all voltages, fluctuations in discharge magnitude and discharge frequency were measured (Figures 5.1 and 5.2). Therefore the calculation of the mean magnitude of the previous or successive discharge, or the calculation of the mean time to the previous or successive discharge as functions of the discharge magnitude are meaningless.

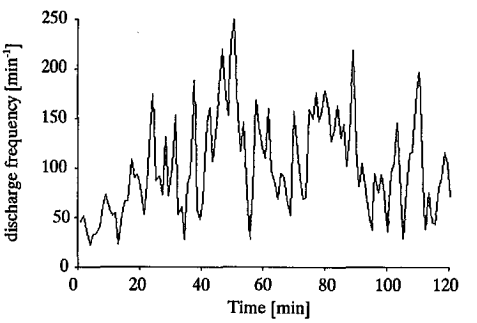

***Figure 5.2** The discharge frequency as time function (one frequency value is calculated each minute); $V_0 = 70$ kV.*

Therefore the histogram of the measured basic quantities (discharge magnitude q_i, and time of occurrence t_i) is proposed for the description of the statistical discharge behaviour. The time of occurrence is replaced by the time between the discharges. Two distributions are possible:

- q-Δt_{pre} histogram (see Figure 5.3)
- q-Δt_{suc} histogram (see Figure 5.4)

There is only a slight difference between these two. The distributions are characteristic and differ from those obtained for internal discharges or discharges in air (see chapter 3 and 4).

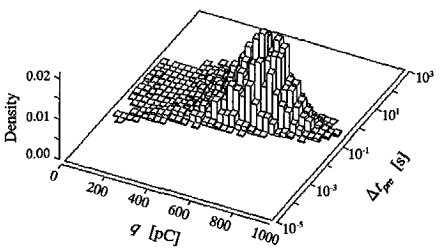

***Figure 5.3** The q-Δt_{pre} histogram; $V_0 = 70$ kV.*

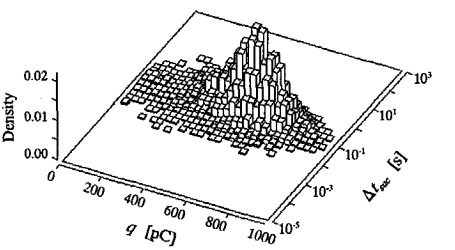

***Figure 5.4** The q-Δt_{suc} histogram; $V_0 = 70$ kV.*

The effect of the test voltage on the discharge behaviour is shown in Figure 5.5. An increased test voltage causes increased discharge magnitude and increased discharge repetition.

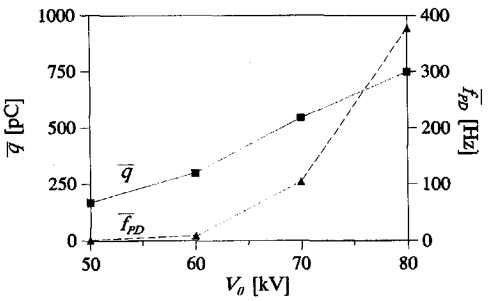

Figure 5.5 *The mean discharge magnitude and the mean frequency as functions of the test voltage.*

5.3 Conclusions

Concerning the behaviour of partial discharge in liquids, the following conclusions are drawn:

1. The discharge inception coincides with the generation of a vaporized region.

2. The discharge behaviour of corona in transformer oil shows a fluctuating pattern.

3. The characterization of corona in transformer oil by statistical means is possible by the q-Δt_{pre} and by the q-Δt_{suc} histograms. Such histograms are proposed for the recognition of defects (see §7.2).

Chapter 6

Ageing and breakdown

The reliable functioning of high voltage components requires the knowledge of ageing at DC voltage. The questions to be discussed concern the lifetime, the effect of a void on ageing and breakdown and the role of partial discharges during ageing.

Measurements have been made for samples containing an cathode-bounded air-filled void (Figures 2.4 and 2.5) and for samples without a void. The set-up is described in §2.3 (Figure 2.6).

6.1 Progressive-stress tests

In order to determine start values for the constant-stress tests a short term breakdown test has been made. The progressive-stress tests have been carried out for the epoxy samples containing an cathode-bounded air filled void (Figures 2.4 and 2.5) and for those without a void. The set-up is described in §2.3 (Figure 2.6). The tests were started with a test voltage of 80 kV. After 24 h the voltage was increased by 10 kV. For the measured breakdown data the WEIBULL distribution is assumed.

$$P_F(V) = 1-\exp[-(\frac{V}{V_S})^{\alpha}] \qquad (6.1)$$

The parameter V_S is known as the voltage-scale parameter (63% breakdown value). The parameter α is the voltage-shape parameter. The values for V_S and α are obtained in this study by the maximum-likelihood method.

The results are shown as WEIBULL plots in Figures 6.1 and 6.2. The

Table 6.1 *The 90% confidence intervals for the V_S and α values as result of the progressive-voltage tests*

90% confidence interval	samples without void	samples with void
V_S	159..176 kV	116..123 kV
α	6.6 .. 16	10 .. 25

90% confidence intervals of the voltage-scale parameter and the voltage-shape parameter are given in Table 6.1. The breakdown voltage is larger for the samples without a void. There may be two reasons: 1. The insulation thickness is larger for the samples without void (2 mm) than for the samples with void (1.5 mm). 2. A field enhancement in the insulation material due to the presence of the void is possible. This field enhancement can be caused by the geometry of the void or by the generation of space charge in the epoxy as a result of the discharge activity in the void.

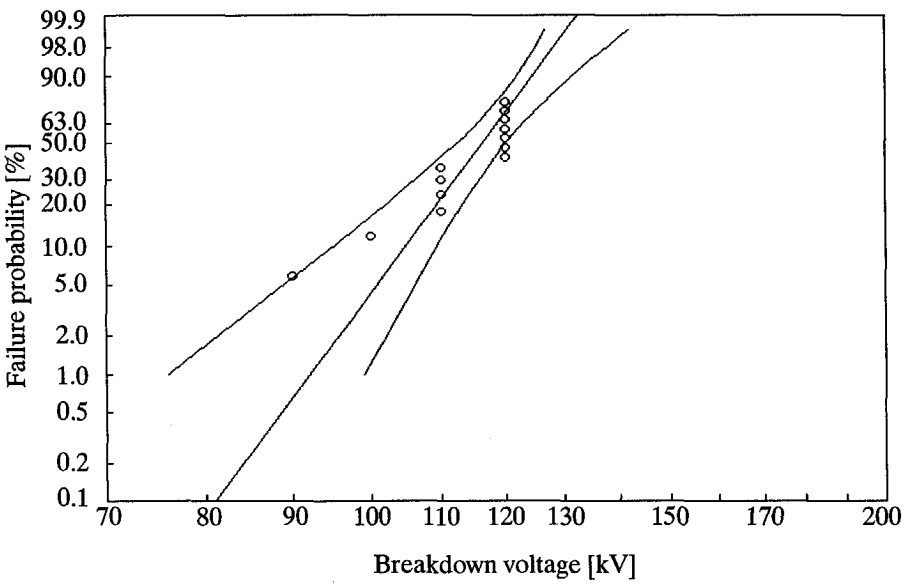

Figure 6.1 *WEIBULL plot with 90% confidence intervals for progressive-stress test for the samples with void (insulation thickness=1.5 mm);* $V_S=119$ *kV,* $\alpha=18$.

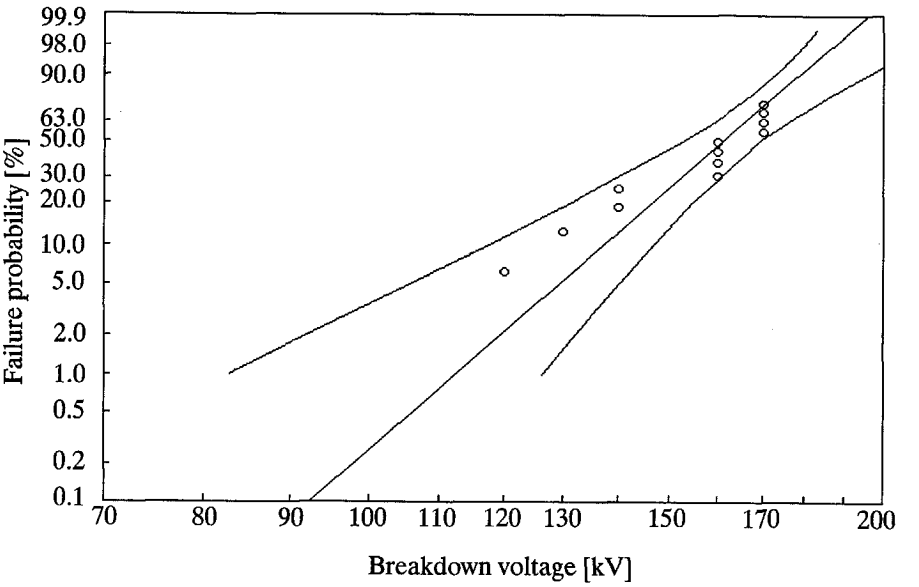

Figure 6.2 *WEIBULL plot with 90% confidence intervals for progressive-stress test for the samples without void (insulation thickness=2 mm); V_S=166 kV, α=12.*

6.2 Constant-stress tests

In order to study the ageing behaviour at DC voltage, constant-stress tests were carried out. Most of the tests were carried out for the epoxy samples containing an cathode-bounded air-filled void (Figures 2.4 and 2.5). One test was made for samples without a void. The set-up is described in §2.3 (Figure 2.6). The test voltage is applied by increasing it within about 1 min up to the test value. Therefore, for breakdowns which occurred during voltage application the time to breakdown was $t_{BD} < 1$ min. These breakdowns are represented by black blocks at the left edge in Figures 6.4-6.7 and 6.10.

The measured time to breakdown t_{BD} and the breakdown location at different test voltages are shown in Appendix C. All breakdowns were used for the evaluation, also those which occurred outside the void. For the measured breakdown data the WEIBULL distribution is assumed.

$$P_F(t) = 1-\exp[-(\frac{t}{t_S})^{\beta}] \qquad (6.2)$$

The parameter t_S is known as the time-scale parameter (63 % breakdown value) to breakdown. The parameter β is the time-shape parameter. The values for t_S and β are obtained here by the maximum-likelihood method.

6.2.1 Samples with a void

The tests were carried out for the test voltages 80 kV, 90 kV, 100 kV, 110 kV and 120 kV. In Figures 6.3-6.7 the measured times to breakdown are plotted on WEIBULL paper. Each of the measured distributions appeared to be bimodal and is represented here as two WEIBULL distributions (*Region 1* and *Region 2* in Figures 6.3-6.7).

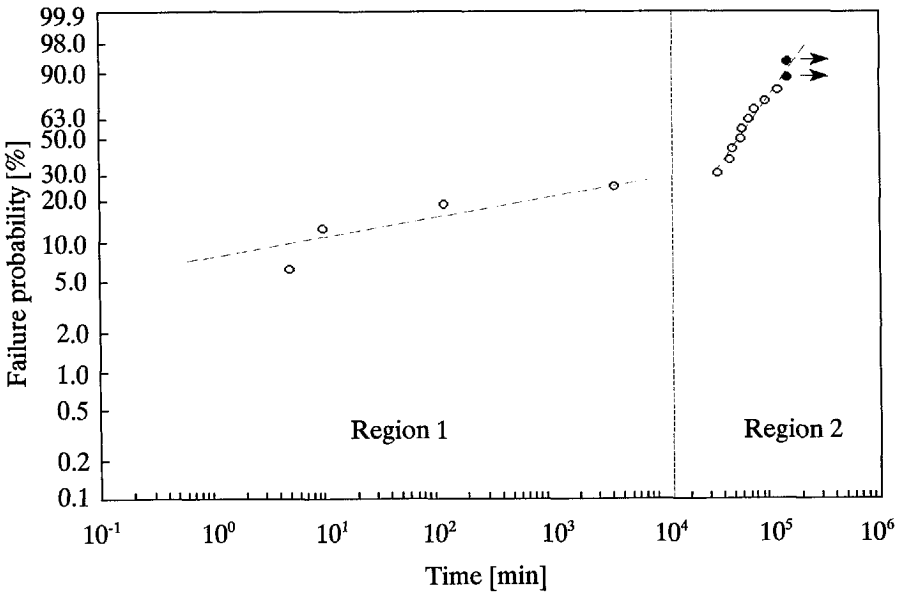

***Figure 6.3** WEIBULL plot for the ageing test at V_0=80 kV.*

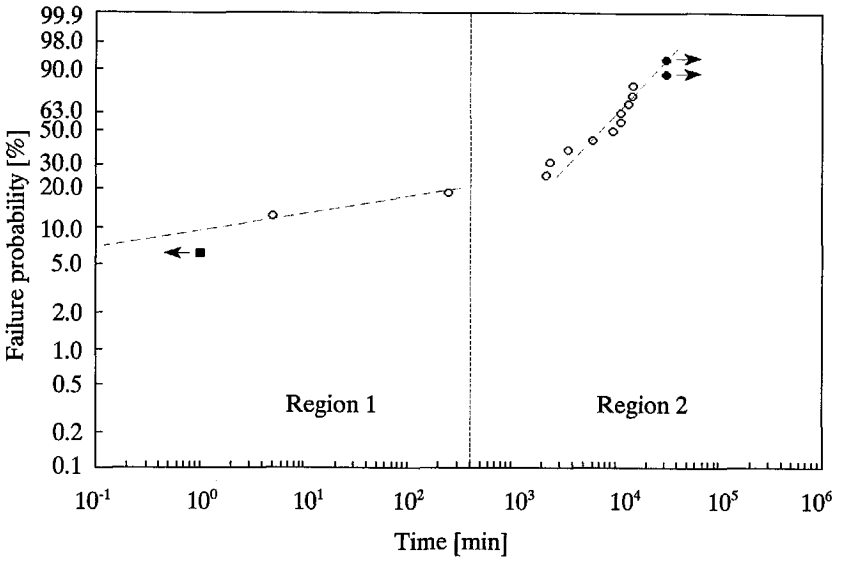

Figure 6.4 *WEIBULL plot for the ageing test at V_0=90 kV.*

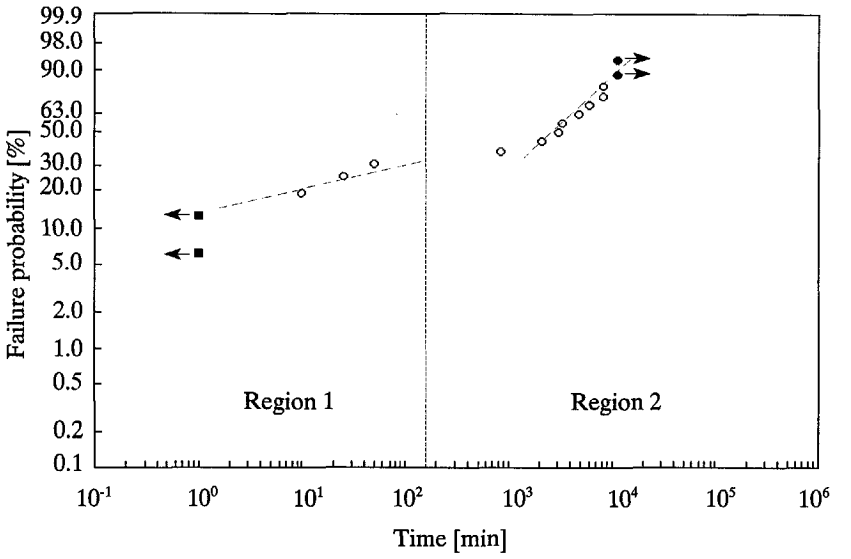

Figure 6.5 *WEIBULL plot for the ageing test at V_0=100 kV.*

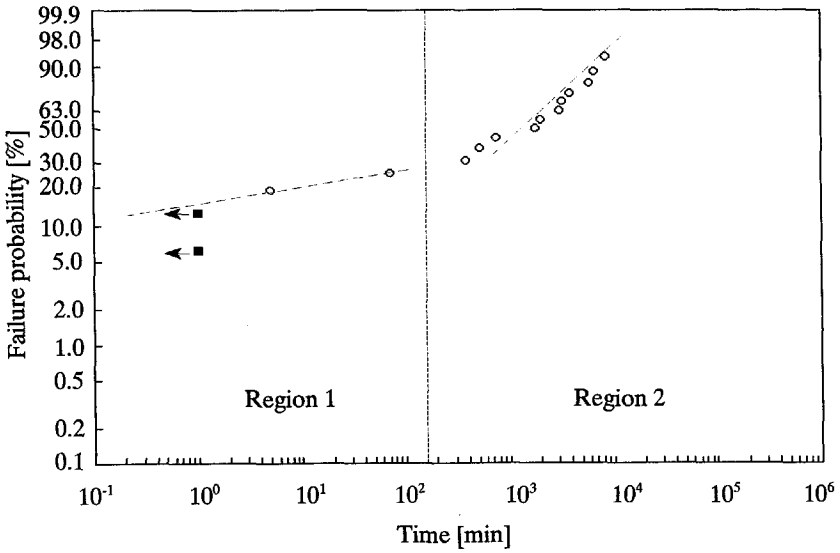

Figure 6.6 *WEIBULL plot for the ageing test at V_0=110 kV.*

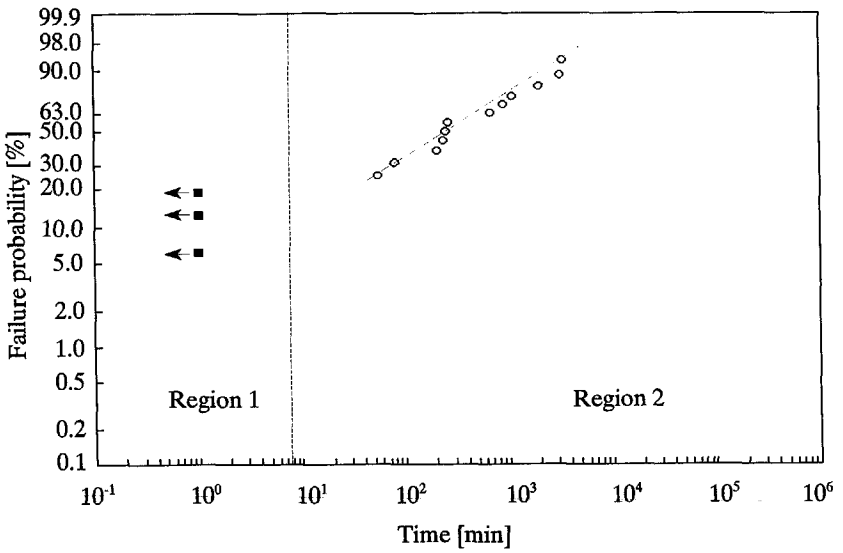

Figure 6.7 *WEIBULL plot for the ageing test at V_0=120 kV.*

Hence, two breakdown mechanisms are concluded to be involved. The WEIBULL parameter t_S and β and their 90% confidence intervals are shown in Table 6.2.

Region 1
A shape parameter $\beta < 1$ is characteristic for *Region 1*. Thus the breakdowns are caused by a conditioning effect. The bad samples break down and the good samples survive. The early breakdowns are assumed to be caused by material faults and not by the presence of the void (see§6.2.2).

Region 2
A shape parameter $\beta > 1$ (except for $V_0 = 120$ kV) is characteristic for *Region 2*. A tendency of increasing β for decreasing V_0 is obtained (Figure 6.8). A $\beta > 1$ means that there is a mechanism which limits the life of the samples. Thus, there is some kind of electric ageing at DC voltage.

***Table 6.2** The WEIBULL parameters and their 90% confidence intervals.*

V_0 [kV]	*Region 1*				*Region 2*			
	t_S [min]	90% confidence interval	β	90% confidence interval	t_S [min]	90% confidence interval	β	90% confidence interval
80	283	8.5..19000	0.38	0.11..0.55	97510	72910..136600	2.0	1.1..2.8
90	35.5	0.8..12000	0.44	–	14610	9310..24420	1.25	0.7..1.7
100	14.6	3.3..78	0.73	0.26..1.1	6955	4570..11540	1.51	0.8..2.1
110	1.1	1..186	0.56	0.16..0.81	3570	2190..5880	1.24	0.7..1.7
120	<1	–	–	–	935	480..1840	0.85	0.5..1.1

The measured ageing behaviour results in a hazard function as shown for 80 kV in Figure 6.9. The decreasing risk of failure in the beginning is caused by the breakdown behaviour in *Region 1*. After the conditioning there is a period of relative stability. The consecutive period of increasing risk for failure is caused by the ageing mechanism in *Region 2*. Such a behaviour is known as a 'bathtub' shape. This behaviour is similar to the ageing found at AC voltage e.g. [41].

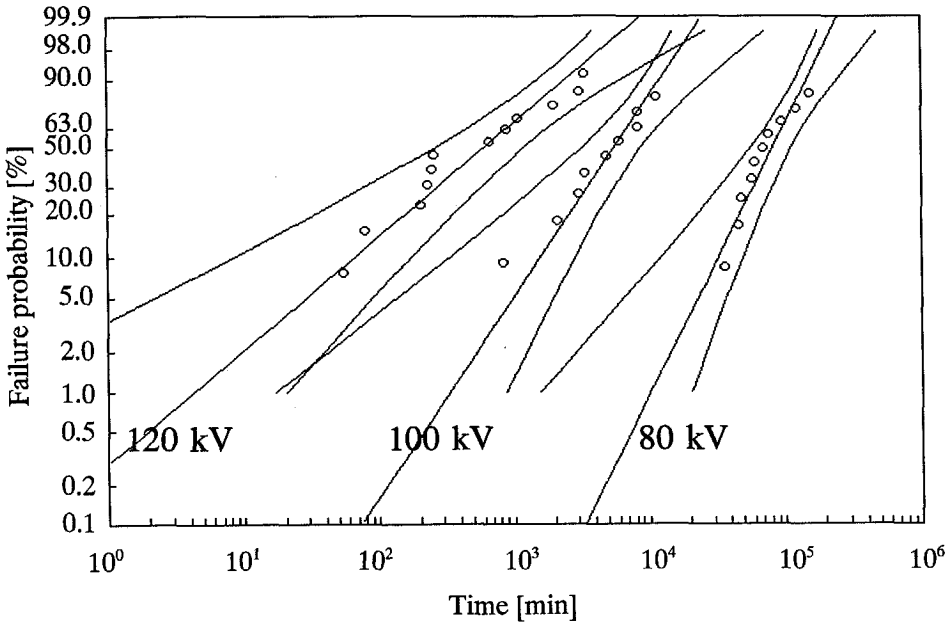

Figure 6.8 *WEIBULL plot for Region 2 at 80 kV, 100 kV and 120 kV for the samples with void.*

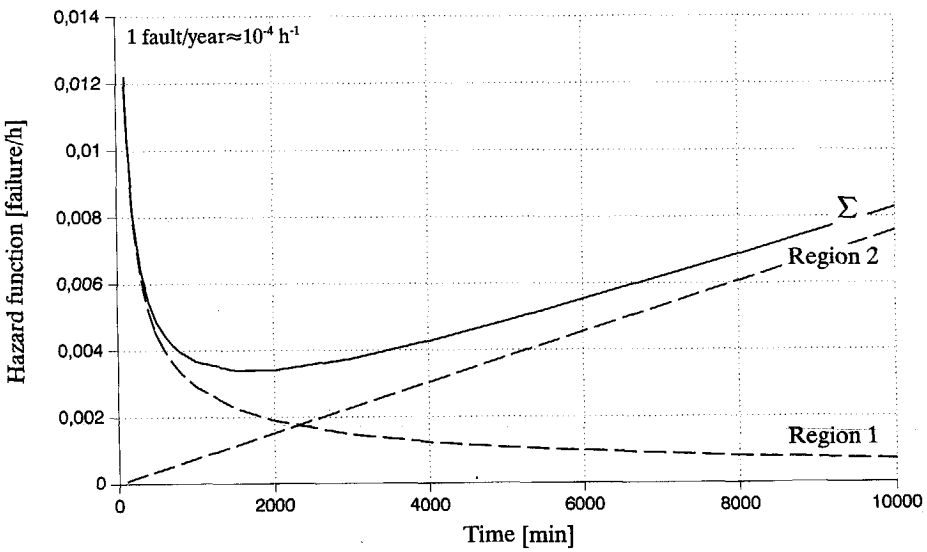

Figure 6.9 *The hazard function at a test voltage of 80 kV containing of the hazard functions for Region 1 and Region 2.*

6.2.2 Samples without a void

As mentioned above, the early breakdowns (*Region 1* in §6.2.1) are assumed to be caused by faults in the dielectric material. In order to check this assumption, a constant voltage test was made for samples without a void. The test voltage was chosen to be 120 kV.

The test results are shown in Figure 6.10. Similar to the tests with a void, two early breakdowns (Region 1 in §6.2.1) were observed. No further breakdown has been observed until 1300 h. This supports the assumption that the early breakdowns may be caused by defects in the dielectric material. Further, as may have been expected, the results show that the presence of a void shortens the lifetime remarkably (compare Figure 6.7).

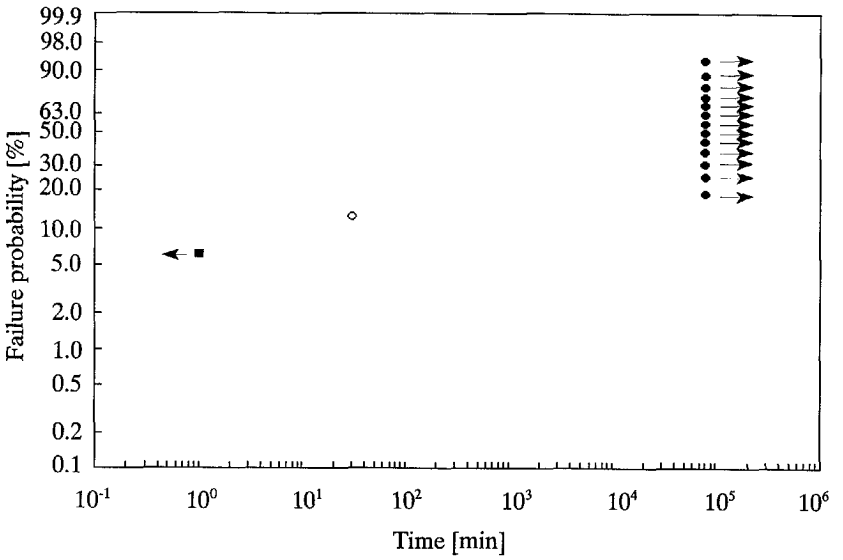

Figure 6.10 *WEIBULL plot for the ageing test at samples without a void at* $V_0 = 120$ *kV.*

6.2.3 Effect of voltage on lifetime

In Figure 6.11, the 90% confidence intervals of the time-scale parameter are shown for the tests on samples with a void. As expected the time to breakdown increases for decreased test voltages. For t_s and V_0 the inverse power law

relation is assumed.

$$t_S \sim V_0^{-n}$$
$$t_S = C^{-1/\beta} V^{-\gamma/\beta} \tag{6.3}$$

This results in a breakdown probability as a function of time and voltage stress:

$$P_F(V,t) = 1-\exp(-Ct^{\beta}V^{\gamma}) \tag{6.4}$$

When plotting the time-scale parameter on double logarithmic paper, the life exponent n (see eq.(6.3)) can be graphicly obtained. In Figure 6.11 the 90% confidence intervals of the time-scale parameter are plotted for *Region 1* and for *Region 2*. As shown in Figure 6.11 the value of n has been obtained to be n=9..12 for *Region 2*. For *Region 1* no life exponent has been determined because of the very wide confidence intervals of the time-scale parameter (see Figure 6.11).

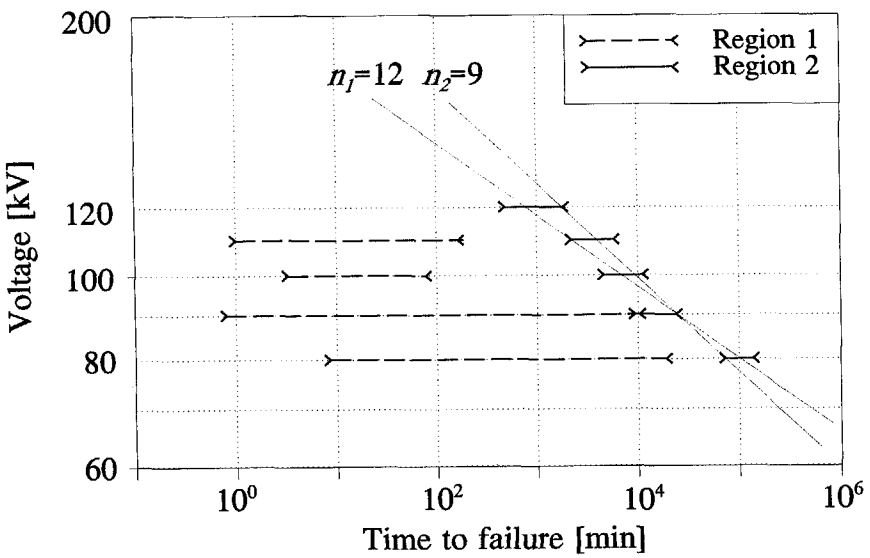

***Figure 6.11** 90% confidence intervals of the time-scale parameter for the two ageing mechanisms (Region 1, 2) for the samples with void.*

6.3 Partial discharges and ageing

Discharge measurements were carried out on virgin samples and on two samples aged at 80 kV for 2550 h. The test voltage for the discharge measurements was 70 kV. The measurement duration was 60 min. After voltage application there is a period of intense discharge activity (>1000 discharges/min) for about one minute. After that time the discharge frequency drops and reaches a more or less stable state (Figures 6.12-6.13).

The discharge frequency as a time function is shown in Figures 6.12 and 6.13. The discharge frequency appears to be somewhat larger for the aged samples (Figure 6.13). The distribution function of the aged and the virgin samples are shown in Figures 6.14 and 6.15. The discharge magnitude is somewhat larger for the aged samples. However, no remarkable differences have been found. Although no significant relation between partial discharge behaviour and ageing has been obtained, partial discharges indicate weak spots in the insulation construction.

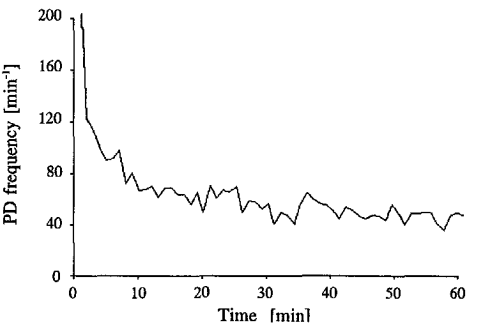

Figure 6.12 *Discharge frequency of a virgin epoxy sample at 70 kV, sensitivity 3.3 pC.*

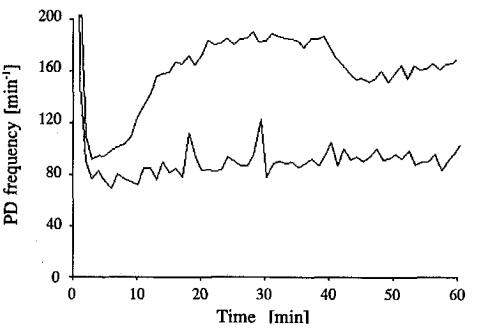

Figure 6.13 *Discharge frequencies of two aged epoxy samples at 70 kV; aged at 80 kV for 2550 h, sensitivity 3.3 pC.*

Breakdown occurred during the discharge measurement of a virgin sample. An increased discharge frequency several minutes before breakdown is remarkable (Figure 6.16). The discharge magnitude, however, remained constant.

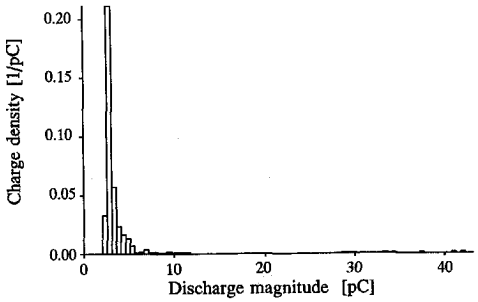

Figure 6.14 *Discharge density of a virgin epoxy sample at 70 kV, sensitivity 3.3 pC.*

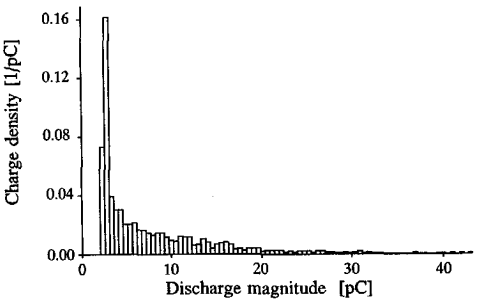

Figure 6.15 *Discharge density of an aged epoxy sample at 70 kV; aged at 80 kV for 2550 h, sensitivity 3.3 pC.*

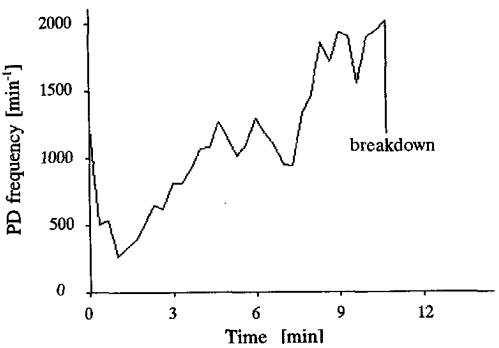

Figure 6.16 *Time behaviour of the discharge frequency of a virgin sample before breakdown; V_o=70 kV, sensitivity 3.3 pC.*

6.4 Conclusions

Concerning the ageing and breakdown behaviour at DC voltage, the following can be stated.

1. The presence of a void causes a decrease in breakdown voltage by
   - reducing the insulation distance
   - local field enhancement in the remaining dielectric.

2. Concerning ageing in the presence of a void, the well-known 'bathtub' shape is valid. Two mechanisms leading to breakdown have been observed. One mechanism causes a conditioning effect which leads to early breakdowns. The second mechanism determines the life of the insulation.

3. The inverse power law relation $L \sim E^{-n}$ can be assumed, where L is the life of the insulation. For epoxy samples containing air-filled voids, values $9 < n < 12$ were obtained.

4. The role of internal partial discharges is not yet clear. However, discharges indicate weak spots. In one case the discharge frequency was observed to increase before breakdown.

Chapter 7

Testing and diagnostics

An important aspect of production is to secure the quality of the product. A qualitatively good product does not contain defects which may affect the reliable functioning of the product during its lifetime. Therefore the ability to detect, locate and recognise defects is required.

Testing answers the question as to the presence of a defect. The answer is either yes or no. For the evaluation of a product in terms of good or bad, this information is sufficient. In order to detect defects, tests are carried out. A clearly defined test criterium (e.g. breakdown for voltage tests) determines the test result. The different test methods are discussed in §7.1.

If the number of faulty products is unsatisfactorily large, the question as to the reasons for failing should be answered. Therefore the localisation and the recognition of defects is very useful. For defect localization and defect recognition the term 'diagnostics' is usually used. Diagnostics based on the measurement of partial discharges is discussed in §7.2.

7.1 Testing

The aim of testing is to secure the reliable functioning of the device or of a construction for the lifetime it is designed for. In general a distinction can be made between:

- *Type-tests*
- *Routine-tests*

The *type-test* is carried out on prototypes and it evaluates the design of a new product. The *routine-test* is an after production test. It ensures the quality of the product. Each product is tested. Faulty products should be detected.

Both the type test and the routine test can be divided into different test methods. For AC voltage the stability test, the impulse test and the partial discharge test are the common standards. These tests should be carried out at DC as well. In addition to these tests, testing for field transitions is necessary.

7.1.1 Stability test

Type test

In order to ensure that the device to be tested can withstand the operating stress for its entire lifetime, accelerated ageing tests are necessary. Therefore, the knowledge of the 'life-line' is required, i.e. the relation between a measured lifetime L at an overvoltage V and the expected lifetime at the operating voltage must be known. Usually an inverse power law relation is assumed

$$L \sim V^{-n} \tag{7.1}$$

During long-term DC tests on polyethylene discs [18], on polyethylene cables [66] and on different epoxy samples [34] values of $n=8..20$ are reported. For the lifetime experiments carried out in this work, values $9<n<12$ have been found for epoxy samples containing an air-filled void (Figure 6.10). These values n are similar to those obtained for AC voltage [73]. Therefore, concerning the *type-test*, the concept of overvoltage testing for DC voltage is concluded to be similar to that for AC [44]. In agreement with this, testing for 50 days at 2 times the operating voltage is proposed [67] in order to ensure a life of 30 years for a DC XLPE cable (assumed life exponent $n=9$).

Routine test

The time dependence of the breakdown behaviour for the experiments reported in §6 at DC voltage is similar to that found for AC voltage (see hazard function Figure 6.9):

- At the beginning of operation a conditioning effect is observed.
- For a certain time the failure risk remains small.
- Ageing finally leads to an increase of the failure risk again. The end of the electric life is approached.

The test should detect the defect objects which cause the large failure risk in the beginning stage (see hazard function Figure 6.9). The test voltage and test duration must be chosen large enough to ensure the failing of the defect objects. Ageing of the good test objects due to the test should be minimal. This determines an upper level for the test voltage and for the test duration.

7.1.2 Testing for field transitions

Transient fields occur after switching the voltage on or off, or after polarity reversal and are related to processes of charge accumulation (see §1.2). After switching on/off or after a polarity reversal, a certain time is required to reach a steady state electric field. During this time the field may locally exceed the

acceptable field strength (compare Figure 1.2). Therefore all possible situations which might occur during operation must be tested, e.g. polarity reversal for DC cables.

7.1.3 Impulse test

If the test object is expected to be exposed to impulse stress then impulse tests should be carried out. HVDC energy equipment may be exposed to impulse voltages due to a lightning stroke or due to switching of currents. For non-energy HVDC equipment in general, only the impulse stress due to switching has to be taken in account. All these stress situations may occur for AC equipment as well. Many test specifications have been worked out for AC voltage [91] which may be used for DC as well.

7.1.4 Partial discharge testing

At AC voltage the maximal discharge magnitude q_{max}, measured under clearly defined conditions [90], has been accepted as a criterium for a 'GO/NO GO' test. The discharge frequency is not taken into account, because the minimal discharge frequency is determined by the power frequency (50 or 60 Hz).

At DC, the discharge frequency depends very much on the resistivity of the insulating material and on the test voltage. In practice, the discharge frequency can range between 0.1 min^{-1}...10000 min^{-1}. Therefore it has to be taken in account.

The following proposal is made concerning the GO/NO GO test [44]. The discharge magnitude is plotted at the abscissa (Figure 7.1). The number of discharges larger than the abscissa value are plotted at the ordinate. Such a display was first reported in [69] and it is called here the f_{PD}-q function. Depending on experience, a GO area and a NO GO-area can be defined [44] (see Figure 7.1). If the f_{PD}-q function crosses the NO GO area, the tested product is recognized to be of bad quality. As mentioned

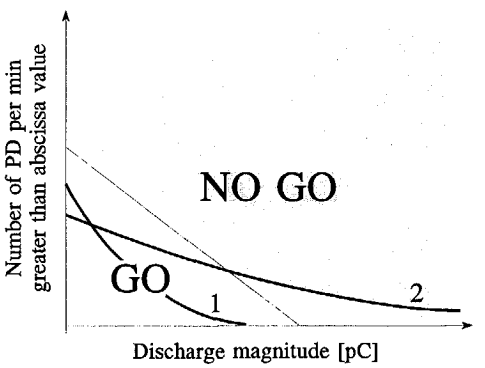

Figure 7.1 *The f_{PD}-q functions for a product of good quality (1) and for a product of bad quality (2).*

earlier, the locations of the GO area and the NO GO area must be determined by experience. The experience can be gained by testing on products of known quality or by comparing the discharge behaviour of different defects [44]. Feedback (for instance customer complaints/comments) must be used when reshaping the GO area and the NO GO area, so that after some time a reliable test procedure will have been developed.

Example

Discharge measurements were carried out for a filament transformer (Figure 7.2), which is used in a 150 kV (-75 kV, + 75 kV) power supply for an X-ray tube. The filament transformer provides the heating current for the filament at the cathode of the X-ray tube in order to promote electron emission.

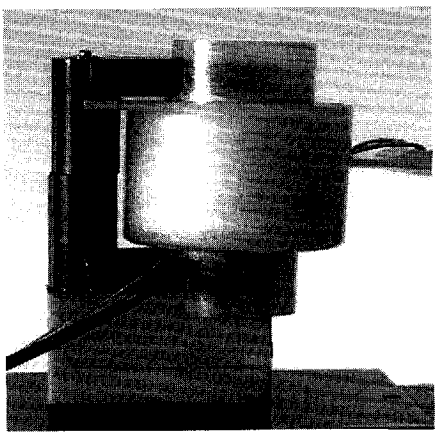

***Figure 7.2** Filament transformer.*

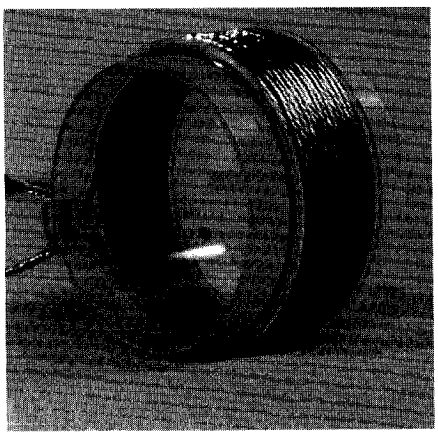

***Figure 7.3** High voltage coil of the filament transformer.*

The measurements were carried out at 75 kV DC. The measurement time was about 60 min. Two types of high voltage coils have were tested (Figure 7.3). Based on visual inspection, type 1 was of good quality, whereas the coils of type 2 were observed to contain small defects (scratches, voids). The measured f_{PD}-q functions (3 of each type) are shown in Figure 7.4.

A GO area can be defined so that the measurements of type 1 are recognised as good and the measurements of type 2 are recognised as bad. The thus defined GO area can be used for a quality check. As mentioned above, a refining of the GO area in course of time is necessary.

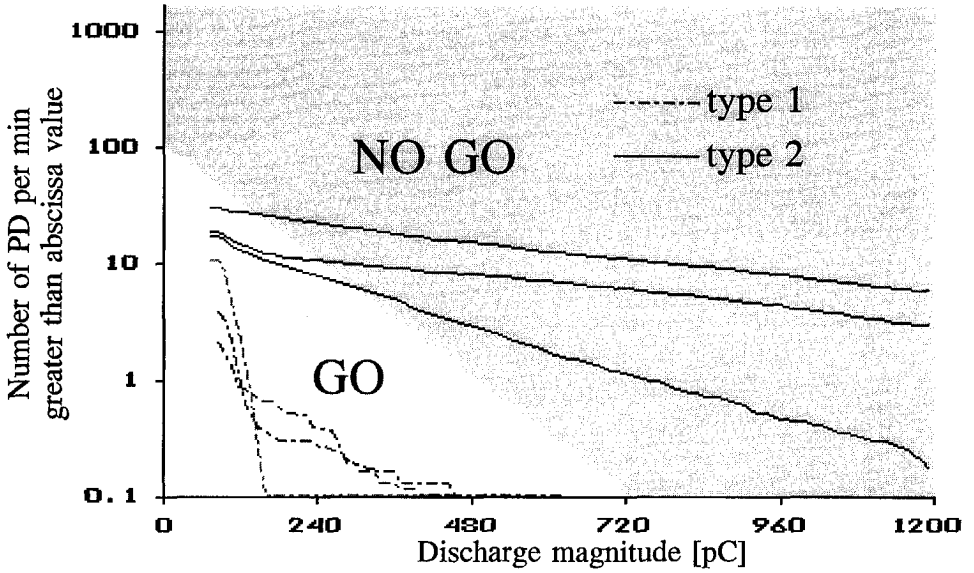

Figure 7.4 *Measured f_{PD}-q function for a filament transformer with different high voltage coils.*

7.1.5 Combined test

Non-electric parameters (temperature, mechanical stress etc.) can affect electric stability. For instance, non-pressurized paper-insulated HVDC cables showed a reduction of the dielectric strength of the order of 50% during the cooling phase of a thermal cycle [26]. Therefore these non-electric parameters have to be taken into consideration as well. The foregoing indicates the necessity for the development of combined tests (e.g. electrical stress combined with heating cycles) which should simulate the operating conditions.

7.2 Discharge diagnostics

In addition to the *type-test* and the *routine-test*, diagnostic tools are needed which enable the localization and recognition of defects. These methods can be used to find the reason for product failure and they will finally lead to the improvement of the design or the production.

The main principle of discharge diagnostics is the following. Partial discharges occur in the test object. The discharges can be measured and a 'fingerprint'

can be derived for the defect generating the discharges. By comparing the fingerprint of an unknown defect with the fingerprints of known defects the unknown defect may be recognised.

(a) Discharge diagnostics at AC voltage

The recognition and classification of partial discharges was first developed for AC voltage [64]. For each single discharge, the discharge magnitude q and the phase angle φ can be measured. These quantities are called basic quantities. As mentioned above, a fingerprint for the discharging defect is derived from the measured basic quantities. In the beginning, the discharge pulses were displayed superimposed on the cycle of the test voltage. The optical image was used as the fingerprint [64]. An expert was required to relate the fingerprints (characteristic discharge patterns) to certain types of defects. The availability of computers and the development of classification procedures made automated discharge classification and recognition possible. Therefore characteristic parameters are calculated from the measured data. These characteristic parameters, the fingerprints, are stored in a data bank. By comparing the characteristic parameters of an unknown defect with the parameters in the data bank, the recognition of the unknown defect may be possible. For AC the following approaches are known to the author.

1. One group of classification procedures is based on two dimensional histograms, for instance the phase angle histogram or the discharge magnitude histogram. Characteristic parameters, for instance skewness and kurtosis (see Appendix D), are used [27,28,63] to describe the shape of the measured distributions. These characteristic parameters can be stored in a data base. The classification is made by comparing the measured characteristic parameters with those stored in the data base. In order to compare the characteristic parameters, different mathematical procedures, for instance neural networks [28,63] or the centour score method [42,47] are reported.

2. Another group of classification procedures is based on the three dimensional discharge magnitude-phase histogram $H(q,\varphi)$. Characteristic parameters are used to describe the histogram $H(q,\varphi)$. For instance, the surface of the $H(q,\varphi)$ histogram was described with fractal features, such as fractal dimension and lacunarity [71]. The fractal dimension can be used as a measure of the surface roughness and the lacunarity is used as a measure of the denseness of a fractal surface [8,35]. These fractal features were further used as characteristic parameters. Another approach is reported in [31,75], where the three dimensional discharge magnitude-

phase histogram $H(q,\varphi)$ is directly used as a set of characteristic parameters. The classification is made by neural networks [31,75].

All the two dimensional distributions used in the first group can be derived from the three dimensional discharge magnitude-phase histogram $H(q,\varphi)$. Therefore, it can be stated that for AC voltage, most of the known characteristic parameters can be derived from the three dimensional discharge magnitude-phase histogram $H(q,\varphi)$, see Figure 7.5.

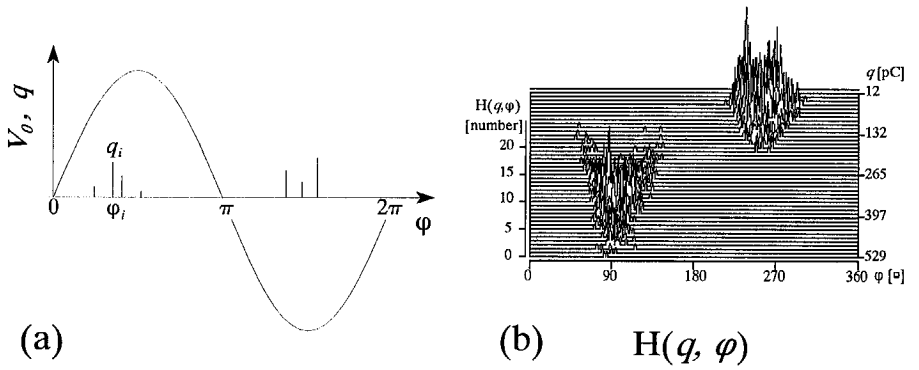

Figure 7.5 *The discharge process at AC: (a) time function with discharge magnitude q_i and phase angle φ_i as basic quantities; (b) the H(q, φ) distribution as characteristic discharge function* [45].

(a) Discharge diagnostics at DC voltage

At DC voltage, no approach to the classification and recognition of discharge defects is known to the author. The basic quantities which can be measured for each single discharge are the discharge magnitude q_i and the time of occurrence t_i.

If, for AC, all known classification procedures can be based on the three dimensional discharge magnitude-phase histogram $H(q,\varphi)$ then the classification for DC should be based on a three dimensional distribution as well. This distribution must contain the discharge magnitude as one parameter and an additional time parameter (similar to the phase φ used for AC). The author suggests the use of the $H(q,\Delta t_{suc})$ histogram as a base for classification and

recognition procedures at DC voltage (see Figure 7.6). Because of the mathematical similarity of $H(q,\varphi)$ and $H(q,\Delta t_{suc})$ all knowledge gained of discharge pattern recognition at AC voltage (based on $H(q,\varphi)$) can be applied for the recognition of partial discharge patterns at DC voltage based on $H(q,\Delta t_{suc})$.

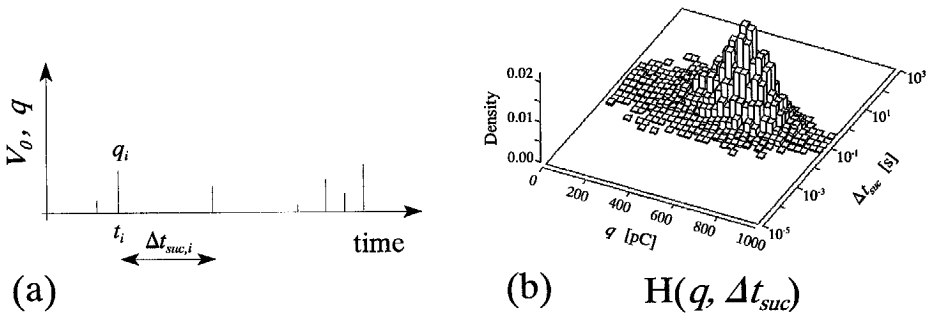

Figure 7.6 *The discharge process at DC: (a) time function with discharge magnitude q_i and time of occurrence t_i as basic quantities; (b) the $H_n(q, \Delta t_{suc})$ distribution as characteristic discharge function.*

In the previous chapters the three dimensional $H(q,\Delta t_{suc})$ histogram has been found to be characteristic for specific types of discharges (see Figures 7.7-7.9). This means that discharge classification and recognition at DC voltage should be possible. Based on the $H(q,\Delta t_{suc})$ histograms, an expert could visibly recognise some defects. For instance, for corona in air, a very narrow peak is characteristic (Figure 7.8).

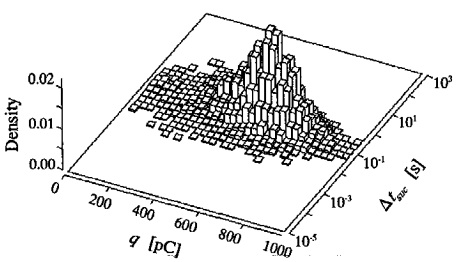

Figure 7.7 *$H_n(q, \Delta t_{suc})$ histogram for corona in oil at 70 kV (needle radius ≈ 35 μm)*

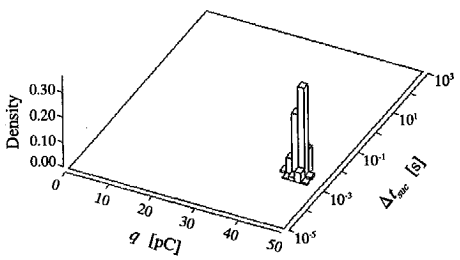

Figure 7.8 *$H_n(q, \Delta t_{suc})$ histogram for corona in air at 8 kV (needle radius ≈ 40 μm)*

For internal discharges (Figures 7.9) the maximum density is registered for the smallest measured discharges.

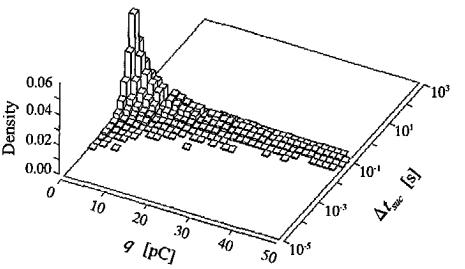

Figure 7.9 *$H_n(q, \Delta t_{suc})$ histogram for internal discharges in polyethylene (sample height 0.6 mm, void diameter 10 mm, void height 0.2 mm)*

In order to automate, the classification must be based on a set of characteristic parameters. Automated classification is made by comparing the characteristic parameters of known defects with those of unknown defects. Similar to the case of AC, there are the following possibilities.

1. The three dimensional $H(q,\Delta t_{suc})$ histogram could be used as a set of characteristic parameters and stored in a data base. For the classification, neural networks could be used as reported for AC in [31,75].

2. Fractal features could be used as characteristic parameters to describe the surface of the three dimensional $H(q,\Delta t_{suc})$ histogram as reported in [22].

3. Some two dimensional histograms such as the discharge magnitude histogram $H(q)$ or the time separation histogram $H(\Delta t_{suc})$ can be derived from the $H(q,\Delta t_{suc})$ histogram. Skewness *Sk* and kurtosis *Ku* (see Appendix D) could be used as characteristic parameters to describe the shape of these two dimensional histograms. The differences in the three dimensional histograms (Figures 7.7-7.9) lead to differences in the derived two dimensional histograms as well (Figures 7.10-7.12). The classification and recognition should not just be based on a single two dimensional histogram. For instance, the values of kurtosis and skewness of the magnitude histogram for corona in air (Figure 7.10(a)) and corona in oil (Figure 7.11(a)) do not differ very much. But there are clear differences in the *Sk* and *Ku* values for the time separation histogram of both defects in Figures 7.10(b) and 7.11(b). The presence of a ripple on the DC test voltage can affect the distribution of the time separation

(Figure 7.12) which can influence the result of recognition.

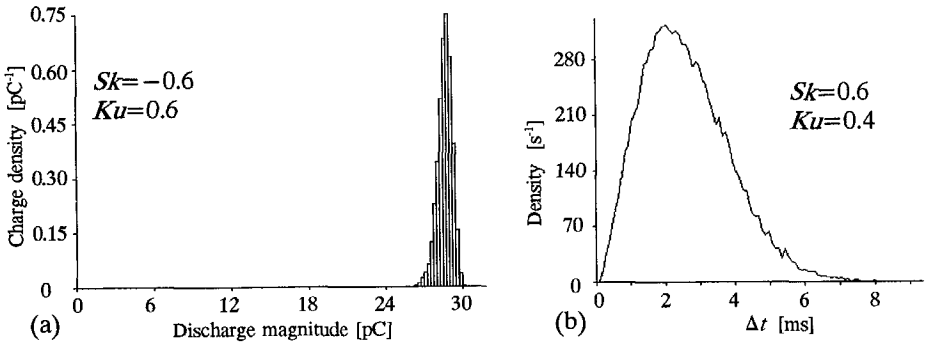

Figure 7.10 *The discharge magnitude histogram H(q) (a) and the time separation histogram H(Δt) (b) for corona in air ($V_0 = -7$ kV).*

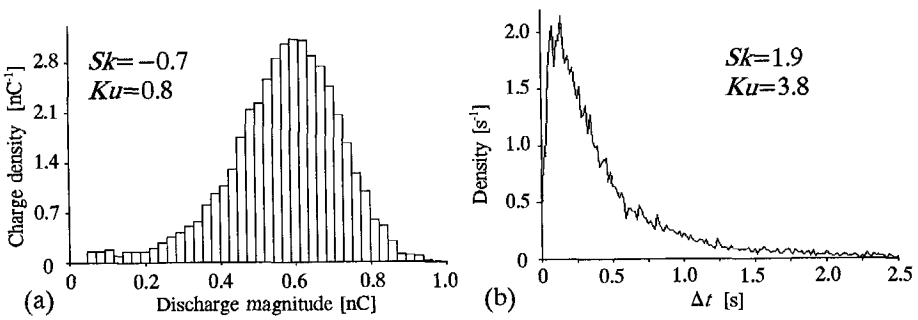

Figure 7.11 *The discharge magnitude histogram (a) and the time separation histogram H(Δt) (b) for corona in oil ($V_0 = 70$ kV).*

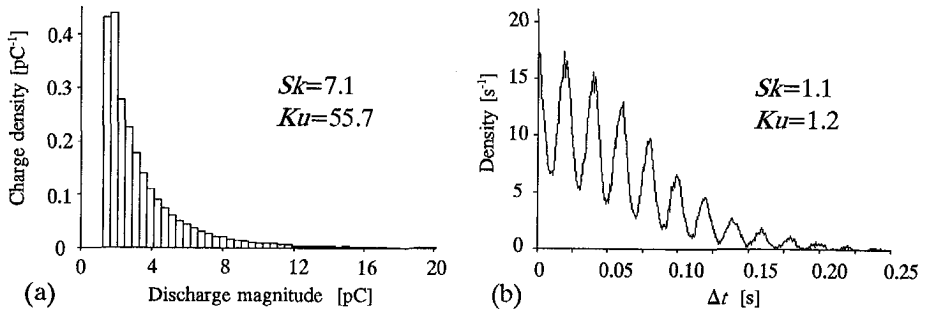

Figure 7.12 *Histogram of the discharge magnitude (a) and of the discharge separations (b) for internal discharges (h_S=0.3 mm, h_V=0.1 mm, d_V=6 mm, V_0=20 kV). The oscillation in (b) is caused by an AC ripple on the DC test voltage (see §3.3.2).*

7.3 Conclusions

(a) testing

The dependence of the ageing process on the electric field stress at DC has been found to be similar to that at AC. Therefore accelerated ageing tests used at AC (based on the assumption of a 'lifeline') can be used at DC as well. Therefore, concerning the *type-test*, the concept of overvoltage testing for DC voltage is concluded to be similar to that for AC [44].

The time behaviour of ageing at constant stress observed at DC is similar to that found for AC. The 'bathtub' shape is characterized by a conditioning effect in the beginning, succeeded by a certain time with a small failure risk. Finally, the failure risk increases again. The *routine-test* should lead to the conditioning caused by breakdown of the defect objects enhancing the risk of failure in the beginning.

At DC voltage, transient fields are caused by switching on/off or by polarity reversal. These situations must be tested as well.

The electrical stress due to impulse voltages is similar for AC and DC, so the test procedures could be similar as well.

The test conditions should include non-electric parameters (similar to the operation conditions), because the non-electric parameters such as temperature, mechanical stress etc. affect the dielectric behaviour.

For the partial discharge testing, a GO/NO GO test is suggested.

(b) Partial discharge diagnosis
The author suggests the use the three dimensional $H(q, \Delta t_{suc})$ histogram as a base for discharge classification and recognition at DC voltage.

If the classification of partial discharge patterns at DC voltage is based on the three dimensional $H(q, \Delta t_{suc})$ histogram, then all classification methods used for AC voltage can be used for DC as well.

Chapter 8

Conclusions

Partial discharges at DC voltage

1. Based on time-resolved measurements for internal discharges at DC voltage, the Townsend-like discharge mechanism has been found to be dominant.

2. A model to describe the statistical discharge behaviour has been developed that is based on the mutual relation of time lag, discharge magnitude and recovery time. The model proved to be valid for internal discharges and for corona in air.

Ageing and breakdown at DC voltage

3. The inverse power law relation $L \sim E^{-n}$ can be assumed, where L is the life of the insulation. For epoxy samples containing air-filled voids values $9 < n < 12$ were obtained.

4. The time behaviour of ageing observed at DC at constant stress is similar to that found at AC. The 'bathtub' shape is characterized by a conditioning effect in the beginning, succeeded by a certain time with a small failure risk. Finally the failure risk increases again.

Partial discharge and breakdown testing at DC voltage

5. Accelerated ageing tests used at AC (based on the assumption of a 'life-line') can be used at DC as well, based on conclusion 3.

6. For the partial discharge testing a simple GO/NO GO test is suggested.

Remarks:

At DC voltage, transient fields are caused by switching on/off or by polarity reversal. These situations must be tested and they must be taken into account by means of field calculation.

The electrical stress due to impulse voltages is similar for AC and DC, so the test procedures should be comparable as well.

The test conditions should include non-electric parameters (similar to the operating conditions), because the non-electric parameters such as temperature, mechanical stress etc. affect the dielectric behaviour.

Partial discharge diagnosis

7. The author suggests the use of the three dimensional $H(q,\Delta t_{suc})$ histogram as a base for discharge classification and recognition at DC voltage.

8. If the classification of partial discharge patterns at DC voltage is based on the three dimensional $H(q,\Delta t_{suc})$ histogram, then all classification methods used for AC voltage can be used for DC as well.

Suggestions for further study

1. In order to use the discharge diagnostics at DC voltage for actual technical objects, the methods for discharge diagnostics used for AC should be implemented for use at DC. The ability of the different methods to discriminate between different defects should be studied.

2. Most of the failures at DC voltage occur along interfaces. Therefore the following subjects are of special interest for further study.
   - mechanism of charge accumulation at interfaces
   - discharges along interfaces

3. Chemical reactions under the influence of high DC field strength may cause ageing. These reactions may occur at interfaces between different materials as well as in the bulk of a dielectric. Further investigations are required to understand these phenomena.

The aim of the studies pointed out in 2. and 3. should be to develop a set of characteristic parameters to describe the behaviour of electrode/insulator and insulator/insulator interfaces. These parameters will probably be based on the micro-structure (chemical structure, impurities, surface roughness) of the materials in contradiction to the macroscopical description (based on conductivity and permittivity) used today.

4. More work is required to understand ageing at DC voltage. Further investigation of the statistical breakdown behaviour should be related to the investigation of the physical ageing mechanism.

Appendix A

Charge accumulation in inhomogeneous materials [33]
In an electroquasistatic field, MAXWELL's equations can be written as

$$\nabla \times \boldsymbol{E} = 0 \tag{A.1}$$

$$\nabla \cdot \boldsymbol{D} = \nabla \cdot \epsilon \boldsymbol{E} = \rho \tag{A.2}$$

$$\nabla \cdot \boldsymbol{J} + \frac{\delta \rho}{\delta t} = 0 \,, \tag{A.3}$$

where $\boldsymbol{D}$ is the flux density, $\boldsymbol{E}$ is the electric field strength, $\boldsymbol{J}$ is the current density in the dielectric, while ϵ and ρ are the dielectric permittivity and the free space charge density respectively. $\boldsymbol{J}$ obeys Ohm's law

$$\boldsymbol{J} = \sigma \boldsymbol{E} \,, \tag{A.4}$$

where σ is the conductivity of the material.

Equations (A.2) and (A.4) result in

$$\boldsymbol{J} \cdot \nabla \frac{\epsilon}{\sigma} + \frac{\epsilon}{\sigma} \nabla \cdot \boldsymbol{J} = \rho \tag{A.5}$$

The elimination of $\nabla \cdot \boldsymbol{J}$ with eq.(A.3) and eq.(A.5) leads to

$$\frac{\delta \rho}{\delta t} + \frac{\sigma}{\epsilon} \rho = \frac{\sigma}{\epsilon} \boldsymbol{J} \cdot \nabla \frac{\epsilon}{\sigma} \tag{A.6}$$

In the pure DC state the accumulated space charge remains constant, so that eq.(A.6) becomes

$$\rho = \boldsymbol{J} \cdot \nabla \frac{\epsilon}{\sigma} \tag{A.7}$$

With (A.4) equation (A.7) becomes

$$\rho = \sigma \boldsymbol{E} \cdot \nabla \frac{\epsilon}{\sigma} \tag{A.8}$$

Appendix B

Data loss due to the polarity dependent noise rejection

Noise due to discharges outside the sample can be rejected because of its opposite discharge polarity. During the rejection of a disturbance impulse the system can not record a discharge signal for the blind time t_{blind}. During the measurement of the time $t_{measure}$, the total blind time t_{tot} is

$$t_{tot} = N_{outside} \cdot t_{blind} \quad , \tag{B.1}$$

where $N_{outside}$ is the number of discharges outside the sample, so that the frequency $f_{outside}$ of disturbances due to discharges outside the sample is given by

$$f_{outside} = \frac{N_{outside}}{t_{measure}} \tag{B.2}$$

Assuming independence of the discharge occurrences inside and outside the sample, the number of not recorded discharge N_{NR} is

$$N_{NR} = N_{inside} \cdot \frac{t_{tot}}{t_{measure}} \quad , \tag{B.3}$$

where N_{inside} is the number of discharges inside the sample. Then the data loss is given by

$$L_{data} = \frac{N_{NR}}{N_{inside}} = \frac{t_{tot}}{t_{measure}} = t_{blind} \cdot f_{outside} \tag{B.4}$$

Appendix C

Results of the ageing tests for the samples without void
The breakdown times depend on the test voltages

120 kV min	**110 kV** min	**100 kV** min	**90 kV** min	**80 kV** min
<1	<1	<1	<1	5
<1	<1	<1	5	10
<1	5	10	245	120
55	70	25	2185	4230
80	380	50	2335	35820
205	520	840	3565	45720
235	745	2120	6040	48360
250	1770	3040	9500	56880
260	1985	3370	11340	59760
670	3050	4860	11405	69000
895	3235	6020	13645	76200
1085	3805	8200	14620	96600
1985	5955	8200	15110	123600
3100	6545	>11400	>31800	>153000
3370	8640	>11400	>31800	>153000

The breakdown locations (see Figure C.1)

	no BD	in the void	corner	outside the void	void or corner
120 kV	-	5	5	1	4
110 kV	-	6	6	1	2
100 kV	2	4	7	2	-
90 kV	2	7	2	2	2
80 kV	2	3	5	2	3

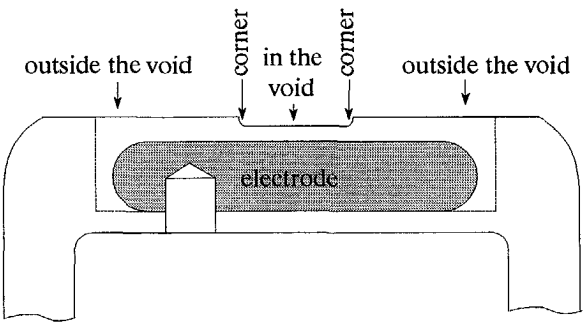

Figure C.1 *The breakdown locations.*

Appendix D

Skewness and kurtosis as characteristic parameters of two dimensional distributions

For pattern recognition purposes, the information contained in the discharge distributions is quantified. This is achieved by description of their shapes by various statistical parameters. Among others, skewness and kurtosis are used for discharge recognition at AC voltage [27].

Skewness, *Sk*, describes the asymmetry of the distribution with respect to a normal distribution. It is defined as

$$Sk = \frac{\sum (x_i - \mu)^3 \cdot P_i}{\sigma^3} \tag{D.1}$$

where x_i is the recorded value, P_i is the probability of appearance for that value x_i in the i-th phase window, μ is the mean value

$$\mu = \sum x_i \cdot P_i \tag{D.2}$$

and σ is the variance

$$\sigma^2 = \sum (x_i \cdot \mu)^2 \cdot P_i \,. \tag{D.3}$$

For a symmetric distribution, $Sk=0$, if it is asymmetric to the left, $Sk>0$, and if it is asymmetric to the right, $Sk<0$, see Figure D.1.

Kurtosis, *Ku*, represents the sharpness of the distribution with respect to the normal distribution,

$$Ku = \frac{\sum (x_i - \mu)^4 \cdot P_i}{\sigma^4} - 3 \,. \tag{D.4}$$

If the distribution has the same sharpness as a normal distribution, $Ku=0$. If it is sharper than normal, $Ku>0$, and if it is flatter, $Ku<0$, see Figure D.1.

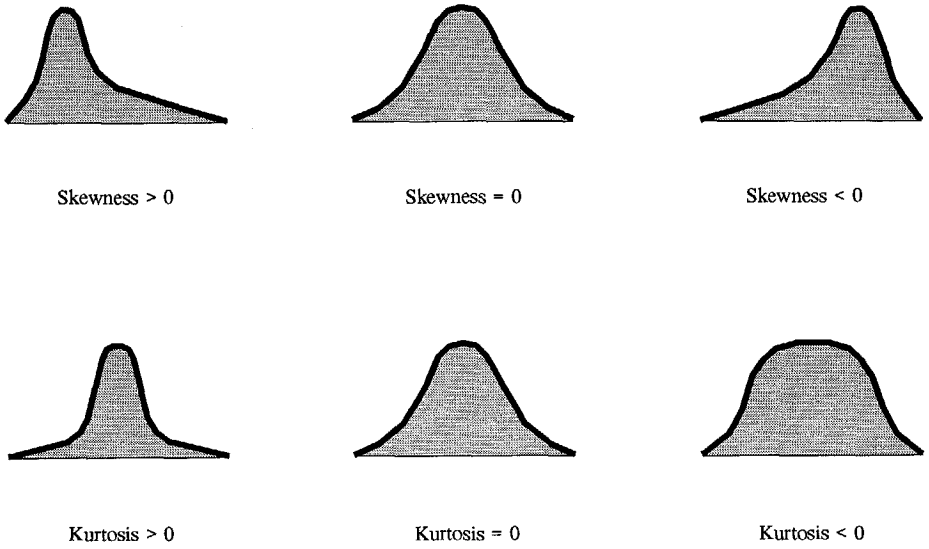

Figure D.1 *Examples of distributions and their resulting skewness and kurtosis.*

List of symbols

C	capacitor
$\boldsymbol{D}$	electric flux density
d_V	diameter of the void
$\boldsymbol{E}$	electric field intensity
f_{outside}	frequency of discharges outside the sample (see Appendix B)
$H(q)$	histogram of the discharge magnitude
$H(q, \Delta t_{suc})$	three dimensional histogram of discharge magnitude and the time to the successive discharge
h_V	height of the void
h_S	height of the sample
i_{PD}	discharge current (see Figure 1.4)
$\boldsymbol{J}$	current density
k_{AC}	voltage excess for AC (see eq. 3.6)
k_{DC}	voltage excess for DC (see eq. 3.10)
Ku	kurtosis (Appendix D)
L_{data}	data loss due to polarity dependent noise rejection
n	life line exponent eq.(6.3)
P_F	failure probability (§6)
q	discharge magnitude
Sk	skewness (Appendix D)
R	resistor
t	time
t_{blind}	blind time of the classical discharge detection system (see Appendix B)
t_L	time lag (Figure 3.17)
t_R	recovery time (Figure 3.17)
t_S	time scale parameter (§6)
Δt_{pre}	time to the predecessor of a discharge
Δt_{suc}	time to the successor of a discharge
V	voltage
V_0	test voltage
V_{cap}	maximal voltage across a void at AC if no discharge would occur, Figure 3.1
V_{con}	maximal voltage across a void at DC if no discharge would occur, Figure 3.2
V_i	ignition voltage (e.g. Figure 3.1, 3.2)
V_{inc}	inception voltage
V_{min}	minimal breakdown voltage (e.g. Figure 3.1, 3.2)
V_r	residual voltage after discharge extinction (Figure 3.4)
V_S	voltage scale parameter (§6)
ΔV	overvoltage above the minimal breakdown voltage (see Figure 3.1, 3.2)
v_{PD}	voltage pulse caused by the discharge current (see Figure 1.4)

α	time shape parameter eq.(6.1)
β	voltage shape parameter eq.(6.2)
ϵ	permittivity
σ	conductivity
ρ	space charge

Bibliography

[1] *Atten*, P.; *Saker*, A., "Streamer propagation over a liquid/solid interface". IEEE Trans. EI, Vol. 28 (1993), No. 2, pp. 230-242.

[2] *Bartnikas*, R., "Note on discharges in helium under ac conditions". Brit. J. Appl. Phys. (J. Physics D.), Vol. 1 (1968), pp. 659-661.

[3] *Bever*, R.S., "Ramp technique for DC partial discharge testing". IEEE Trans. EI, Vol. 20 (1985), No. 1, pp. 38-45.

[4] *Bilodeau*, T.M.; *Sarjeant*, W. J., "High-voltage and partial discharge testing techniques for space power systems". IEEE Electrical Insulation Magazine, Vol. 5 (1989), No. 2, pp. 12-21.

[5] *Brinkmann*, K., Einführung in die elektrische Energiewirtschaft, F. Vieweg&Sohn GmbH, Braunschweig, 1971 (in German)

[6] *van Brunt*, R.J., "Stochastic properties of partial-discharge phenomena". IEEE Trans. EI, Vol. 26 (1991), No. 5, pp. 902-948.

[7] *van Brunt*, R.J.; et. al., "Recent advances in partial discharge measurement capabilities at the National Institute of Standards and Technology". IEEE Trans. EI, Vol. 27 (1992), No. 1, pp. 114-129.

[8] *Chen*, S.S.; *Keller*, J.M., "On the calculation of fractal features from images". IEEE Trans. on Pattern Analysis and Machine Intelligence, Vol. 15 (1993), No. 10, pp. 1087-1090.

[9] *Craig Miller*, H., "Surface flashover of insulators". IEEE Trans. EI, Vol. 24 (1989), No. 5, pp. 765-786.

[10] *Dakin*, T.W. et al, "Breakdown of gases in uniform fields - Paschen curves for N_2, air and SF_6". Electra no. 32, 1974, pp. 61-82.

[11] *Devins*, J.C.; *Rzad*, S.J.; *Schwabe*, R.J., "Breakdown and prebreakdown phenomena in liquids". J. Appl. Phys. 52 (7), pp. 4531-4545, 1981.

[12] *Devins*, J.C., "The physics of partial discharges in solid dielectrics". IEEE Trans. EI, Vol. 19 (1984), No. 5, pp. 475-495.

[13] *Dissado*, L.A.; *Fothergill*, J.C.; *Wolfe*, S.V.; *Hill*, R.M., "Weibull statistics in dielectric breakdown; theoretical basis, application and implications". IEEE Trans. on EI, Vol. 19 (1984), No. 3, pp. 227-233.

[14] *Dissado*, L.A.; *Fothergill*, J.C., Electrical degradation and breakdown in polymers. Peter Peregrinus Ltd., London, 1992.

[15] *Douglas*, J.L.; *Parr*, D.J., "Evaluation of 100 kV direct voltage extruded polythene cable". Direct Current, Vol. 2 (1971), No. 3, pp.100-103.

[16] *Eeman*, J.C.J., "Experimental partial discharge detection equipment for DC and DC ramp high voltage testing". Proc. of the Europ. Space Power Conf., Florence 2-6 Sep. 1991, (ESA SP-320, August 1991).

[17] *Eoll*, C.K., "Theory of Stress Distribution in Insulation of High-Voltage DC Cables". IEEE Trans. EI, Vol. 10 (1975), pp. 27-35 and 49-54.

[18] *Favrie*, E.; *Pelet*, Y., "Etude du polyéthylène basse densité pour l'isolation des câbles d'énergie à courant continu à très haute tension". RGE, Tome 88, Vol. 1 (1979), pp. 27-35.

[19] *Forster*, E.O., "Progress in the field of properties of dielectric liquids". IEEE Trans. on EI, Vol. 25 (1990), No. 1, pp. 45-53.

[20] *Forster*, E.O. , "Partial discharges and streamers in liquid dielectrics". IEEE Trans. EI, Vol. 28 (1993), No. 6, pp. 941-946.

[21] *Forster*, E.O.; et. al., "The effect of the electrode gap on breakdown in liquid dielectrics". IEEE Trans. DEI (1994), Vol. 1, No. 3, pp. 440-445.

[22] *Fromm*, U., "Partial discharge classification at DC voltage". 9th ICSD, July 10-13, 1995, Leicester (UK), paper 7.1.9.

[23] *Fromm*, U.; *Morshuis*, P.H.F., "The discharge mechanism in gaseous voids at DC voltage". 9th ISH, August 28-September 1, 1995, Graz (Austria), paper 4154.

[24] *Fromm*, U.; *Kreuger*, F.H., "Statistical Behaviour of Internal Partial Discharges at DC voltage". Jpn. J. Appl. Phys., Vol. 33 (1994), Part 1, No. 12A, pp. 6708-6715.

[25] *Fruth*, B., *Niemeyer*, L., "The Importance of Statistical Characteristics of Partial Discharge Data", IEEE Trans. EI, Vol. 27 (1992), pp. 60-69.

[26] *Gazzana*, P., *Metra*, P.; *Miramonti*, G., "Research on the breakdown under type test of non-pressurized paper-insulated HVDC cables", ETEP, Vol. 3 (1993), No. 5, pp. 321-330.

[27] *Gulski*, E., Computer-aided Recognition of Partial Discharges Using Statistical Tools, Ph.D Thesis, Delft University of Technology (the Netherlands), Delft University Press, 1991, ISBN 90-6275-728-6.

[28] Gulski, E., Krivda, A., "Neural Networks as a Tool for Recognition of Partial Discharges", IEEE Trans. EI, Vol. 28 (1993), pp. 984-1001. *Errata* in IEEE Trans. DEI, Vol. 1 (1994), p. 351.

[29] *Hamid*, S.H.; *Amin*, M.B.; *Maadhah*, A.G., Handbook of polymer degradation, Marcel Dekker, INC., New York, Basel, Hong Kong 1992.

[30] *Hammer*, F.; *Küchler*, A., "Insulating systems for HVDC power apparatus". IEEE Trans. EI Vol. 27 (1992), No. 3, pp. 601-609.

[31] *Hozumi*, N., *Okamoto*, T., *Imajo*, T., "Discrimination of Partial Discharge Patterns Using a Neural Network", IEEE Trans. EI, Vol. 27 (1992), pp. 550-556.

[32] *Ieda*, M.; *Nawata*, M., "DC treeing breakdown associated with space charge formation in polyethylene". IEEE Trans. EI, Vol. 12 (1977), No. 1, pp. 19-25.

[33] *Jing*, T., Surface charge accumulation in SF_6. Ph.D Thesis, Delft University of Technology (the Netherlands), Delft University Press, 1993, ISBN 90-6275-848-7.

[34] *Karapetyan*, M.M.; *Khachatryan*, A.S.; *Bortnik*, I.M., "Short- and Long-Term Strength of Polymer Composite Materials with DC and AC Voltages", Power engineering (USSR Acad. of Sciences), Vol. 29 (1991), No. 1, pp. 99-105.

[35] *Keller*, J.M.; *Chen*, S.S., "Texture description and segmentation through fractal geometry". Computer Vision, Graphics, and Image Processing, Vol. 45 (1989), pp. 150-166.

[36] *Kelley* et al., "Measurement of partial discharges in hexane under DC voltage". IEEE Trans. EI, Vol. 24 (1989), No. 6, pp. 1109-1119.

[37] *Kimbark*, E.W., Direct current transmission, Wiley-Interscience, Volume I. Wiley-Interscience, 1971.

[38] *König*, D., "Impulslose Teilentladungen in Hohlräumen von Epoxydharzformstoff-Isolierungen". ETZ-Archiv, Vol. 90 (1969), pp. 156-158.

[39] *Kranz*, H.G., *Krump*, R., "Partial Discharge Diagnosis Using Statistical Optimization on a PC-based System", IEEE Trans. EI, Vol. 27 (1992), pp. 93-98.

[40] *Kreuger*, F.H. Partial Discharge Detection in High-Voltage Equipment. Butterworths & Co, 1989.

[41] *Kreuger*, F.H. Industrial high voltage Part II. Delft University Press, ISBN 90-6275-562-3, 1992.

[42] *Kreuger*, F.H.; *Gulski*, E.; *Krivda*, A., "Classification of Partial Discharges", IEEE Trans. EI, Vol. 28 (1993), pp. 917-931.

[43] *Kreuger*, F.H.; *Fromm*, U., "Partial Discharges in Gaseous Voids for DC Voltage". Jpn. J. Appl. Phys., Vol.33 (1994), Part 1, No.2, pp.1079-1084.

[44] *Kreuger*, F.H. Hoge Gelijkspanning. College Dictaat, TU Delft, 1994, to be published as Industrial High DC Voltage, Delft University Press, 1995.

[45] *Krivda*, A., Recognition of discharges. Discrimination and classification. Ph.D Thesis, Delft University of Technology (the Netherlands), Delft University Press, 1995.

[46] *Lewiner*, J.,"Evolution of experimental techniques for the study of the electrical properties of insulating materials" IEEE Trans. EI, Vol 21 (1986), No. 3, pp. 351-360.

[47] *Lindeman*, R.H.; *Merenda*, P.F.; *Gold*, R.Z., Introduction to Bivariate and Multivariate Analysis. pp. 203-204, Scott, Foresman and Company, 1980.

[48] *Löffelmacher*, G.; *Ulrich*, J., "'Faseriges Kanalwachstum', eine Zerstörungsform in hochpolymeren Isolierstoffen bei verringerten Teilentladungen". etz-a, Bd. 97 (1976), H. 8, S. 483-484.

[49] *Luoni*, G.; *Occhini*, E.; *Parmigiani*, B., "Long term tests on a $\pm$600 kV DC cable system". IEEE Trans. on PAS, Vol. 100 (1981), No. 1, pp. 174-183.

[50] *Macur*, J.; *Domansky*, K.; *Sikula*, J., "Stochastic character of partial discharges in insulators". J. Appl. Phys., Vol. 67 (1990), No. 1, pp. 540-542.

[51] *Mahajan*, S.M.; *Sudarshan*, T.S., "Measurement of the space charge field in transformer oil using its Kerr effect". IEEE Trans. on DEI, Vol 1 (1994), No. 1, pp. 63-70.

[52] *Malik*, N.H.; *Alrainy*, A.A., "Statistical variation of dc corona pulse amplitudes in point-to-plane gaps". IEEE Trans. EI, Vol 22 (1987), No. 6, pp. 825-829.

[53] *Melville*, D.R.G.; *Salvage*, B., "Detection and measurement of discharges in gaseous cavities in solid dielectrics under direct voltage conditions". Proc. IEE, Vol. 112 (1965), No. 5, pp. 1071-1073.

[54] *Morshuis*, P.H.F.; *Kreuger*, F.H., "Transition from streamer to townsend mechanisms in dielectric voids". J. Phys. D: Appl. Phys. 23 (1990), pp. 1562-1568.

[55] *Morshuis*, P.H.F., "The spacial distribution and electrical parameters of partial discharges in PE during ageing ". Proc. 4th Int. Conf. Cond. and Breakdown, Italy, 1992.

[56] *Morshuis*, P.H.F., Partial Discharge Mechanisms. Ph.D Thesis, Delft University of Technology (the Netherlands), Delft University Press, 1993, ISBN 90-6275-931-9.

[57] *Müller*, K.B., Über das Verhalten extrudierter PE-Kabel bei hoher Gleichspannungs-Langzeit-Belastung. Diss. TH Darmstadt 1976, Germany.

[58] *Nagao*, M.; *Kitamura*, T.; *Mizuno*, Y.; *Kosaki*, M; *Ieda*, M., "Localized heat generation before breakdown of polyethylene films". Proc. 3rd Int. Conf. Cond. Breakdown in Solid Dielectrics, Trondheim (Norway), 1989, pp.77-81.

[59] *Nakamura*, K.; *Kamijo*, Y., "Fluctuation mechanism of D.C. partial discharge in polyethylene and impulse noise in submarine cables". Jpn. J. Appl. Phys., Vol.15 Part 1 (1976), No.5, pp.865-870.

[60] *Niemeyer*, L.; *Fruth*, B.; *Gutfleisch*, F., "Simulation of Partial Discharges in Insulation Systems". 7th ISH, paper 71.05, 1991.

[61] *O'dweyer*, J.J., The theory of electrical conduction and breakdown in solid dielectrics. Clarendon Press, Oxford, 1973.

[62] *O'dweyer*, J.J., "The role of space charge in the theory of solid-dielectric breakdown". IEEE Trans. EI, Vol 9 (1984), No. 1, pp. 1-9.

[63] *Okamoto*, T., *Tanaka*, T., "Novel Partial Discharge Measurement Computer-aided Measurement Systems", IEEE Trans. EI, Vol.21 (1986), pp. 1015-1019.

[64] "Recognition of Discharges", CIGRE, Electra, No.11 (1969), pp. 61-98.

[65] *Robinson*, P.A.; *Coakley*, P., "Spacecraft charging", IEEE Trans. EI, Vol. 27 (1992), No. 5, pp. 944-960.

[66] *Roman*, E.S., Direct current long-term breakdown strength of cross-linked polyethylene. Diss., Royal Inst. of Technology Stockholm 1980, Sweden.

[67] *Sakamoto*, Y.; *Fukagawa*, H.; *Ninomyia*, K., "Investigation on test method of DC XLPE cable". IEEE Trans. on PAS, Vol. 101 (1982), No. 6, pp. 1352-1362.

[68] *Salvage*, B.; *Steinberg*, N.R., "Discharge repetition in an air-filled cavity in a solid dielectric under direct-voltage conditions". Electronics Letters, Vol. 2 (1966), No. 11, pp. 432-433.

[69] *Salvage*, B.; *Sam*, W., "Detection and measurement of discharges in solid insulation under direct-voltage conditions". Proc. IEE, Vol. 114 (1967), No. 9, pp. 1334-1336.

[70] *Satish*, L., *Gururaj*, B.I., "Use of Hidden Markov Models for Partial Discharge Pattern Classification", IEEE Trans. on Electrical Insulation, Vol.28, pp. 172-182, 1993.

[71] *Satish*, L., "Can fractal features be used for recognizing 3-d partial discharge patterns?". IEEE Trans. DEI, 1995.

[72] *Shihab*, S., Teilentladungen in Hohlräumen von polymeren Isolierstoffen bei hoher Gleichspannung, Diss. TU Braunschweig 1972, Germany.

[73] *Smit*, J.J.; *Ross*, R., "Manufacturing influences on the H.V.-A.C. endurance of epoxy-resin insulation", CIGRE Symposium, Vienna, May 1978, paper 610-10.

[74] *Stricklett*, K.L. et al., "Observation of partial discharges in hexane under high magnification". IEEE Trans. EI, Vol. 26 (1991), No. 4, pp. 692-698.

[75] Suzuki, H., Endoh, T., "Pattern Recognition of Partial Discharge in XLPE Cables Using a Neural Network", IEEE Trans. EI, Vol. 27 (1992), pp. 543-549.

[76] *Takahashi*, E.; *Tsutsumi*, Y.; *Okuyama*, K.; *Ogata*, F., "Partial discharge characteristics of oil-immersed insulation systems under DC, combined AC-DC and DC reversed polarity voltage". IEEE Trans. on PAS, Vol. 95 (1976), No. 1, pp. 411-421.

[77] *Tanaka*, T., "Internal partial discharge and material degradation". IEEE Trans. on EI, Vol. 21 (1986), No. 6, pp. 899-905.

[78] *Trichel*, G.W., "Mechanism of the negative point-to-plain corona near onset". Phys. Rev., Vol. 54 (1938), pp. 1078-1084.

[79] *Wang*, X.; *Huang*, Y; Tu, D., "Trap density as an indication of electrical ageing degree in polymers". Proc. 4th Int. Conf. on PADM, 1994, Brisbane (Australia), paper 7202.

[80] *Watanabe*, K., "D.C. Partial Discharges and Current in Polyethylene". Jpn. J. Appl. Phys., Vol. 17 (1978), Part 1, No. 3, pp. 483-490.

[81] *Weedy*, B.M., Underground transmition of electric power, John Wiley&Sons, 1980.

[82] *Wen*, K.C.; *Zhou* Y.B.; *Fu*, J.; *Jin*, T., "A calculation method and some features of transient field under polarity reversal voltage in HVDC insulation". IEEE Trans. on Power Delivery, Vol. 8 (1993), No. 1, pp. 223-230.

[83] *Werelius*, P.; *Erikson*, R.; *Braun*, J.M.; *Sedding*, H.G.: Temporal characteristics of partial discharge in voids under DC excitation; Nordic Ins. Sym., 1992.

[84] *Whitehead*, S., Dielectric breakdown of solids, Clearendon Press, Oxford, 1951.

[85] *Zeller*, H.R.; *Schneider*, W.R., "Electrofracture mechanism of dielectric ageing". J. Appl. Phys., Vol. 56 (1984), No. 2, pp. 455-459.

[86] *Zimmer*, H.H., "Gleich- und Wechselspannungskorona an technisch relevanten Elektrodengeometrien unter Berücksichtigung des Luftfeuchteeinflusses". thesis Univ. Karlsruhe, Germany, 1985 (in German).

[87] IEEE working group on dielectric tests for HVDC stressed transformers and reactors, "Recommended dielectric test procedures for converter transformers and smoothing reactors". IEEE Trans. on PWRD, Vol. 1 (1986), No. 3, pp. 161-166.

[88] CIGRE Study Committee No. 21, Working Group 21-01, "Recommendations for tests of power transmittion DC cables for a rated voltage up to 600 kV". Electra, N^0 72 (1980), pp. 105-114.

[89] Ansoft Corporation, Four Station Square, Commerce Court Building, Suite 660, Pittsburgh, PA 15219, Tel: 412-261-3200.

[90] IEC-Standard, Publication 270, "Partial discharge measurements", 1981.

[91] IEC-Standard, Publication 60-2, "High voltage test techniques", Part 2: Test procedures, 1973.

Acknowledgements

I would like to thank my promotor Prof. Dr. Ir. F.H. Kreuger for his encouragement of this research project. Thanks go to my colleagues of the High Voltage Laboratory for many fruitful discussions and for their support of the project leading to this thesis.

Samenvatting

Om betrouwbare hoogspanningscomponenten te kunnen leveren zijn geschikte testmethoden noodzakelijk. Om zulke testmethoden te ontwerpen is kennis nodig van de mechanismen die tot veroudering en uiteindelijk tot doorslag van het produkt leiden. In deze dissertatie worden partiële ontladingen en doorslag bij hoge gelijkspanning beschreven. Het uiteindelijke doel is het ontwerpen van testprocedures en diagnostische technieken voor produkten voor hoge gelijkspanning.

Hoofdstuk 1 geeft een inleiding over de specifieke problemen bij de toepassing van hoge gelijkspanning.

De gebruikte experimentele methoden worden in hoofdstuk 2 uiteengezet. Ze omvatten:

- een klassiek ontladingsmeetsysteem gecombineerd met een computer-analysesysteem,
- een systeem om time-resolved metingen te verrichten,
- een opstelling voor verouderingsproeven.

Interne partiële ontladingen worden in hoofdstuk 3 bestudeerd. Het aan ontladingen ten grondslag liggende fysische mechanisme is onderzocht en het statistische gedrag is geanalyseerd. Er wordt een ontladingsmodel beschreven en aan de hand van experimenten getoetst. Het model is gebaseerd op het verband tussen wachttijd, ontladingsgrootte en hersteltijd van een enkele ontlading.

In hoofdstuk 4 wordt het statistische gedrag van partiële ontladingen in lucht beschreven. Het model, zoals beschreven in hoofdstuk 3, kan gebruikt worden voor de beschrijving van corona ontladingen. Het is gebleken dat de fysica van oppervlakte ontladingen complexer is. De 3-dimensionale q-Δt_{suc}-verdeling (aantal ontladingen als functie van ontladingsgrootte en tijd tot de volgende ontlading) kan worden gebruikt voor de beschrijving van oppervlakte ontladingen.

In hoofdstuk 5 worden partiële ontladingen in diëlectrische vloeistoffen behandeld. Een overzicht van de mechanismen die tot doorslag leiden wordt hier gepresenteerd. Er worden meetresultaten van partiële ontladingen in

transformatorolie gegeven.

Veroudering en doorslag onder hoge gelijkspanning is in hoofdstuk 6 onderzocht. Er zijn verouderingsproeven gedaan aan epoxy proefstukken met een luchtgevulde holte. Voor de evaluatie van de resultaten is aangenomen dat de levensduur van de proefstukken met een hoge macht n van de beproevingsspanning afhangt. Hieruit volgde een levensduurexponent van $9<n<12$ voor de epoxy proefstukken.

Testmethoden en diagnostische methoden voor ontladingen onder hoge gelijkspanning worden behandeld in hoofdstuk 7. Er wordt geconcludeerd dat de proeven onder gelijkspanning op soortgelijke manier kunnen worden uitgevoerd als die onder wisselspanning. Verder wordt er een partiële ontladingsproef voorgesteld. De 3-dimensionale q-Δt_{suc}-verdeling wordt voorgesteld als basis voor de classificatie van ontladingen. In dat geval kunnen alle hedendaagse methoden voor wisselspanning ook voor gelijkspaning worden gebruikt.

Zusammenfassung

Die Produktion zuverlässiger und langlebiger Hochspannungskomponenten erfordert entsprechende Testmethoden. Voraussetzung dafür ist die Kenntnis der Alterungs- und Durchschlagsmechanismen in Dielektrika. In der vorliegenden Arbeit werden das Verhalten von Teilentladungen (TE) und elektrischem Durchschlag bei hohen Gleichspannungen untersucht mit dem Ziel, Test- und TE-Diagnoseverfahren für Gleichspannungsapparate zu entwickeln.

Das erste Kapitel beinhaltet eine Einleitung zu den Problemen beim Umgang mit hohen Gleichspannungen.

In Kapitel 2 werden die verwendeten Meßeinrichtungen beschrieben. Das sind:
- ein klassisches TE-Meßsystem in Verbindung mit einem computergestützten TE-Analysator,
- ein extrem breitbandiges TE-Meßsystem zur Untersuchung interner TE,
- ein Meßaufbau für Alterungsuntersuchungen.

In Kapitel 3 werden der physikalische Mechanismus und das statistische Verhalten interner TE untersucht. Ein Modell des statistischen Verhaltens von internen TE wird beschrieben. Das Modell beruht auf der Annahme einer gegenseitigen Abhängigkeit der Verzögerungszeit (notwendig zur Lieferung eines Startelektrons), der TE-Größe und der notwendigen Zeit zum erneuten Erreichen der Durchschlagspannung unmittelbar nach einem TE-Ereignis.

In Kapitel 4 wird das statistische Verhalten von TE in Luft beschrieben. Ein Modell, ähnlich dem für das statistische Verhalten von internen TE, kann auch zur Beschreibung von Koronaentladungen benutzt werden. Zur charakteristischen Beschreibung von Gleitentladungen entlang dielektrischer Oberflächen kann ein dreidimensionales q-Δt_{suc}-Histogramm (Anzahl von TE in Abhängigkeit von der Entladungsgröße und der Zeit zur nachfolgenden Entladung) dienen.

Das Verhalten von TE in dielektrischen Flüssigkeiten wird in Kapitel 5 behandelt. Es wird ein Überblick der zum Durchschlag führenden Mechanismen gegeben. Meßergebnisse von TE in Transformatorenöl werden präsentiert.

Alterung und elektrischer Durchschlag bei hoher Gleichspannung stehen im Mittelpunkt des sechsten Kapitels. Resultate von Alterungsexperimenten an

Hohlraumprüfkörpern aus Epoxydharz werden präsentiert. Bei der Auswertung wird eine exponentielle Abhängigkeit der Lebensdauer von der Testspannung angenommen. Ein Lebensdauerexponent $9<n<12$ wird ermittelt.

In Kapitel 7 werden Test- und TE-Diagnoseverfahren bei Gleichspannung diskutiert. Aus diesen Betrachtungen ergibt sich die Schlußfolgerung, daß Spannungstests bei Gleichspannung ähnlich wie bei Wechselspannung durchgeführt werden sollten. Ein TE-Test wird vorgeschlagen. Bezüglich der TE-Diagnose bei Gleichspannung wird das q-Δt_{suc}-Histogramm als Basis für die TE-Klassifikation vorgeschlagen. In diesem Falle können alle aus der Wechselspannungstechnik bekannten TE-Diagnosetechniken auch bei Gleichspannung angewendet werden.

U. Fromm was born in Koßdorf, Germany, on June 14, 1966. After graduating in 1984 at the Erweiterte Oberschule in Elsterwerda, he studied at the Faculty of Electrical Engineering at the Dresden University of Technology, where he graduated in 1991.

In October 1991 he joined the High Voltage Laboratory of the Delft University of Technology, where he performed research in the field of testing and diagnosis of HVDC components leading to this Ph.D thesis.